MOUNTAIN-PLAINS CONSORTIUM

MPC 22-480 | K. Ng, L. Khatri, and E. Alomari

IMPROVING DESIGN
AND CONSTRUCTION
OF TRANSPORTATION
INFRASTRUCTURE
THROUGH BEDROCK
CHARACTERIZATION

MOUNTAIN-PLAINS CONSORTIUM REGION 8

Technical Report Documentation Page

1. Report No. MPC-632	2. Government Accession No.	3. Recipient's Catalog No.
4. Title and Subtitle Improving Design and Construction of Transportation Infrastructure through Bedrock Characterization		5. Report Date September 2022
		6. Performing Organization Code
7. Author(s) Kam Ng, Ph.D. Lokendra Khatri Esraa Alomari		8. Performing Organization Report No. MPC 22-480
9. Performing Organization Name and Address Dept. of Civil & Architectural Engineering and Construction Management Department of Mathematics & Statistics University of Wyoming 1000 E. University Ave. Laramie, WY 82071		10. Work Unit No. (TRAIS)
		11. Contract or Grant No.
12. Sponsoring Agency Name and Address Mountain-Plains Consortium North Dakota State University PO Box 6050, Fargo, ND 58108		13. Type of Report and Period Covered Final Report
		14. Sponsoring Agency Code

15. Supplementary Notes

16. Abstract

This study evaluates a comprehensive experimental investigation to better understand the mechanical and deformation behavior of Wyoming bedrocks and therefore to improve the design and construction of transportation infrastructure. Fifty-six rock samples were collected from different locations around the state of Wyoming, including different rock types, formations, geologic ages, and depths. The prominent rock types are sandstone, shale, siltstone, claystone, and other less common rock types that represent three geological types: igneous, sedimentary, and metamorphic. Geotechnical investigation and rock sampling were performed to obtain standard rock cores with a diameter to height ratio of 1:2 for laboratory testing. A series of uniaxial and triaxial compression, porosity, and specific gravity tests were conducted on these samples, and the results in terms of Mohr-Coulomb failure parameters, Hoek and Brown failure parameters, and elastic properties were analyzed in this study. Findings of this research includes conducting regression analysis for the dataset in order to establish prediction equations that relate bedrock strength and deformation properties and the failure behavior of bedrocks depending upon rock geology and other contributing factors. Finally, recommendations were provided based on the experimental results that will facilitate the design and construction of transportation infrastructure in Wyoming.

17. Key Word bedrock, construction, deformation, design, disaster resilience, geotechnical engineering, infrastructure, laboratory tests	18. Distribution Statement Public distribution		
19. Security Classif. (of this report) Unclassified	20. Security Classif. (of this page) Unclassified	21. No. of Pages 97	22. Price n/a

Form DOT F 1700.7 (8-72)   Reproduction of completed page authorized

Improving Design and Construction of Transportation Infrastructure through Bedrock Characterization

Prepared by:

Kam Ng, Ph.D., P.E., Associate Professor
Lokendra Khatri, MS Student
Esraa Alomari, Ph.D. Student

Department of Civil & Architectural Engineering and Construction Management
Department of Mathematics & Statistics
University of Wyoming
1000 E. University Avenue
Laramie, Wyoming 82071

September 2022

Acknowledgements

Disclaimer

The contents of this report reflect the views of the authors, who are responsible for the facts and the accuracy of the information presented. This document is disseminated under the sponsorship of the Department of Transportation, University Transportation Centers Program, in the interest of information exchange. The U.S. Government assumes no liability for the contents or use thereof.

ABSTRACT

This study evaluates a comprehensive experimental investigation to better understand the mechanical and deformation behavior of Wyoming bedrocks and therefore to improve the design and construction of transportation infrastructure. Fifty-six rock samples were collected from different locations around the state of Wyoming, including different rock types, formations, geologic ages, and depths. The prominent rock types are sandstone, shale, siltstone, claystone, and other less common rock types that represent three geological types: igneous, sedimentary, and metamorphic. Geotechnical investigation and rock sampling were performed to obtain standard rock cores with a diameter to height ratio of 1:2 for laboratory testing. A series of uniaxial and triaxial compression, porosity, and specific gravity tests were conducted on these samples, and the results in terms of Mohr-Coulomb failure parameters, Hoek and Brown failure parameters, and elastic properties were analyzed in this study. Findings of this research includes conducting regression analysis for the dataset in order to establish prediction equations that relate bedrock strength and deformation properties and the failure behavior of bedrocks depending upon rock geology and other contributing factors. Finally, recommendations were provided based on the experimental results that will facilitate the design and construction of transportation infrastructure in Wyoming.

TABLE OF CONTENTS

LIST OF TABLES

LIST OF FIGURES

1.   INTRODUCTION

1.1   Background

Bedrock is the underlying relatively hard and solid rock beneath the soil, gravel, and other unconsolidated material. The bedrocks are generally igneous, metamorphic, or sedimentary, depending on the formation process they undergo. The rock can be formed by the lithification of loose sediments over time, cooling and hardening of magma, or changing form. Thus, these underlying bedrocks have different strengths based on their formation, age, type, and depth. The age of the bedrock, ranging from the Precambrian to Cenozoic eras, differs in strength and deformation properties. These bedrocks are the parent material for soil materials and take up the loads from civil infrastructure during design and construction. It is, therefore, essential to perform comprehensive experimental investigations on these bedrocks to understand their strength and deformation properties.

In the case of transportation infrastructure in Wyoming, especially bridges, slopes, and roadways, different bedrock formations such as White River, Wasatch, Fort Union, Green River, and Arikaree are often encountered. The engineering properties, such as shear strength, elastic properties, failure parameters, stiffness, and bedrock quality of these bedrock formations, are lacking due to the absence of advanced rock testing equipment. The lack of understanding of rock behaviors and measured engineering parameters has created challenges in the design and construction of transportation infrastructures in Wyoming. Although prediction equations developed and published by researchers have been used to estimate some of these engineering properties, in the absence of measured properties of Wyoming bedrocks, the applicability of these prediction equations has yet been verified.

A site investigation is often performed by The Wyoming Department of Transportation (WYDOT) to determine the subsurface profile and geomaterial properties. The lithology of the Wyoming bedrock formations consists predominantly of shale, sandstone, siltstone, claystone, mudstone, and conglomerate. A standard penetration test, rock quality designation, geological strength index, and uniaxial compressive strength are measured and logged in the bedrock properties database. However, shear strength properties of these bedrocks (friction angle and cohesion) and elastic properties (Young's modulus and Poisson's ratio) are usually estimated but not measured. Understanding and characterizing these Wyoming bedrock properties will yield prediction equations that are more representative of local bedrocks, contribute a more significant economic benefit to the design and construction of transportation infrastructure, and increase the reliability of these infrastructures.

1.2   Problem Statement

The underlying bedrocks have natural variability depending upon the formation process they undergo. This creates increased uncertainty in the subsurface condition for the design and construction of transportation infrastructures. The limited understanding of bedrock behaviors and absence of strength and elastic properties leads to unforeseen construction challenges, especially in the case of deep foundation design in soft rocks (Mokwa and Brooks 2008). This research includes measuring the rock properties of different lithology and locations within the state of Wyoming to advance the development of a geomaterial classification system (Adhikari et al., 2019). The comprehensive test data of the bedrocks will reduce the uncertainties and discrepancy between design outcome and construction performance by improving the engineering design efficiency.

During the construction of driven piles, especially in the soft rocks, AASHTO (2020) recommends that the pile be driven in the same manner as soil. The static analysis method for soft rocks is not readily available for pile resistance estimation; hence, pile resistances are usually under-predicted (Ng and

Sullivan 2017). The piles do not satisfy the LRFD strength limit at the end of driving and, occasionally, at the beginning of the last strike. Significant discrepancies between estimated and measured pile resistances were reported (Ng et al., 2015). This high uncertainty in pile performance could lead to construction challenges, especially in the case of a bridge project where foundation construction is critical. This research, therefore, can provide a database of bedrock properties that can be utilized to calibrate the static analysis method to improve the pile resistance estimation and decrease the discrepancy between the estimated and measured pile resistance in soft rocks. This will reduce the design and construction costs. The empirical prediction equations for the Hoek and Brown parameters are developed based on general bedrocks that might not represent the Wyoming bedrocks. The measured properties of intact rock samples, along with unconfined compressive strength (qu) and geological strength index (GSI) records in the WYDOT Bedrock Properties Database, can be used to calibrate the Hoek and Brown parameters, improve the qp estimation, and increase the reliability of drilled shaft design and construction in Wyoming. This improvement can reduce the depth of the bedrock socket and eventually the overall construction cost.

Landslides and rock falls are common occurrences in Wyoming. This research will generate measured shear strength properties (friction angle and cohesion) and elastic properties (Young's modulus and Poisson's ratio) of Wyoming bedrocks used in rock stability evaluation and mitigation strategies for rock slope stabilization. This will increase the stability and reduce the cost of rock slope stabilization. The design of spread footing on shallow bedrock requires the determination of Hoek and Brown parameters (Cater and Kulhawy 1988) or shear strength properties (Goodman 1989). Due to the challenges with determining the nominal bearing resistance on rocks, a shallow footing may be over-designed or under-designed, leading to unforeseen changes in cost and design. This research will provide the necessary parameters to reduce the need for an expensive plate load test to determine the nominal bearing resistance.

Rock rippability, or the ease of mechanical evacuation of rock, is commonly encountered during road construction. The rock rippability depends on the geology and engineering properties of the bedrock. Seismic lines are run at sites to correlate drilling characteristics and seismic velocities to the rock rippability. Still, high torque and horsepower drills have made the comparison more difficult. The measured bedrock properties from this research will provide the technical background to improve rock rippability evaluation and excavation effort prediction, enhancing the preparation of construction schedules and cost estimates.

Bedrock is a parent material of base aggregates used in flexible and rigid pavements. Although the laboratory-measured properties and resilient modulus of the local base materials in Wyoming have been recently quantified (Ng et al., 2019), little is known about the Wyoming bedrock as the parent material. A study by the Virginia DOT concluded that limestone aggregates have a higher resilient modulus than granite aggregates (Hossain and Lane 2015). Hence, this research will provide the basis for future assessment of suitable bedrock sources for base aggregates in terms of degradation behavior, particle breakage, and mechanical properties.

1.3   Objectives

The main objective of the research is to understand the strength and deformation behaviors of Wyoming bedrocks to improve the design and construction of transportation infrastructure. The research outcome will also look to address WYDOT's strategic goals: acquiring and responsibly managing resources, providing a safe, reliable, and effective transportation system, and encouraging and supporting innovation to increase the efficiency in the design and construction of transportation infrastructures.

This research also aims to reduce the design and construction challenges due to the lack of measured engineering properties of bedrock representing the Wyoming formations. The objectives of the research are as follows:

1. To determine the strength and deformation properties of bedrocks. This includes the shear strength properties (friction angle and cohesion) and elastic properties (Young's modulus and Poisson's ratio).
2. To develop locally calibrated relationships for bedrock properties in terms of index parameters, rock quality, and unconfined compressive strength (qu). These parameters will be used to better define the Hoek and Brown (HB) criterion to achieve a more cost-effective design of drilled shafts and driven piles.
3. To expand the WYDOT database of rock properties. This database currently has 2,100 project and rock test records, and 523 were identified as tertiary formations. The database has measured bedrock density, percentage recovery, rock quality designation (RQD), and geological strength index (GSI) but lacks shear strength and elastic properties.
4. To improve the understanding between Wyoming geology and bedrock behaviors.

1.4   Tasks

The research objectives are accomplished by completing the five research tasks described below.

1.4.1   Task 1. Literature Review

The first research task is to conduct a literature review pertinent to rock mechanics and bedrock properties. This task includes a review of documents, books, papers, reports, catalogs, manuals, notes, and presentation slides about bedrock quality and properties relevant to civil engineering applications. This task will also include documentation and reviewing the current knowledge and practice related to bedrock classification, description, testing, and properties. This research task will also identify gaps in the knowledge and review of current specifications and guidelines by DOTs, AASHTO, and other agencies.

1.4.2   Task 2. Assessment of WYDOT Electronic Database and Rock Inventory

The second research plan task includes assessing the WYDOT electronic database and rock inventory data. In this task, a review and analysis of usable records like rock quality description, qu value, and geology description from the WYDOT database shall be conducted for subsequent studies. This task will help identify relevant cores and usable rock samples from the WYDOT geology storage for laboratory testing.

1.4.3   Task 3. Geotechnical Investigation and Rock Sampling

The third task is the geotechnical investigation and rock sampling. This task includes obtaining new rock samples from the geotechnical investigation on highway projects. The geology program will perform the geotechnical investigation to obtain standard rock cores of diameters about 1.91 inches. The standard core run will be 5 feet depending upon the RQD. The geotechnical reports and subsurface profiles of the projects were assessed to determine the underlying bedrock characteristics, stratigraphy, geological formation, and discontinuity. A minimum of three rock samples with a diameter to height ratio of 1:2 will be obtained for laboratory testing.

1.4.4 Task 4. Laboratory Rock Testing

The fourth task is to conduct laboratory testing of the collected rock samples from Task 3. The laboratory testing will include the uniaxial and triaxial compressive tests following the ASTM D7012 (2014) using the servo-controlled testing system (GCTS RTR-1500). This task will include testing 50 rock samples, i.e., at least 150 specimens, collected from all around Wyoming. These 50 rock samples will consist of the typical lithology of the Wyoming bedrock formations, predominantly shale, sandstone, siltstone, claystone, mudstone, and conglomerate.

1.4.5 Task 5. Data Analysis and Correlation Development

The fifth task includes data analysis and prediction equation development using the data collected from the literature review in Task 1, collected data from the database in Task 2, and the laboratory-measured data from Task 4. This task will focus on understanding the bedrock failure and deformation behaviors. Combining triaxial and uniaxial test results, Hoek-Brown parameters and Mohr-Coulomb shear strength parameters were determined. The measured rock properties and the rock quality description will be compiled for each Wyoming bedrock formation and lithology. The properties will be presented with model comparison criteria.

1.5 Report Focus and Organization

This report aims to better understand the mechanical and deformation behavior of Wyoming bedrocks to improve the design of WYDOT transportation infrastructures. Chapter 1 presents the background, objectives, and tasks of this research. A literature review follows in Chapter 2. Chapter 3 focuses on laboratory rock testing and samples preparation. Chapter 4 describes the summary of experimental testing of different rock types. Chapter 5 presents the research methods and datasets used in the analysis. Finally, recommendations and conclusions are given in Chapter 6, which is followed by the references.

2. LITERATURE REVIEW

2.1 Introduction

Based on the process of formation, rocks generally are of three types: igneous, sedimentary, and metamorphic. The mechanical properties of these rocks, like the stress and strain, the compressive strength, and elastic constants (Young's modulus, shear modulus, bulk modulus, and Poisson's ratio), are affected by numerous factors. The compressive strength and Young's modulus are affected by constitutive properties of the rock and test conditions. The constitutive properties include porosity, mineralogy, anisotropy, geological age, and density, whereas the test conditions are the confinement, strain rate, temperature, and sample condition. Table 2.1 shows the geological time scale of rocks that can be used to describe the age and process of formation. The pores influence the strength and deformation properties of rocks (Franklin and Dusseault, 1989; Rui Song et al., 2019).

Table 2.1 Geological time scale (Lyn Topinka, 1997)

Era	Period or System	Epoch or Series
Cenozoic (66 million years ago to present)	Quaternary (2 million years ago - Present)	Holocene (12000 years ago- Present)
		Pleistocene (2 million - 12000 years ago)
	Tertiary (66 million - 2 million years ago)	Pliocene (5-2 million years ago)
		Miocene (24-5 million years ago)
		Oligocene (37-24 million years ago)
		Eocene (58-37 million years ago)
		Paleocene (66-58 million years ago)
Mesozoic (250 - 66 million years ago)	Cretaceous (135-66 million years ago)	Early / Late
	Jurassic (205-135 million years ago)	Early / Late
	Triassic (250-205 million years ago)	Early / Late
	Carboniferous (365-290 million years ago)	Pennsylvanian (310-290 million years ago)
		Mississippian (365-310 million years ago)
	Devonian (400-365 million years ago)	Early / Middle / Late
	Silurian (425-400 million years ago)	Early / Middle / Late
	Ordovician (500-425 million years ago)	Early / Middle / Late
	Cambrian (570-500 million years ago)	Early / Middle / Late
Precambrian (Beginning of Earth to 570 million years ago)		

2.1.1 Mechanical Anisotropy

Rock masses are complex nature materials that consist of intact rock pieces and fractures and bedding planes at different orientations. These characteristics of rock masses affect their mechanical behaviors and cause anisotropy. Anisotropy is the variation of properties concerning the directions in analyzing the rock structure. The anisotropic nature of rock creates variation in the strength and deformation behaviors in different directions. The strength envelopes of these anisotropic rocks vary significantly with axial and confining pressures.

An anisotropy is generally observed in sedimentary rocks because of the orientation of clay, aligned fractures, cracks and pores, and fine layering (Nasseri et al., 2003). Rock anisotropy can be described as intrinsic and induced. The intrinsic anisotropy is caused by bedding planes, discontinuities, and constituting minerals whereas the induced anisotropy is caused by overburden pressure and sediment changes. The rock anisotropy interacts with stress, deformability, and strength, and it is important in rock masses (Amadei and Savage, 1989; Amadei, 1996).

The anisotropy plays an important role when microstructural observations are made of argillaceous rocks like shale and claystone. These rocks consist of porous fine-grained clay with embedded silt/sand grains. Therefore, the mechanical properties are altered by the ratio of these contents. The anisotropic properties of these rocks are rarely available or measured from small rock samples as they do not contain fractures with varying sizes, orientations, and beddings at large scales. Therefore, evaluating the anisotropic nature of the rocks is still a challenge in rock mechanics. The mechanical properties like Young's modulus and Poisson's ratio often describe the rocks' anisotropic behaviors.

2.1.2 Young's Modulus

Young's modulus is defined as the measure of rock's stiffness or resistance to elastic deformation under the applied load. The lower the Young's modulus, the more ductile the rock, and the higher the Young's modulus, the more brittle the rock. The elastic modulus is a critical parameter in describing rock behavior under loading due to the quasi-brittle nature of rocks (Bieniawski, 1989; Hoek & Brown, 1980). The International Society of Rock Mechanics (ISRM) has described three methods for determining Young's modulus: the tangent, secant, and average. The Young's modulus determined in this research is calculated by plotting the axial stress in the y-axis and the axial strain as a percentage in the x-axis. The linear portion of the curve given as a straight line is identified, and the gradient of this line is calculated. The strain by definition is non dimensional and expressed in percentage. To express the Young's modulus in the same unit as the stress, the gradient is then multiplied by 100 so that the strain is in dimensionless decimal instead of percentage. Eq. (2.1) represents the formula for the calculation of the Young's modulus.

$$\varepsilon = \frac{Axial\ stress}{Axial\ strain\ (\%)} \times 100 \tag{2.1}$$

2.1.3 Poisson's Ratio

Poisson's ratio is a ratio of change in width (radial deformation) to the change in length (axial deformation) of the rock under loading. Poisson's ratio measures the compressibility of rocks and provides a valuable measure of how much a material deforms under stress. The maximum value of Poisson's ratio in the case of rock is considered as 0.5. Rock will have a Poisson's ratio of 0.5 if it deforms elastically at a low strain rate. The Poisson's ratio of a rock core subjected to an axial load is expressed in dimensionless ratio of lateral strain to axial strain, shown in Figure 2.1 (a), and method of calculation from unconfined compression test (UCS), as shown in Figure 2.1 (b). Eq. (2.2) and for the Poisson's ratio (ν) has a negative sign because the material will contract in the transverse direction when compressed or expand when stretched.

$$\nu = -\frac{\frac{\Delta R}{R}}{\frac{\Delta L}{L}} = -\frac{\varepsilon_l}{\varepsilon_a} \tag{2.2}$$

Where ε_l is the lateral strain, and ε_a is the axial strain.
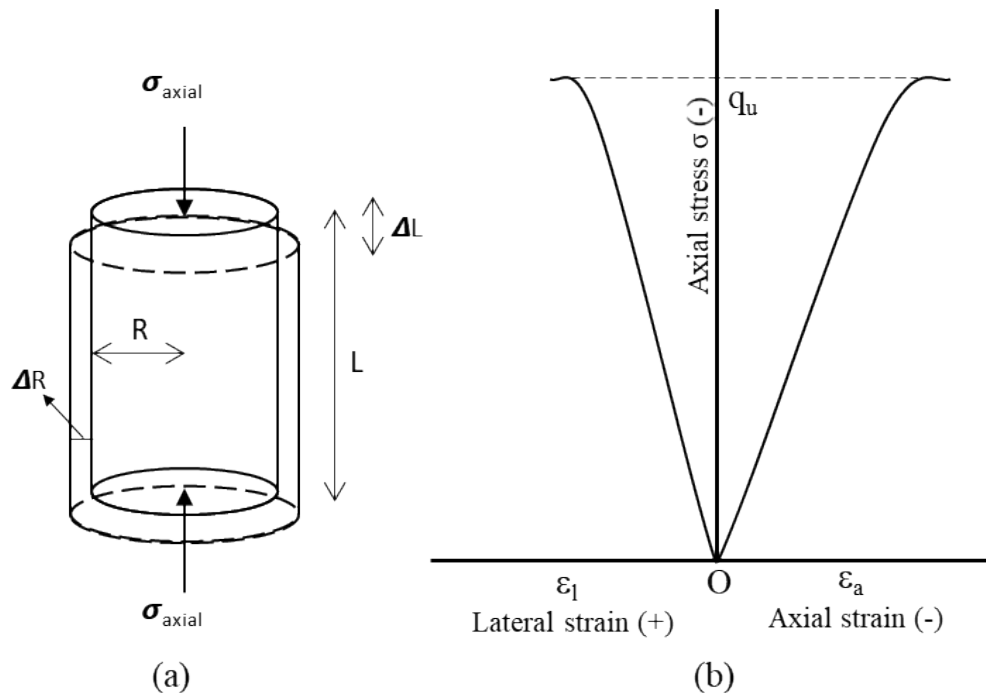
Figure 2.1 (a) Deformation of cylindrical specimen under uniaxial stress; (b) UCS results to illustrate method for calculating Poisson's ratio (from ASTM D7012, 2014)

2.2   Shear Strength

The shear strength of an intact rock developed along a potential rupture surface is described by two parameters: internal angle of friction (φ) and cohesion (c). When the cohesion becomes zero, i.e., when a planar, clean fracture occurs in rocks with no infilling material, the shear strength of rock is a function of friction angle. The shear strength of rock is typically described by the cohesion and the friction angle. The cohesion and friction angle are determined from a Mohr-Coulomb envelope given by Eq. (2.3) plotted against a series of Mohr's circles, as shown in Figure 2.2. The τ is the shear stress, c is the y-intercept, σ is the normal stress, and φ is the internal angle of friction. The Mohr's circle is defined as the locus of points that represent the state of stress on individual planes at all their orientations.

$$\tau = c + \sigma \, tan\varphi \tag{2.3}$$

Strength and stiffness of intact rocks depend on factors like the rock type, degree of weathering, and mineralogy. Depending up on these factors, the strength of intact rock can vary across different rocks, and sometimes within the same rock type if the rock is anisotropic. Table 2.2 shows the representative strengths for different types of intact rocks developed by Goodman, 1989.

7
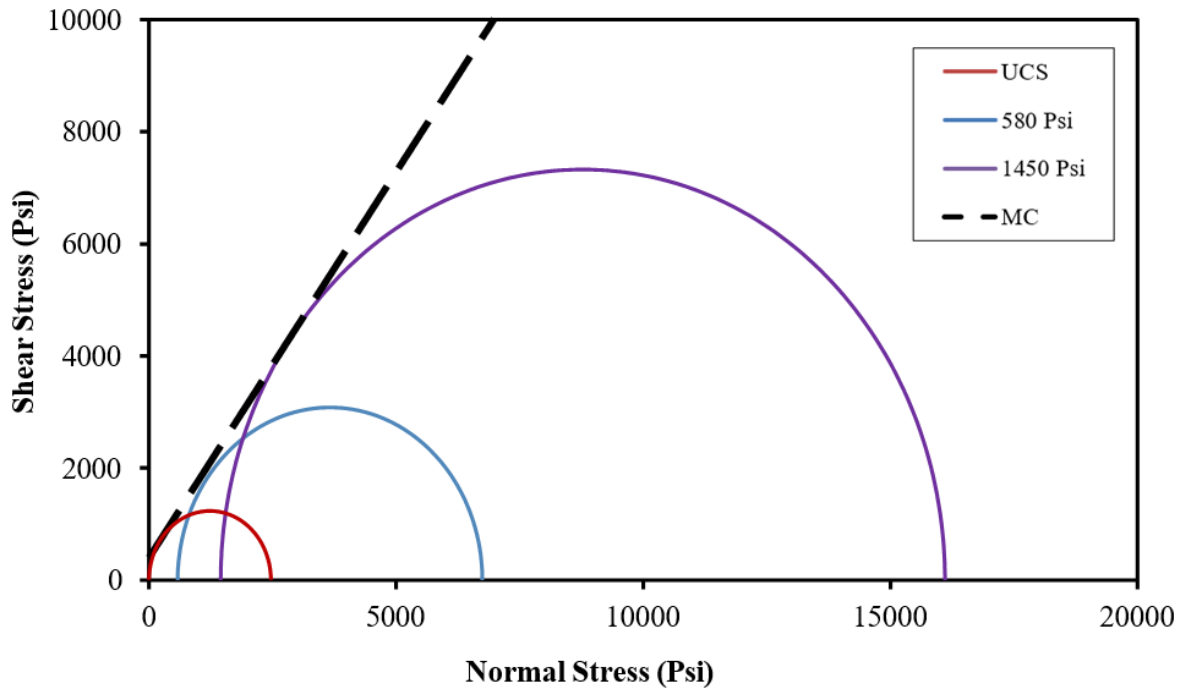
Figure 2.2 Plot of series of Mohr circle for the determination of cohesion and friction angle

Table 2.2 Representative strengths for different types of intact rocks (after Goodman, 1989)

Intact Rock Material	q_u (psi)	Ratio (q_u/q_t)
Berea Sandstone	10702.35	9137.394
Navajo sandstone	31038.13	3770.988
Tensleep sandstone	10502.2	-
Hackensack siltstone	17804.86	6019.077
Monticello Dam s.s. (greywacke)	11502.96	-
Solenhofen limestone	35509.65	8890.829
Bedford limestone	7401.289	4684.727
Tavernalle limestone	14203.57	3625.95
Oneota dolomite	12603.8	2857.249
Lockport dolomite	13102.73	4322.132
Flaming Gorge shale	5100.986	24308.37
Micaceous shale	10902.51	5264.879
Dworshak Dam gneiss (45° to foliation)	23506.31	3408.393
Quartz mica schist ($\perp$ schistosity)	8001.746	14561.82
Baraboo quartzite	46412.16	4220.606
Taconic marble	8992.356	7687.014
Cherokee marble	9703.042	5424.421
Nevada Test Site granite	20505.47	1754.96
Pikes Peak granite	32809.05	2755.722
Cedar City tonalite	14703.95	2306.104
Palisades diabase	34958.51	3060.302
Nevada Test Site basal	21506.23	1638.929
John Day basalt	51513.15	3553.431
Nevada Test Site tuff	1650.532	1450.38

**q_u is the unconfined compressive strength; q_t is the splitting tension strength

2.2.1 Cohesion (c)

The cohesion is an integral part of shear strength independent of inter-particle friction. The cohesion of rock is also known as inherent strength. Cohesion (c) is the y-intercept of the Mohr-Coulomb (MC) criterion given by Eq. (2.3). Table 2.3 shows the cohesion values of some typical rock types reported in the literature (Goodman, 1980). These cohesion values represent the specific rock types and can only be used as a reference while laboratory testing of individual rock types is recommended.

Table 2.3 Typical range of friction angle for a variety of rock types (Goodman, 1980)

Rock Type	Cohesion (psi)
Berea Sandstone	3945.034
Muddy Shale	5569.459
Stone Mt. Granite	3074.806
Georgia Marble	3074.806
Sioux Quartzite	10239.68
Indiana Limestone	971.7546

2.2.2 Friction Angle (φ)

The size and shape of particle grains exposed on a fracture surface during failure determine the friction angle of the rock. Granular rocks like sandstone and siltstone have different friction angle values depending on their grain size. Rocks can be categorized into three groups based on their grain sizes (fine, medium, and coarse). Fine-grained rocks like the schists and shales generally have low friction angles. The medium-grained rocks like sandstones, siltstones, and gneiss have medium friction angles; and the coarse-grained rocks like basalt, granite, limestone, and conglomerate have high friction angles. Table 2.4 shows the typical range of friction angles for various rock types (Barton, 1973; Jaeger and Cook, 1976; Willie and Norrish, 1996). Besides grain size, asperity, surface roughness, and shape of grains can also affect the friction angle. Hence, laboratory testing of rocks should be conducted to determine the friction angle.

Table 2.4 Typical range of friction angles for various rock types (Wyllie et al., 1996)

Rock Class	φ Range (Degree)	Typical Rock Type
Low Friction	20 to 27	Schists, Shale, Marl
Medium Friction	27 to 34	Sandstones, Siltstones, Gneiss, Chalk, Slate
High Friction	34 to 40	Basalt, Granite, Limestone, Conglomerate

2.3   Relationship between Stress-Strain and Failure Behavior

The stress-strain relationship describes the deformation of a material under loading. The point of failure in the stress-strain curve is the maximum strength of the rock. The stress-strain relationship for rocks is not linear and can be categorized into three distinct segments, as shown in Figure 2.3. Region 1 is non-linear due to the closure of the void spaces, region 2 shows approximately elastic behavior, and region 3 shows approximately plastic behavior until failure. The rock loses all shear strength at failure and shows either a brittle response or ductile response. The ductile or brittle response depends on whether the rock can undergo substantial permanent strain without macroscopic fracture (Paterson and Wong, 2004). The brittle failure responds in a mostly elastic fashion until failure, as shown in Figure 2.4 (a), and the ductile

failure responds elastically until the elastic limit then in plastic fashion until failure, as shown in Figure 2.4 (b).
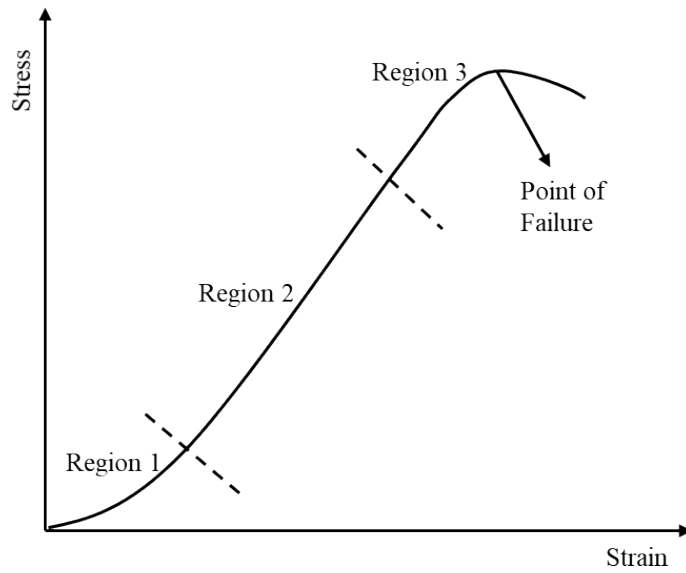
Figure 2.3 Generalized stress-strain curve for rock
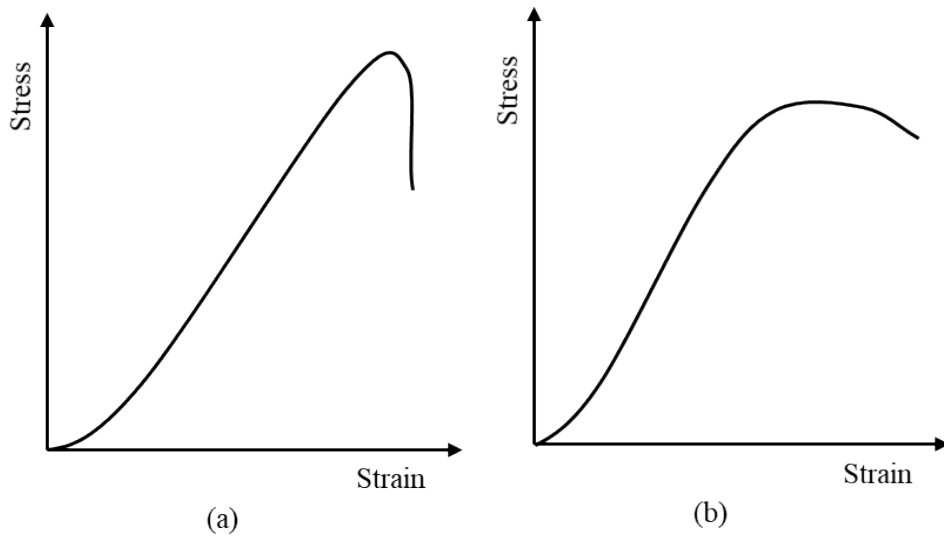
Figure 2.4 Failure response (a) brittle and (b) ductile responses of rocks
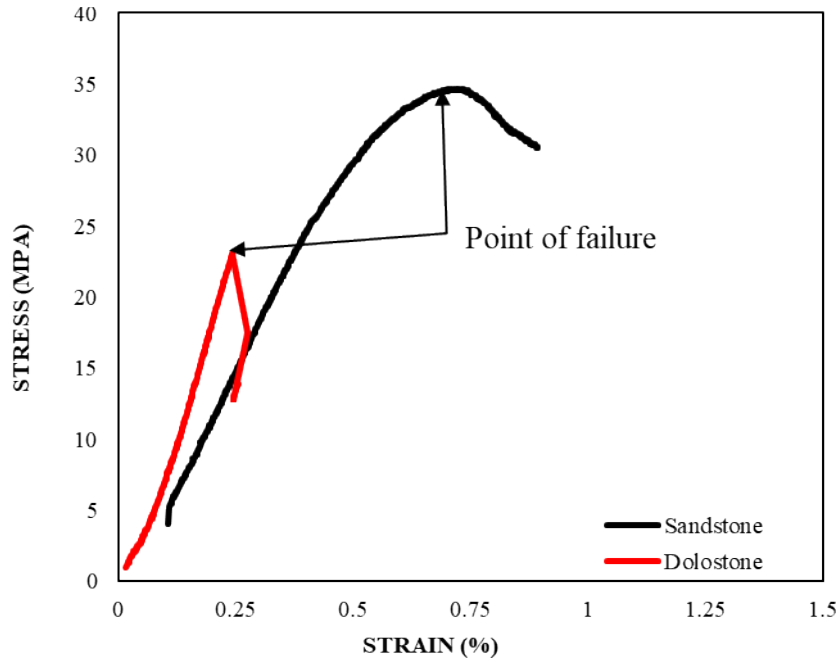
Figure 2.5 The stress-strain plot for sandstone and dolostone (lab measured)

The stress-strain plot for the sandstone in Figure 2.5 represents a ductile failure with a smooth curve after the point of failure while the dolostone shows a brittle failure with a sharp decrease in the stress-strain plot after the point of failure.

2.3.1 Failure Modes

The failure behavior of rock depends on the inherent rock materials, rock types, loading conditions, confining pressure, and discontinuities. The mechanism of failure in rocks and failure modes have been studied and documented (Tien, Kuo, and Juang, 2006; Wong and Baud, 2012; Xie et al., 2011).

Depending upon the bedding angle of the parent rock and applied confinement, there are four failure modes in transversely isotropic rocks, as shown in Figure 2.6: a) sliding failure across discontinuities, b) sliding failure along discontinuities, c) tensile fracture across discontinuities, and d) tensile splitting along discontinuities. The UCS tests on rocks with 0-, 15-, 30-, and 90-degree bedding angles exhibit tensile failures; whereas, with the application of the confining pressure, rocks with all bedding angles exhibit sliding failure (Tien, Kuo, and Juang, 2006). In the case of anisotropic rocks like shales, failure occurs by tensile splitting at low confinement and shear failure occurs at higher confinement, so the failure mode differs with confining pressure (Ambrose et al., 2014).

(a) Sliding failure across discontinuities   (b) Sliding failure along discontinuities

(c) Tensile failure across discontinuities   (d) Tensile failure across discontinuities

Figure 2.6 Different failure modes observed in tested samples

2.4 Failure Criteria Overview

The rock failure criterion describes the shear strength of rock under different normal stresses. A failure criterion, either linear or nonlinear, describes the maximum shear stress at maximum normal stress (σ_n) at which the rock will fail. The failure behavior depends upon the rock type, confinement applied, and discontinuities present. A discontinuity of a rock mass largely governs the failure behavior. Some other principal factors are mineral composition, bedding, water content, and state of stress in the rock mass. Rock failure criteria can be classified as isotropic or anisotropic depending on their application on rocks that exhibit anisotropic behavior or not. In the case of anisotropic rocks like shale, Ambrose et al. (2014),

from the computed tomography (CT) scans, reported that shales at bedding angles of 0º to 10º and at 90º show tensile failure, shales at 45º to 75º show shear failure along the plane of weakness, and shales between 15º and 30º show transitional failure, i.e., mixed failure mode of tensile and shear. Similar findings were reported by Tien et al. (2006) for reconstituted argillaceous rocks under unconfined conditions.

The failure mode is also found to be dependent on confining pressure as most UCS showed brittle failure, and as the confinement is increased, the failure mode gradually changed to ductile failure. Table 2.5 summarizes the classification of anisotropic failure criteria, as summarized by Deveau et al. (1998) and updated by Ambrose et al. (2014).

Table 2.5 Classification of anisotropic failure criteria (Deveau et al., 1998; Ambrose et al., 2014)

Continuous Criteria		Discontinuous Criteria
Mathematical Approach	**Empirical Approach**	
Von Mises (1928) Hill (1984) Olszak and Urbanowicz (1956) Goldenblat (1962) Goldenblat and Kopnov (1966) Boehler and Sawczuk (1970, 1977) Tsai and Wu (1971) Pariseau (1968) Boehler (1975) Dafallas (1979, 1987) Allirot and Boehler (1979) Nova and Sacchi (1979) Nova (1980, 1986) Boehler and Raclin (1982) Raclin (1984) Kaar et al. (1989) Cazacu (195) Cazacu and Cristescu (1999) Kusabuka, Takeda and Kojo (1999) Pietruszczak and Mroz (2001) Lee and Pietruszczak (2007) Mroz and Maciejewski (2011)	Casagrande and Carrillo (1944) Jaeger Variable Shear (1960) Mclamore and Gray (1967) Ramamurthy, Rao, and Singh (1988) Ashour (1988) Zhao, Liu, and Qi (1992) Singh, et al. (1998) Tien and Kuo (2001) Tien, Kuo and Juang (2006) Tiwari and Rao (2007) Saroglou and Tsiambaos (2007a) Zhang and Zhu (2007) Lee, Pietruszczak and Choi (2012)	Jaeger (1960, 1964) Walsh and Brace (1964) Hoek (1964, 1983) Murrell (1965) Barron (1971) Ladanyi and Archambault (1972) Biemiawski (1974) Hoek and Brown (1980) Smith and Cheatham (1980a) Yoshinaka and Yamabe (1981) Duveau and Henry (1997) Pei (2008) Zhang (2009)

Many failure criteria have been proposed by researchers over the decades. The failure criteria discussed in this thesis are the Mohr-Coulomb (MC) and the Hoek-Brown (HB) failure criteria because of their wide acceptance in engineering practice, mainly due to their simplicity and the sheer volume of experimental data availability. The MC and HB are linear and nonlinear failure criteria, respectively.

2.4.1 Mohr-Coulomb (MC) Failure Criterion

The MC criterion is a linear failure criterion most widely used for quasi-brittle material like rocks. This criterion is commonly used in engineering practice because its material parameters have a clear physical meaning in terms of cohesion and internal angle of friction. This criterion assumes that failure is controlled by maximum shear stress, and the shear stress at failure depends on the normal stress. It also assumes that the intermediate principal stress (σ_2) does not affect the failure. The MC failure line is a straight line that best touches the Mohr circles, as shown in Figure 2.7.

The MC failure criterion can be written as a function of major and minor principal stresses or normal and shear stresses. MC can be plotted in the major and minor principal stress plane or in a normal and shear stress plane (Jaeger and Cook, 1979). The derivation of the MC failure criterion in a normal stress (σ) versus shear stress (τ) 2D plane is described by Eqs. (2.4), (2.5), and (2.6).
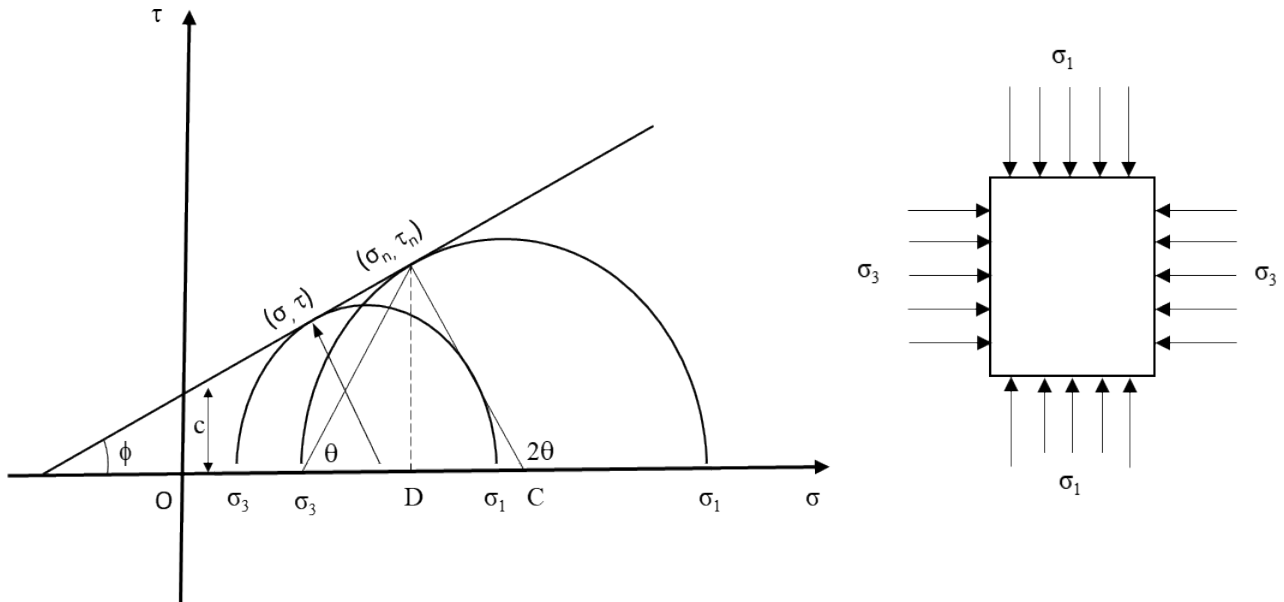
Figure 2.7 Illustration of Mohr-Coulomb failure criterion in 2D

From the Mohr circles we have,

$$\sigma = \sigma_m - \tau_m \, sin\varphi \tag{2.4}$$

$$\tau = \tau_m \, cos\varphi \tag{2.5}$$

Where, τ_m is the max shear; σ_m is the mean principal stress; σ_1 and σ_3 are major and minor principal stresses, respectively. The MC criterion can therefore be written as:

$$\tau_m = \sigma_m \, sin\varphi + c \, cos\varphi \tag{2.6}$$

In terms of the normal stress (σ_n) and shear stress (τ_n) on a failure plane (Figure 2.8) are given by Eq. (2.7) and (2.8), respectively.

$$\sigma_n = \frac{\sigma_1+\sigma_3}{2} + \frac{\sigma_1-\sigma_3}{2} \, cos\,(2\varphi) \tag{2.7}$$

$$\tau_n = \frac{\sigma_1 - \sigma_3}{2} \sin(2\varphi) \tag{2.8}$$
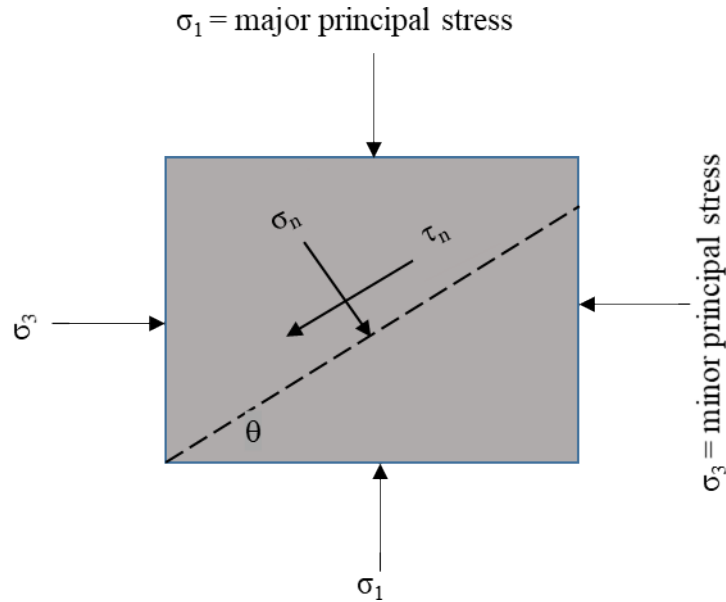
Figure 2.8 σ_n and τ_n are the normal and shear stresses acting on the failure plane

Table 2.6 Common modified Mohr-Coulomb diagrams (FHWA, 2017)

Diagram	Abscissa	Ordinate	MC Cohesion	MC Friction Angel
p-q diagram	$p = \frac{(\sigma_1 + \sigma_3)}{2}$	$q = \frac{(\sigma_1 - \sigma_3)}{2}$	$c = \frac{d}{cos\varphi}$	$\varphi = sin^{-1}(tan\theta)$
p-q diagram	$p = \frac{(\sigma_1 + 2\sigma_3)}{3}$	$q = (\sigma_1 - \sigma_3)$	$c = \frac{d(3 - sin\varphi)}{6cos\varphi}$	$\varphi = sin^{-1}\left(\frac{3}{1 + \frac{6}{tan\theta}}\right)$
$(\sigma_1 - \sigma_3) vs\ \sigma_3'$	$(\sigma_1 - \sigma_3)$	σ_3'	$c = \frac{d(1 - sin\varphi)}{2cos\varphi}$	$\varphi = sin^{-1}\left(\frac{1}{1 + \frac{2}{tan\theta}}\right)$
$\sigma_1'\ vs\ \sigma_3'$	σ_1'	σ_3'	$c = \frac{d(1 - sin\varphi)}{2cos\phi}$	$\varphi = sin^{-1}\left(\frac{tan\theta - 1}{tan\theta + 1}\right)$

$d\ and\ \theta$ are the intercept and slope of the failure envelope

2.4.2 Hoek-Brown (HB) Failure Criterion

Dr. Evert Hoek and Dr. Tom Brown introduced the HB failure criterion in 1980. HB is a nonlinear failure criterion, and in the case of full Mohr circle resembles a parabola. This criterion was derived from the brittle fracture criterion of intact and jointed rock mass (Griffith, 1924). Hoek focused on rock fracture propagation and failure of rock samples following fracture initiation in the compression stress field, whereas Griffith's theory predicted failure strength in the tensile stress field.

The HB criterion given by Eq. (2.9) is based on the major principal stress (σ1) and minor principal stress (σ3) at failure and is the function of uniaxial compressive strength (σci), the rock mass constant mb, and HB fitting coefficients a and s, which depend upon the characteristics of the rock mass (Hoek and Brown, 1980). This criterion assumes the rock isotropic and does not consider tensile failure, i.e., neglects the value of confining stress less than 0.

The rock material constants *a*, *s*, and *mb* can be calculated using Eqs. (2.10), (2.11), and (2.12), respectively, based on the geological strength index (GSI) and disturbance factor (D). The *mb* constant for a rock mass is also related to the constant *mi* for an intact rock.

$$\sigma_1 = \sigma_3 + \sigma_{ci} \sqrt[a]{m_b \frac{\sigma_3}{\sigma_{ci}} + s} \tag{2.9}$$

$$a = \frac{1}{2} + \frac{1}{6} \left(e^{\frac{-GSI}{15}} - e^{\frac{-20}{3}} \right) \tag{2.10}$$

$$s = exp \left(\frac{GSI-100}{9-3D} \right) \tag{2.11}$$

$$m_b = m_i \exp\left(\frac{GSI - 100}{28 - 14D} \right) \tag{2.12}$$

The GSI can be estimated directly from the rock mass rating (RMR), and the D factor depends on the degree of disturbance that the rock suffers during blast damage and stress relaxation. The generalized HB criterion Eq. (2.13) for an intact rock can be derived by substituting the s = 1 and a = 0.5.

(a) Material Constant mi

Material constant (*mi*) is one of the three input parameters required to describe the HB- failure criterion. It can be estimated from triaxial compressive strength results, or the reference Table 2.7 provided by Hoek and Brown (1980). A poor prediction equation between lithology and *mi* values was observed in the analysis of the existing database. The statistical analysis of the triaxial and tensile tests is the most accurate method for determining *mi* values (Read and Richard, 2011).

$$\sigma_1 = \sigma_3 + \sqrt{m\sigma_{ci}\sigma_3 + s\sigma_{ci}^2} \tag{2.13}$$

Table 2.7 Estimated values of the constant mi in parenthesis (Hoek and Brown, 1980)

Rock Type	Class	Group	Texture			
			Coarse	Medium	Fine	Very Fine
Sedimentary	Clastic		Conglomerate (22)	Sandstone (19)	Siltstone (9)	Claystone (4)
			Greywacke (18)			
	Non-Clastic	Organic	Chalk (7)			
			Coal (8-21)			
		Carbonate	Breccia (20)	Sparitic Limestone (10)	Micritic Limestone (8)	
		Chemical		Gypstone (16)	Anhydrite (13)	
Metamorphic	Non-Foliated		Marble (9)	Hornfels (19)	Quartzite (24)	
	Slightly Foliated		Migmatite (30)	Amphibolite (25-31)	Mylonites (6)	
	Foliated		Gneiss (33)	Schists (4-8)	Phyllites (10)	Slate (9)
Rock Type	Class	Group	Texture			
			Coarse	Medium	Fine	Very Fine
Igneous	Light		Granite (33)		Rhyolite (16)	Obsidian (19)
			Granodiorite (30)		Dacite (17)	
			Diorite (28)		Andesite (19)	
	Dark		Gabbro (27)	Dolerite (19)	Basalt (17)	
			Norite (22)			
	Extrusive Pyroclastic		Agglomerate (20)	Breccia (18)	Tuff (15)	

(b) Geological Strength Index (GSI)

The GSI proposed by Hoek and Brown (1997) uses field observation, the blockiness of rock mass, and surface joint characteristics to determine the rock mass classification. There are several methods used for the rock mass classification: rock quality designation (RQD) (Deere, 1964), rock structure rating (Wickham et al., 1972, 1974), rock mass rating (Bieniawski, 1973, 1976, 1989), Q-System (Barton et al., 1974) and rock mass index (Palmstrom 1995, 1996 a, b). The GSI differs from other classification systems as it relies on the visual inspection of rock mass structure and the condition of the discontinuity surface without involving any quantitative measurements.

Hoek and Brown proposed using a range of GSI values instead of an absolute number as it is subjective to the observer's differentiation between the surface condition and structure type. Figure 2.9 (a) shows the GSI table (Hoek and Brown, 1997), and Figure 2.9 (b) shows the Hoek and Marinos (2000) GSI chart. Hoek and Marinos (2000) introduce laminated/sheared as a new structure type in addition to the intact or massive, blocky, very blocky, blocky/distributed, and disintegrated structure types proposed by Hoek and Brown (1997). The laminated/sheared represents lack of blockiness, which may be caused by closely spaced shear planes. Hoek et al. (2013) further introduced a revised GSI chart, which can be used to quantify the GSI by joint condition and RQD, as shown in Figure 2.10. As GSI is recommended as a range instead of a specific value from the lithology, structure, and observed discontinuities, the quantification using joint condition (JCond89) and RQD by Eq. (2.14) is more suitable.

$$GSI = 1.5 JCond_{89} + \frac{RQD}{2} \qquad (2.14)$$

(a)   (b)

Figure 2.9 Geological strength index table for jointed rock (a) Hoek and Brown (1997),
(b) Hoek and Marinos (2000)

GEOLOGICAL STRENGTH INDEX (GSI) FOR JOINTED BLOCKY ROCK MASSES

From the lithology, structure and observed discontinuity surface conditions, estimate the average GSI based on the descriptions in the row and column headings. Alternatively, from logged RQD values and Joint Condition ratings (from Bieniawski, 1989), estimate $GSI = 1.5\,JCond_{89} + RQD/2$ based on the scales attached to the chart axes.

For intact or massive rock with GSI > 75, check for brittle spalling potential. For sparsely jointed rock with GSI > 75, failure will be controlled by structurally defined blocks or wedges. The Hoek-Brown criterion should not be used for either of these conditions.

This chart applies to tunnels of about 10 m span and slopes < 20 m high. For larger caverns and slopes consider reducing GSI to account for decreasing block interlocking.

SURFACE CONDITIONS

VERY GOOD — Very rough, fresh unweathered surfaces

GOOD — Rough, slightly weathered, iron-stained surfaces

FAIR — Smooth, moderately weathered and altered surfaces

POOR — Slickensided, highly weathered surfaces with compact coatings or fillings of angular fragments

VERY POOR — Slickensided, highly weathered surfaces with soft clay coatings or infillings

STRUCTURE   DECREASING SURFACE QUALITY ⇨

BLOCKY - well interlocked undisturbed rock mass made up of cubical blocks formed by three sets of intersecting joints

VERY BLOCKY - interlocked, partially disturbed rock mass, multi-faceted angular blocks formed by 4 or more joint sets

BLOCKY, DISTURBED/SEAMY - folded with angular blocks formed by many intersecting joint sets. Persistence of bedding planes or schistosity

DISINTEGRATED - poorly inter-locked, heavily broken rock mass with mixture of angular and rounded rock pieces

DECREASING INTERLOCKING

(Chart contour values: 80, 70, 60, 50, 40, 30, 20, 10)

RQD/2 axis (right): 40, 35, 30, 25, 20, 15, 10, 5, 0

$1.5\,JCond_{89}$ axis (bottom): 45, 40, 35, 30, 25, 20, 15, 10, 5, 0

Figure 2.10 Quantification of GSI from joint condition and RQD (Hoek et al., 2013)

(c) Disturbance Factor (D)

The disturbance factor refers to the degree of disturbance caused by the blast damage and stress relaxation on the rock mass and is measured in a range from 0 to 1, where 0 is for undisturbed in-situ rock masses and 1 is for very disturbed rock masses (Hoek and Brown, 1997). As it is difficult to reach a very high

disturbance factor, Hoek and Brown (2019) emphasized that the disturbance factor should be applied to the limited thickness and not the whole rock mass.

It has been reported that the use of disturbance factor to the entire rock mass in which excavation is conducted leads to an extremely conservative and inappropriate design. Therefore, the common thickness for disturbed zones is around 1.64 to 3.28 feet. Figure 2.11 shows the determination of the disturbance factor proposed by Hoek and Brown (1997) based on the description of the rock mass after blasting. The study from Lorig and Varona (2000), Sonmez and Ulusay (1999), and Cheng and Liu (1990) reported that the disturbance factor is influenced by many factors and cannot be precisely quantified; however, after the study by Kim et al. (2015), it was found that the factor D can be found quantitatively by measuring the speed of acoustic wave in rock mass as the blasting causes loosening and damaging of intact rock.

Appearance of rock mass	Description of rock mass	Suggested value of D
	Excellent quality controlled blasting or excavation by Tunnel Boring Machine results in minimal disturbance to the confined rock mass surrounding a tunnel.	D = 0
	Mechanical or hand excavation in poor quality rock masses (no blasting) results in minimal disturbance to the surrounding rock mass.	D = 0
	Where squeezing problems result in significant floor heave, disturbance can be severe unless a temporary invert, as shown in the photograph, is placed.	D = 0.5 No invert
	Very poor quality blasting in a hard rock tunnel results in severe local damage, extending 2 or 3 m, in the surrounding rock mass.	D = 0.8
	Small scale blasting in civil engineering slopes results in modest rock mass damage, particularly if controlled blasting is used as shown on the left hand side of the photograph. However, stress relief results in some disturbance.	D = 0.7 Good blasting D = 1.0 Poor blasting
	Very large open pit mine slopes suffer significant disturbance due to heavy production blasting and also due to stress relief from overburden removal. In some softer rocks excavation can be carried out by ripping and dozing and the degree of damage to the slopes is less.	D = 1.0 Production blasting D = 0.7 Mechanical excavation

Figure 2.11 Disturbance factor estimation (Hoek and Brown, 1997)

2.5 Current Site Investigation and Methods for Estimating Rock Properties

There are various methods for site investigation and estimation of rock properties. Agencies like the American Association of State Highway and Transportation Officials (AASHTO), the American Society of Testing and Materials (ASTM), the Federal Highway Administration (FHWA), and other private organizations have developed various standard methods of practice for estimation of rock properties. Different states follow one or more of these agencies in developing a geotechnical manual for practice. Not all states have a geotechnical manual prepared. This section will have a description of all agencies and states that have standards for site investigation and estimation of rock properties.

2.5.1 The American Association of State Highway and Transportation Officials (AASHTO)

AASHTO has a standard practice for conducting a geotechnical subsurface investigation, known as AASHTO R13, and a standard method of test for diamond core drilling for site investigation, known as AASHTO T225. These standards are widely followed by the states when preparing a geotechnical manual. The description of these standards is discussed below.

2.5.1.1 AASHTO R13

This standard practice deals with investigation, sampling, testing, and evaluation of subsurface conditions to provide the required information for a better understanding of the underlying soil and bedrock properties. The first step in any subsurface investigation process is the reconnaissance of the project area. This involves topographic maps, air photos, satellite imagery, geologic maps, statewide and countrywide soil surveys, mineral resource surveys, information from landowners, local well drillers, and representatives of the local construction industry.

The second step is to prepare an exploration plan. This involves a review of available data on geology history, rock, soil, and groundwater conditions followed by a field reconnaissance for identification of surficial geologic conditions, mapping of stratigraphic exposures and outcrops, and examination of existing structures. This is followed by the on-site investigation of the surface and subsurface materials by geophysical surveys, borings, or test pits to recover a representative disturbed sample for laboratory classification and undisturbed sample for engineering properties pertinent to the investigation.

The selection of the equipment and procedures for use in exploration depends largely on subsurface material, the depth of exploration, the nature of the terrain, and the intended use of data. The geophysical investigations method using ground-penetrating radar can be used in defining soil and rock layers in the depth range of 0.98 to 32.8 feet. AASHTO recommends that the exploration records should be kept in a systematic manner, including a description of each test hole, boring, test pit, or geophysical test site. The identification of rock materials should be based on ASTM C119 or ASTM C294.

2.5.1.2 AASHTO T225

This standard deals with the procedure for diamond core drilling designed to secure intact samples of rocks. The equipment required are a rotary drilling machine for providing a rotary motion, water or drilling mud pump to deliver sufficient drilling fluid volume and pressure, and core barrels as required. The single-tube core barrel is generally not preferred, and a double-tube core barrel is considered as a minimum standard. The sizes of core barrels suggested by AASHTO are shown in Table 2.8 and the standard sizes of casing are shown in Table 2.9.

Table 2.8 Standard sizes of core barrels (AASHTO)

Size	Hole Diameter		Core Diameter	
	In.	mm	In.	mm
EWX, EWM	1.5	38.1	0.812	20.6
AWX, AWM	1.957	49.2	1.375	30.2
BWX, BWM	2.375	60.3	1.625	41.3
NWX, NWM	3	76.2	2.125	54
69.9 by 98.4 mm	3.875	98.4	2.687	68.3
102 by 140 mm	5.5	140	3.937	100
152 by 197 mm	7.75	197	5.937	151

Table 2.9 Standard sizes of casing (AASHTO)

Size	Outside Diameter		Inside Diameter		Will fit hole drilled by:
	In.	mm	In.	mm	
EX	1.8125	46.0	1.5	38.1	AWX, AWM
AX	2.25	57.2	1.906	48.4	BWX, BWM
BX	2.875	73.0	2.187	60.3	NWX, NWM
NX	3.5	88.9	3.0	76.2	by 98.4 mm

2.5.2 The Federal Highway Administration (FHWA)

The Geotechnical Site Characterization, Geotechnical Engineering Circular No. 5 (2017), describes various data sources to be considered during the desk study and field reconnaissance along with their uses and sources, as shown in Table 2.10.

Table 2.10 Useful maps and data sources for existing information (FHWA, 2017)

Map/Data Source	Use	Source(s)
USGS Topographic Maps	•Topography •Crude recent and historical land use	USGS
Aerial Photographs	•Historical and recent land use & vegetation •Structure, roadway, stream locations, etc. •Identification of potential hazards	Google EarthTM, Google MapsTM, NAIP, Other public and commercial sources
Physiographic Landforms	•General soil/rock type	USGS, state agencies
Surficial geology	•General soil/rock type at surface	USGS, state agencies
Bedrock geology	•General rock type, age at depth	USGS, state agencies
Bedrock Depth Contours	•Crude bedrock depths	State agencies
Soil Survey Maps and Data	•Map scale characterization of general soil types and characteristics •Quantitative classification data •Identification of problematic soils	NRCS, state agencies
Fault Maps	• Identification of potential hazards	USGS, state agencies
Flood inundation maps	•Identification of potential flooding and related hazards (e.g., scour)	FEMA, USGS, USACE, state agencies
Stream gage records	•Identification of potential hazards (e.g., scour)	USGS National Water Information System
Climatic data	•Historical climate records for temperature, precipitation, and stream gage records	NOAA National Centers for Environmental Information
Map/Data Source	**Use**	**Source(s)**
Mine location/type	•Aggregate source •Rock type	Federal and state agencies
Sinkhole/karst maps	•Identify karst hazard	Federal and state agencies
Natural Hazards Information	•Identification of potential hazards	Federal and state agencies, http://www.usgs.gov/hazards/
Landfill/Superfund Sites Maps	•Identification of potential hazards	Federal and state agencies
Impaired Streams and Waterways Maps	•Identification of potential hazards or special environmental requirements	Federal and state agencies
Hydrologic maps	•Identification of springs and other groundwater hazards	Federal and state agencies
Utility maps	•Selecting investigation locations	Public and private sources
Well maps and well logs	•Indications of groundwater conditions	State agencies
Sanborn Fire Insurance Maps	•Historical land use •Identification of potential environmental hazards	Library of Congress, state & university libraries, http://www.loc.gov/collections/sanborn-maps/

For the classification of rocks, grain-size, weathering, rock color, and relative rock strength are generally used parameters. The grain size is relevant based on the type of rock as sedimentary rocks have different grain sizes and shapes when compared with igneous rock. FHWA provides the criteria for defining rock grain size, shown in Table 2.11, and rock color notation based on the 1977 rock color chart from the Geologic Society of London, shown in Table 2.11. In terms of relative rock strength, the classification criteria are shown in Table 2.12. For the classification of the rock mass, FHWA recommends three classification systems: alternative rock mass classification system, rock mass rating (RMR) classification system, and geological strength index (GSI) classification system.

Table 2.11 Criteria for defining rock grain size (FHWA, 2017)

Grain Size	Description	Criteria
< 0.003 in. (< 0.075 mm)	Very Fine-Grained	Cannot be distinguished by unaided eye. Few to no mineral grains are visible with a hand lens
0.003–0.02in. (0.075 – 0.425 mm)	Fine-Grained	Few crystal boundaries are visible; grains can be distinguished with difficulty by the unaided eye but can be somewhat distinguished by hand lens
0.02 – 0.8 in. (0.425 – 2 mm)	Medium-Grained	Most crystal boundaries are visible; grains distinguishable by eye and with hand lens
0.8 – 2 in. (2 – 4.75 mm)	Coarse-Grained	Crystal boundaries are visible; grains distinguishable with naked eye
2 in. (> 4.75 mm)	Very Coarse-Grained	Crystal boundaries are clearly visible; grains are distinguishable with the naked eye

Table 2.12 Rock color descriptor (after Geologic Society of London, 1977)

Grade	Description	Field Identification	Approx. Compressive Strength (MPa)
R0	Extremely Weak Rock	Specimen can be indented by thumbnail.	0.24 –1.03
R1	Very Weak Rock	Specimen crumbles under sharp blow with point of geological hammer and can be peeled with a pocketknife.	1.03-5
R2	Weak Rock	Shallow cuts or scrapes can be made in a specimen with a pocketknife. A firm blow with a geological hammer creates shallow indents.	5-24.14
R3	Medium Strong Rock	Specimen cannot be scraped or cut with a pocketknife. Specimen can be fractured with a single firm blow with a geological hammer point.	24.14-50
R4	Strong Rock	Specimen requires more than one firm blow of the point of a geological hammer to fracture.	50.00-100.00
R5	Very Strong Rock	Specimen requires many firm blows from the hammer end of a geological hammer to fracture.	100-250
R6	Extremely Strong Rock	Specimen can only be chipped with firm blows from the hammer end of a geological hammer.	> 250

2.5.3 Sabatini et al., 2002

Sabatini et al. (2002) selected the southwest portion of the Piedmont Province in west-central Alabama to discuss the index properties, deformation modulus, and strength properties of the rocks. Recommendations on the selection of appropriate design values are provided based on the field and laboratory data. The boring methods for rocks are summarized in Table 2.13.

Table 2.13 Rock core drilling methods (Sabatini et al., 2002)

Method	Procedure	Type of Sample	Applications	Limitations/Remarks
Rotary Core of Rock (ASTM D 2113; AASHTO T225)	Outer tube with diamond bit on lower end rotated to cut annular hole in rock; core protected by stationary inner tube, cuttings flushed upward by drill fluid.	Rock cylinder 0.87- to 3.94-inch wide and as long as 9.84 ft, depending on rock soundness. Standard coring size is 2.13-inch diameter.	To obtain continuous core in sound rock (percent of core recovered depends on fractures, rock variability, equipment, and driller skill)	Core lost in fracture or variable rock; blockage prevents drilling in badly fractured rock; dip of bedding and joint evident but not strike
Rotary coring of rock, wire line	Same as ASTM D 2113, but core and stationary inner tube retrieved from outer core barrel by lifting device or "overshot" suspended on thin cable (wire line) through special large-diameter drill rods and outer core barrel	Rock cylinder 1.10- to 3.35-inch wide and 4.92- to 9.84-ft long	To recover core better in fractured rock, which has less tendency for caving during core removal; to obtain much faster cycle of core recovery and resumption of drilling in deep holes	Core lost in fracture or variable rock; blockage prevents drilling in badly fractured rock; dip of bedding and joint evident but not strike
Rotary coring of swelling clay, soft rock	Similar to rotary coring of rock; swelling core retained by third inner plastic liner	Soil cylinder 1.12- to 2.09-inch wide and 23.62- to 59.06-inch long encased in plastic tube	In soils and soft rocks that swell or disintegrate rapidly in air (protected by plastic tube)	Sample smaller; equipment more complex than other soil sampling techniques

The rock cores extracted from these methods are then tested in the laboratory for the estimation of various properties. Table 2.14 shows the list of tests, ASTM standards for these tests, a brief procedure, and their applications.

Table 2.14 Summary information on rock laboratory test methods (FHWA-IF-02-2002)

Test Category	ASTM Test Designation	Procedure	Applicable Rock Types	Applicable Rock Properties	Limitations / Remarks
Point Load Test	D 5731	Rock specimens in the form of core, cut blocks, or irregular lumps are broken by application of concentrated load through a pair of spherically truncated, conical platens.	Generally not appropriate for rock with uniaxial compressive strength less than 3626 psi	Provides an index of uniaxial compressive strength	Can be performed in the field with portable equipment or in the laboratory; in soft or weak rock, test results need to be adjusted to account for platen indentation
Compressive Strength	D 2938	A cylindrical rock specimen is placed in a loading apparatus and sheared under axial compression with no confinement until peak load and failure are obtained.	Intact rock core	Uniaxial compressive strength	Simplest and fastest test to evaluate rock strength; fissures or other anomalies will often cause premature failure
Direct Shear Strength	D 5607	A rock specimen is placed in the lower half of the shear box and encapsulated in either synthetic resin or mortar. The specimen must be positioned so that the line of shear force lies in the plane of discontinuity to be investigated. The specimen is then mounted in the upper shear box and normal load and shear force applied.	Used to assess peak and residual shear strength of discontinuity	Peak and residual shear strength	May need to perform in-situ direct shear test if design is controlled by potential slip along a discontinuity filled with very weak material
Durability	D 4644	Procedure is similar to that for unconfined compressive strength of intact rock. Lateral strains are also measured	Intact rock core	Modulus and Poisson's ratio	Modulus values (and Poisson's ratio) vary due to nonlinearity of stress-strain curve.
Strength-Deformation	D 3148	Dried fragments of rock are placed in a drum made of wire mesh that is partially submerged in distilled water. The drum is rotated, the sample dried, and the sample is weighed. After two cycles of rotating and drying, the weight loss and the shape of size of the remaining rock fragments are recorded.	Shale or other soft or weak rocks	Index of degradation potential of rock	

2.5.4 State Department of Transportation (DOT)

(1) Alabama

The Alabama Department of Transportation (ALDOT) has published a geotechnical manual for Alabama. There are three sections for planning geotechnical explorations, field exploration, and laboratory testing methods, and field exploration procedures and considerations. These guidelines are not exhaustive and only serve as an aid to the engineer in planning and executing geotechnical explorations.

a) Planning Geotechnical Explorations

A site review comprising the review of available data and field reconnaissance is conducted before formulating a geotechnical exploration plan. ALDOT recommends the use of the maintenance bureau's surveying and mapping section, interviews with local ALDOT division and district personnel, and Alabama Department Of Environmental Management (ADEM) data apart from the usual procedure to get a better knowledge of the local conditions. The field reconnaissance will provide relevant findings and observations, such as site hazards, rock outcrops, existing rock cut slopes, accessibility for fieldwork, and other unusual features pertinent to the project area. This information is vital for the preparation of the geotechnical exploration plan discussed in Table 2.15.

b) Field Exploration and Laboratory Testing Methods

The field sampling and testing methods for rock coring involve using a core barrel equipped with coring bits. The rock mass is cut through with the coring bits to recover continuous samples to evaluate bedrock characteristics. Qualitative and structural characteristics such as weathering, hardness, discontinuities, lithology, and formation can be obtained. The logging, marking, preserving, placing, packaging, and transportation of the rock cores should be in accordance with ASTM D 5079. Some minimum information such as size, type, and design of core barrel, length, recovery, and RQD of each core, rock lithology and structural description, and remarks concerning drilling time and character such as mechanical fractures should be noted during coring and logging.

Laboratory testing of the rock cores, such as uniaxial compressive strength, elastic modulus, and slake durability, determine the rock mass's strength, stiffness, and durability properties, respectively. The rock core preparation should follow ASTM D 4543 and uniaxial test ASTM D 7012.

c) Field Exploration Procedure and Considerations

The boring procedures are performed according to AASHTO T-306: Progression Auger Borings for Geotechnical Explorations. In the case of the SPT test, the termination criteria will be based on minimum penetration into bedrock or competent material (defined in terms of SPT N-value, RQD, material type, etc.) and not a target boring depth alone. The rock mass encountered during drilling will be classified according to RMR and GSI system.

Table 2.15 Summary of guidelines on boring frequency and depth (ALDOT, 2021)

Exploration Type	Boring Frequency Guidance	Boring Depth Guidance
Bridge Foundations	**General** — At least one boring per substructure (abutment/bent). At least two borings per substructure/ footing for footing widths >70 feet	Through unsuitable material and into competent material for foundation support, with competent material to be defined by the engineer for the project. For all projects, if a review of the available nearby geotechnical information suggests that compressible layers may be present underlying upper harder/denser layers, sufficient borings drilled deeper than outlined below should be advanced to characterize that possibility.
	Driven Piles — At least one boring within 50 feet of planned piles	Rock bearing piles: At least 10 feet into continuous (i.e., ≥95% recovery) bedrock
	Drilled Shafts — At least one boring within 20 feet of redundant shafts where bearing materials are variable. At least one boring at the shaft location per non-redundant shaft	Rock bearing: To at least 30 feet into bedrock for each boring, and with at least one boring per bent to at least 50 feet into bedrock; the bottom 30 feet of cored bedrock should have recovery ≥95% and RQD ≥50%
	Micro piles — Following guidance for shafts	Following guidance for rock bearing shafts
	Spread Footings — Boring at each corner for variable bearing conditions (such as on hillsides, over karst bedrock conditions, etc.)	Rock bearing: Extending below the bearing elevation to a depth of at least 2B

(2) Alaska

The Alaska Department of Transportation and Public Facilities (Alaska DOT&PF) in the Alaska Geological Field Investigations Guide (2007) provides a table for specifications and standards followed by the state to conduct the geotechnical field investigation. Table 2.16 shows the Alaska DOT&PF specification and standards table.

Table 2.16 Specifications and standards for geotechnical field investigation (Alaska DOT&PF, 2007)

SUBJECT	ASTM	AASHTO
Conducting Geotechnical Subsurface Investigations	-	R13
Decommissioning Geotechnical Exploratory Boreholes	-	R22-97
Diamond Core Drilling for Site Investigation	D 2113	T 225
Standard Guide to Site Characterization for Engineering, Design, and Construction Purposes	D 420	T 86
Preserving and Transporting Rock Core Samples	D 5079	-
Standard Guide for Field Logging of Subsurface Explorations of Soil and Rock	D 5434	-
Seismic Refraction Method for Subsurface Investigation	D 5777	-

(3) California

The California Department of Transportation's (Caltrans) Soil and Rock Logging, Classification, and Presentation Manual (2010) provides the department's practices and procedures for rock description, identification, classification, and preparation of boring logs. Caltrans follows a hybrid of the International Society of Rock Mechanics (ISRM) (1981) and the Bureau of Reclamation's Engineering Geology Field Manual (2001) for rock classification and description procedure. The description of the rocks based on the grain-size for crystalline igneous and metamorphic rocks are shown in Table 2.17; the bedding thickness or spacing-based description of sedimentary or bedded volcanic rocks are shown in Table 2.18. Caltrans' Geotechnical Manual divides the geotechnical investigations and refers to AASHTO Subsurface Exploration for the number, locations, and depths of exploratory borings.

Table 2.17 Grain-size for crystalline igneous and metamorphic rock (Caltrans, 2010)

Description	Average Crystal Size, S (Inch)
Very coarse-grained or pegmatite	$0.37 \leq S$
Coarse-grained	$0.19 < S \leq 0.37$
Medium-grained	$0.031 < S \leq 0.19$
Fine-grained	$0.004 < S \leq 0.031$
Aphanitic	$S \leq 0.004$

Table 2.18 Bedding spacing for sedimentary or bedded volcanic rocks (Caltrans, 2010)

Description	Thickness/Spacing, Sb
Massive	$9.84 \text{ ft} < Sb$
Very thickly bedded	$3.28 \text{ ft} < Sb \leq 9.84 \text{ ft}$
Thickly bedded	$3.22 \text{ ft} < Sb \leq 3.28 \text{ ft}$
Moderately bedded	$0.33 \text{ ft} < Sb \leq 0.98 \text{ inch}$
Thinly bedded	$0.98 \text{ inch} < Sb \leq 3.94 \text{ inch}$
Very thinly bedded	$0.24 \text{ inch} < Sb \leq 0.98 \text{ inch}$
Laminated	$Sb \leq 0.24 \text{ inch}$

(4) Colorado

The Colorado Department of Transportation (CDOT) mentions that the extent of rock coring during subsurface exploration should be at least 10 feet below the top of bedrock or the depths indicated in Table 2.19. Single-tube core barrels are not permitted and selection among double- or triple-tube core barrel depends upon the nature of rock and required quality of retrieved core. The boring designation, run number, run depths, recovery, and RQD should be in accordance with ASTM D 6032.

(5) Connecticut

The Connecticut Department of Transportation (CTDOT) limits the use of single-tube core barrel to non-critical application while considering the double-tube as the minimum standard for determining rock quality or strength. The rock cores are stored in wood or other durable material boxes, and the top of first core runs should start at the uppermost left corner of the box. Unlike Alaska DOT&PF, the mechanical breaks in the rock cores are marked with three parallel lines instead of two. The listing of the recovery and RQD for each core run is listed on the inside part of the lid. The preserving and transportation of the rock core samples should be in accordance with ASTM D 5079. The minimum boring depths required for different structures are shown in Table 2.20 as the subsurface exploration guideline.

Table 2.19 Minimum requirement for subsurface explorations (CDOT)

Structure	Exploration Frequency	Recommended Minimum Exploration Depth
Pavement Design	Refer to CDOT Pavement Design Manual	
Foundations	See AASHTO LRFD Bridge Design Specifications	
Retaining walls	See AASHTO LRFD Bridge Design Specifications.	
Culverts	See requirements for spread footings in AASHTO LRFD Bridge Design Specifications	
Sign Structures	Required at foundation locations where CDOT M&S Standards are not used or applicable. See AASHTO LRFD Specifications for Structural Supports for Highway Signs, Luminaires, and Traffic Signals	
Landslide Evaluation	3 m along center of slide and at least one boring above and below sliding area	3 m below slip surface or as needed to design proposed mitigation.
Cut Slopes	Every 61 to 183 m, depending on subsurface conditions and proposed construction.	3 m below base of cut and into stable soil/rock.
Embankments	Every 61 to 183 m, depending on subsurface conditions and proposed construction.	2.0 times the embankment height, or 1.5 m into bedrock, whichever occurs first. Test holes for wide embankments on compressible soils are required to characterize any compressible materials, regardless of embankment height.

Table 2.20 Subsurface exploration guideline (CTDOT)

Proposed Construction	Boring Layout	Minimum Boring Depth Requirements
Bridge Foundation	For substructures less than 30 m wide, provide a minimum of one boring. For substructures over 30 m wide provide a minimum of two borings. Additional borings should be provided in variable subsurface conditions	For spread footings, the borings should extend a minimum 10 m below the footing elevation. For deep foundations, the boring shall extend at least 6 m beyond the anticipated pile/shaft tip elevation or at least 3 m into bedrock
Retaining Walls	A minimum of one boring should be provided for each retaining wall. The maximum spacing between borings should generally not exceed 46 m. The location of borings should be staggered between the toe of the wall and area behind the wall to define the soil conditions at the foundation and within the backfill of the wall.	Use criteria for bridge borings.

The CTDOT follows the standard rock laboratory tests shown in Table 2.21.

Table 2.21 Common rock laboratory tests (CTDOT)

Test Category	Name of Test	ASTM Test Designation
Point Load Strength	Suggested method for evaluating point load strength	D 5731
Compressive Strength	Compressive strength of intact rock core specimen	D 2938
Direct Shear Strength	Laboratory direct shear strength tests for rock specimens under constant normal stress	D 5607
Durability	Slake durability of shales and similar weak rocks	D 4644
Strength Deformation	Elastic moduli of intact rock core specimens in uniaxial compression	D 3148

(6) Florida

McVay et al. (2019) used two datasets for the analysis of unconfined compression test (q_u), splitting tension test (q_t) and dry bulk density (r_{dt}), of the highly porous carbonate rocks of Florida. The report focuses on the rocks' identification, geological setting, laboratory tests, properties observed, strength envelope, and possible prediction equations. Strength envelopes, such as Hoek-Brown (1980, 1988, and 2018) and Johnston (1985), used high-strength rocks, and the results, when applied to the weaker carbonate rock formations of Florida, may need modification. The highly heterogeneous carbonate rocks of Florida show low RQD of less than 50%, as shown in Figure 2.12.

Figure 2.12 Rock cores from bore hole RC-3 (McVay et al., 2019)

a) Porosity

The carbonate rocks used are sedimentary rocks from shallow depths and Eocene Epoch that belongs to the tertiary period of the Cenozoic Era, which is only 58 million years old. This relatively young age and shallow depth of formation mean that the carbonate rocks exhibit high porosity up to 60%, with a median of 37%. The porosity determination was according to the AASHTO Method T-85 and ASTM Method D6473. Based on the results, a description of the rocks in terms of porosity is in Table 2.22.

31

Table 2.22 Proposed porosity description (McVay et al., 2019)

ϕ	0-15%	15-30%	30-45%	>45%
Bulk Porosity	Dense	Slightly Porous	Porous	Very Porous

b) Splitting Tension Strength Test (q$_t$)

This test indirectly evaluates the tensile strength of rocks. A continuous load at a constant rate until failure on a horizontally placed specimen is applied parallel to the core's axis by steel bearing plates. ASTM D-3967 is followed except for the higher L/D (length to diameter) ratio due to the nature of the rocks tested (FDOT 2018). The vugs' (holes/cavities) orientation and distribution affect the strength of the rock under this testing method. The type of splitting is often dictated by these vugs as the failure occurs through the weakest path. Due to the low RQD and low rock core recovery, not all the cores were of even diameter, and the cores with uneven diameter exhibited much lower q$_t$ than expected. The general prediction equation between the q$_t$ and the bulk dry unit weight is as shown in Eq. (2.15).

$$q_t = 26.64 \, e^{(0.191 \times \rho_d \times B)} \tag{2.15}$$

Where, q_t is the tensile strength, ρ_d is the dry bulk density, and B is the fitting coefficient

c) Unconfined Compression Test (UCS)

The unconfined compressive strength (UCS) q$_u$ is the most common strength parameter of the rock. The UCS tests are conducted per ASTM D-7012. The specimens in the UCS test are loaded axially so that the failure is observed within two to 15 minutes, and the pressure at failure is considered the q$_u$. The typical carbonate rock strengths from the literature are shown in Table 2.23.

Table 2.23 The typical carbonate rock strengths from the literature

Carbonate Rock	Qu (Psi)	Reference
Solenhofen Limestone	31908-36260	Jaeger and Cook, 1969; Goodman, 1989
Bedford Limestone	6962-7977	Goodman, 1989
Tavernelle Limestone	14504	Goodman, 1989
Malaysian Limestone	7977-15954	Nazir et al., 2013
Virginia Limestone	47863	Jaeger and Cook, 1969
Australian Limestone and Dolostone	5511-75420	Johnston, 1985
Limestone	6382-29008	Hoek and Brown, 1980
Dolostone	21756-72519	Hoek and Brown, 1980

Among the tested samples for the UCS, 80% resulted in a UCS value of less than 1305 Psi with a median value of 435 Psi. This UCS value is much less than the literature values shown in Table 2.23. The equation for the prediction equation of the UCS value with the bulk dry density is shown in Eq. (2.16)

$$q_u = 40.3 \, e^{(0.225 \times \rho_d \times B)} \tag{2.16}$$

Where, q_u is the UCS, ρ_d is the dry bulk density, and B is the fitting coefficient.

On comparing Equation 2.15 and 2.16, we observe the relationship between q_u and q_t by Eq. (2.17).

$$q_u = 0.51 \times q_t^{\frac{4}{3}}$$ (2.17)

d) Triaxial Compression Tests

The triaxial compression tests were conducted in the Hoek-cell. The confining pressure considered for the test was between 14.5 and 3002 Psi. The test results showed that the porous carbonate rocks showed 30% brittle rupture failures with volumetric dilation, whereas 42% of specimens experienced ductile failure with a contractive volumetric response. The remaining samples showed behavior in between and were described as transition failure. The confining pressure was related to the bulk dry unit weight to predict the type of failure, as shown in Table 2.24.

Table 2.24 Approximate behavior type table of Florida carbonate rocks

σ_3 (Psi)	Bulk Dry Unit Weight Range (slugs/ft3)					
	1.86-2.02	2.06-2.64	2.68-3.41	3.45-3.72	3.80-4.04	4.04-4.27
14.5	Transition	Transition	Brittle	Brittle	Brittle	Brittle
49.3	Ductile	Transition	Transition	Brittle	Brittle	Brittle
129.1	Ductile	Ductile	Transition	Transition	Brittle	Brittle
200.2	Ductile	Ductile	Ductile	Transition	Transition	Brittle
298.8	Ductile	Ductile	Ductile	Ductile	Transition	Transition
600.5-999.3	Ductile	Ductile	Ductile	Ductile	Ductile	Transition
999.3-3000.8	Ductile	Ductile	Ductile	Ductile	Ductile	Ductile

(7) Illinois

The Illinois Department of Transportation (ILDOT) in the Geotechnical Manual (2015) recommends using bedrock sounding using sufficient soundings or probes to delineate the profiles and cross-section of the bedrock surface. Preliminary soundings at intervals of approximately 200 feet can be done to determine if rock will be encountered at an elevation above the proposed depth. If preliminary soundings show the possibility of bedrock, additional soundings at 49.2-ft intervals are done.

ILDOT has a standard rock core log form that should be typewritten and contain the physical properties and arrangement of the rock layers in full description. The bore log should indicate core recovery ratio, RQD, the average rate of time per foot, and other laboratory tests plotted on the vertical scale that allows logging 19.7 feet of depth in 4.9-ft increments. For the compressive strength of the rocks, ILDOT recommends testing according to ASTM D 7012 at the field moisture conditions as departmental experience noted moisture has significant effect upon the indicated strength.

(8) Indiana

The Indiana Department of Transportation (INDOT) Geotechnical Design Manual prohibits rock coring to start or end in weathered bedrock, such as weathered shale and limestone, or in coal seams unless absolutely necessary. Recovery and RQD should be calculated and recorded before transporting the rock cores for storage and testing. A minimum of 9.84 feet into the rock is required at each substructure with a minimum recovery of 75% and a minimum RQD of 50%. If the required recovery and RQD is not obtained in the first 9.84 feet, an additional 4.92-ft coring should be completed. If there are layers of soft

materials, voids in the cored rock, or other geological uncertainties, an additional 9.84-ft coring should be done.

The rock coring should be done with 2-inch core barrels, double or triple-tube, with diamond core bits of NX, NWG, or NWPAM sizes. The maximum allowable run for the core barrel is 4.92 feet. In some special cases, wireline coring is permitted with pre-approved authorization from the INDOT Geotechnical Engineering division. Shale and other non-durable sedimentary rock cores should be wrapped in aluminum of plastic foil to prevent in situ moisture content.

(9) Kansas

The Kansas Department of Transportation (KDOT) Geotechnical Manual (2007) recommends using core barrels with diamond or tungsten-carbide tipped bits for rock coring. The single-tube core barrel results in poor recovery rate in limestone, hence double- or triple-tube core barrels are recommended. The double-tube barrel used in accordance with ASTM D 2113 results in desired core recovery in most rock masses, whereas the triple-tube barrel is best in cases of fractured and poor quality rocks.

KDOT recommends obtaining rock cores to a depth where predicted stress from foundation loading is less than 10% of the original overburden pressure or until a minimum of 9.84 feet of competent rock is cored. If the data for predicting foundation stress are not available, the boring is extended until at least 29.52 feet of bedrock is encountered, and the rock core samples are preserved and transported in accordance with ASTM D 5079. In Kansas, only sedimentary rocks are encountered within practical depths for foundations whose fundamental characteristics are bedding. These bedding thickness and splitting characteristics impact the geotechnical characteristics of the rocks. The bedding descriptors and splitting descriptors of the sedimentary rocks are shown in Tables 2.25 and 2.26, respectively.

Table 2.25 Bedding descriptors (KDOT, 2007)

Bedding Thickness	Description
>3.28 ft	Very Thick
0.98 ft-3.28 ft	Thick Bedded
0.33 ft-0.98 ft	Medium
0.98 ft-0.33 ft	Thin
0.35 inch-0.98 inch	Very Thin
0.35 inch	Laminated

Table 2.26 Splitting descriptors (KDOT, 2007)

Splitting Thickness	Description
>3.28 ft	Massive
0.98 ft-3.28 ft	Blocky
0.33 ft-0.98 ft	Slabby

(10) Kentucky

The Kentucky Transportation Cabinet's Geotechnical Guidance Manual (2005) follows AASHTO T 225: Standard Method of Diamond Core Drilling for Site Investigation for rock core drilling. The use of wire line drilling equipment is permitted. In the case of soft materials, if the recovery is less than 85%, changes in the type of barrel or drilling procedure or a change to soil sampling is made. If consecutive corings produce less than 85% recovery, they are not accepted and shall be re-cored from adjacent borings. Laboratory testing of rock samples for geotechnical purposes include the jar slake (JS) and slake

durability index (SDI) and unconfined compression test (UCS). The testing frequency shall be one test for each 4.92 feet in shale and 9.84 feet in sandstone.

(11) Michigan

The Michigan Department of Transportation (MDOT) Geotechnical Manual (2019) rock core sampling section recommends the use of double- or triple-tube core barrels for all MDOT projects. Individual core runs should not exceed a 4.92-ft length. Use of wireline recovery methods can be adopted if the core lengths are longer than 9.84 feet. ASTM D 2113 should be followed when labeling, preserving, and transporting the rock cores. Rock core recovery and RQD must be mentioned in the individual core boxes. Core orientation is vital as the discontinuities govern the strength of the rock; hence, specialized core barrels that scribe a reference mark on the side of core is preferred, and the degree of rock fractures based on the spacing of the fractures is given in Table 2.27.

Table 2.27 Terms to describe degree of rock fractures (MDOT, 2019)

Description	Spacing
Unfractured	>9.84 ft
Intact	3.28 ft-9.84 ft
Slightly Fractured	0.98 ft-3.28 ft
Moderately Fractured	0.33 ft-0.98 ft
Fractured	1.97 inch-3.94 inch
Highly Fractured	<1.974 inch

(12) Montana

The Montana Department of Transportation (MDT) Geotechnical Manual (2008) recommends the use of diamond core bits for drilling in rocks in accordance with AASHTO T 225 and ASTM D 2133. The core barrels used should be double- or triple-tube for better recovery and better quality of rock core. The length of each core run may extend up to a maximum 9.84 feet, but in highly fractured or weathered rock zones core lengths should be reduced to 4.92 feet or less below the rock surface. The depth of core for at least 9.84 feet is to ensure the rock is actual bedrock and not a boulder. MDT recommends the use of clear water as drilling fluid, however, drilling mud may be required to stabilize collapsing holes.

MDT prefers wooden boxes for storing and transporting rock cores, but they are expensive; hence, for most applications, a cardboard box is accepted. The mechanical fractures that occur during or after coring are marked with three short parallel lines across the fracture trace. Each box should be marked using an indelible black marking pen with clear indication of core recovery percent and RQD calculated in the field. If laboratory testing is planned, it is desirable to wrap the cores in plastic wrap to maintain in situ moisture content.

(13) Nebraska

The Nebraska Department of Transportation follows ASTM D 2113 Standard Practice for Diamond Core Drilling for site excavation and ASTM D 5079 for preserving and transporting rock cores. A double-tube barrel equipped with a diamond drill bit in the inner and outer tubes is used. In a rigid type of core barrel, both inner and outer tubes rotate, whereas in swivel core barrels, only the outer tube rotates. Mostly sedimentary rocks are encountered in Nebraska, and during the field identification of the rocks, rock type, color, moisture condition, grain size, shape, texture, and weathering data should be noted. Descriptions of the field characteristics of Nebraska sedimentary rocks are shown in Table 2.28. When the rock cores are

obtained, core recovery percentage and RQD should be calculated and noted on the core boxes. The RQD value describes the rock quality, as noted in Table 2.29.

Table 2.28 Field characteristics of Nebraska sedimentary rocks

Type of Rock	Grain Size	Hardness	Breaks Into	Reacts with HCL
Sandstone	Up to 6 mm	Varies	Pieces	No
Siltstone	Fine Powder	Varies	Pieces	No
Shale	Not visible	Varies	Layers	No
Mudstone/Claystone	Not visible	Soft to Hard	Pieces	No
Limestone	Not visible	Hard	Pieces	Rapidly
Dolomite	Not visible	Hard	Pieces	Slowly

Table 2.29 Relationship between RQD and rock quality

RQD (%)	Rock Quality
90 – 100	Excellent
75 – 90	Good
50 – 75	Fair
25 – 50	Poor
0 - 25	Very Poor

(14) New Mexico

The New Mexico Department of Transportation (NMDOT) Geotechnical Design Guide (2021) recommends rotary drilling and wireline drilling methods for obtaining the rock cores. The procedure and applicability of these methods are shown in Table 2.30.

Table 2.30 Rock coring types and applications

Boring Method	Procedure Utilized	Applicability
Rotary Drilling (AASHTO T 225)	Power rotation of drilling bit as circulating fluid removes cuttings from hole. Stratum changes indicated by rate of progress, action of drilling tools, and examination of cuttings in drilling fluid. Casing usually not required, except near surface.	Relatively fast and economical method to advance borings through wide variety of materials, including large boulders and broken rock. Typical Uses: • Obtaining rock cores. Probe drilling. • Instrumentation installation. Foundation, landslide, and rock cut investigations.
Wireline Drilling	Rotary-type drilling method where coring device is integral part of drill rod string, which also serves as casing. Core samples obtained by removing inner barrel assembly from core barrel portion of drill rod. Inner barrel is released by retriever lowered by wireline through the drilling rod.	Efficient method for recovering quality core samples of rock. Typical Uses: • General rock coring applications. • Foundation, landslide, rock cut, and material source investigations.

(15) New York

The New York State Department of Transportation (NYSDOT) published its official Geotechnical Design Manual (GDM) for geotechnical field investigation, rock classification, and logging. Rock boring in the state is accomplished by advancing a double-tube core barrel through the rock with application of downward pressure during rotation. ASTM D 2113 is followed as a standard for rock coring and sampling. A continuous coring length of 4.92 feet is obtained, and at any time the core barrel is withdrawn more than 25 mm, the core barrel is removed from the hole and core is removed from the barrel. Rock core recovery of less than 85% is considered unacceptable and coring shall continue for another 4.92 feet. Depending on the RQD, NYSDOT recommends the allowable bearing pressure as shown in Table 2.31. Laboratory tests are conducted on the extracted rock cores to determine their performance properties. Table 2.32 shows the proposed laboratory tests on the rock core samples. The NYSDOT also describes the fracture density of the rock mass from the core recovered lengths and degree of healing, as shown in Table 2.33 and Table 2.34, respectively.

Table 2.31 Recommended allowable bearing pressure for footing on rock (NYSDOT, 2013)

Material	RQD	Allowable Contact Pressure (Psi)
Such igneous and sedimentary rock as crystalline bedrock, including granite, diorite, gneiss, traprock; and hard limestone, and dolomite, in sound condition:	75 – 100%	1666.5
	50 – 75%	902.1
	25 – 50%	416.3
	0 – 25%	139.2
Such metamorphic rock as foliated rocks, such as schist or slate; and bedded limestone, in sound condition:	> 50%	55.1
	< 50%	139.2
Sedimentary rocks, including hard shales and sandstones, in sound condition:	> 50%	346.6
	< 50%	139.2
Soft or broken bedrock (excluding shale), and soft limestone:	> 50%	166.8
	< 50%	111.7
Soft shale:		55.1

Table 2.32 Laboratory tests on rock core samples to obtain performance properties (NYSDOT, 2022)

Name of Test	Standard	Procedure
Resonant Frequency Test	ASTM C 215	Fundamental frequencies of the rock cores are determined from the waveform recorded in the output of the accelerometer. These frequencies are directly related to rock's elastic properties.
UCS Test	ASTM D 7012	Specimens with length to diameter ratio of 2:1 to 2.5:1 are axially loaded to failure.
Indirect Tensile Strength Test	ASTM D 3867	A cylindrical specimen is loaded diametrically across the circular cross section, which causes tensile failure as loading causes tensile deformation perpendicular to the loading direction.
Point Load Test	ASTM D 5731	A specimen with core diameter between 25 mm and 75 mm is subjected to compressive force to induce tensile stress and obtain point load strength index and UCS.

Table 2.33 Description of degree of fracture (NYSDOT, 2013)

Degree of Fracture	Description
Fractured	No observed fractures
Very slightly fractured	Core recovered in lengths greater than 3.28 ft.
Slightly to very slightly fractured	Core recovered in lengths from 0.98 to 3.28 ft.
Slightly fractured	Core recovered mostly in lengths from 0.98 to 3.28 ft with few scattered lengths less than 0.98 ft.
Moderately to lightly fractured	Core recovered mostly in lengths averaging 0.98 ft.
Moderately fractured	Core recovered mostly in lengths from 0.33 to 0.98 ft with most lengths about 0.66 ft.
Intensely to moderately fractured	Core recovered mostly in lengths of 0.33 to 0.66 ft with most lengths about 0.49 ft.
Intensely fractured	Core recovered mostly in lengths from 1.2 to 3.9 inch with most lengths less than 3.9 inch and with fragmented intervals.
Very intensely to intensely fractured	Core recovered as short core lengths averaging less than 1.2 inch
Very intensely fractured	Core recovered mostly as chips and fragments with a few scattered short core lengths.

Table 2.34 Description of degree of healing (NYSDOT, 2013)

Degree of Healing	Description
Totally healed	Fracture is completely healed or re-cemented to a degree at least as hard as surrounding rock.
Moderately healed	Greater than 50% of fracture material, fracture surfaces, or filling is healed or re-cemented and/or strength of the healing agent is less hard than surrounding rock.
Partly healed	Less than 50% fracture material, filling or fracture surface is healed or re-cemented.
Not healed	Fracture surface(s), fracture zone, or filling is not healed or re-cemented.

(16) Ohio

The Ohio Department of Transportation (ODOT) specification for geotechnical explorations recommends AASHTO T225 for coring of rocks and use of double-tube core barrel as a minimum standard. A type N series core barrel, either NX or NQ, is preferred. The initial coring should not exceed 4.92 feet below the top of rock. In case of cores in fractured or highly fractured rocks, the core length should be limited to 4.92 feet; however, if 90% core recovery is achieved in rocks that are moderately fractured or better, core run lengths can be increased to a maximum of 9.84 feet.

In terms of texture, ODOT differentiates the bedrocks as boulder, cobbles, gravel, and sand, as shown in Table 2.35. ODOT describes the bedding thickness as the average perpendicular distance between bedding surfaces, and the differentiation is shown in Table 2.36. The description of degree of fracturing in bedrock and the condition of fractures are shown in Table 2.37 and 2.38, respectively. When necessary for design, the testing on the rocks is performed according to the standards mentioned in Table 2.39.

Table 2.35 Texture of bedrock (ODOT, 2022)

Component		Particle Size	
Boulder		Larger than 12 in.	Larger than 300 mm
Cobbles		3 in. to 12 in.	75 mm to 300 mm
Gravel		0.08 in. to 3 in.	2 mm to 75 mm
Sand	Coarse	0.02 in. to 0.08 in.	0.5 mm o 2 mm
	Medium	0.01 in. to 0.02 in.	0.25 mm to 0.5 mm
	Fine	0.005 in. to 0.001 in.	0.125 mm to 0.25 mm
	Very Fine	0.003 in. to 0.005 in.	0.074 m to 0.125 mm

Table 2.36 Bedding thickness of bedrock (ODOT, 2022)

Description	Thickness
Very Thick	Greater than 36 in. (>1000 mm)
Thick	18 in. to 36 in. (500 -1000 mm)
Medium	10 in. to 18 in. (250 – 500 mm)
Thin	2 in. to 10 in. (50 – 250 mm)
Very Thin	0.4 in. to 2 in. (10 – 50 mm)
Laminated	0.1 in. to 0.4 in. (2.5 – 10 mm)
Thinly Laminated	Less than 0.1 in. (< 2.5 mm)

Table 2.37 Degree of fracturing in bedrock (ODOT, 2022)

Description	Spacing
Unfractured	Greater than 3 m
Intact	1 m to 3 m
Slightly Fractured	0.3 m to 1 m
Moderately Fractured	0.1 m to 0.3 m
Fractured	50 mm to 0.1 m
Highly Fractured	Less than 50 mm

Table 2.38 Condition of fracture in bedrock (ODOT, 2022)

A. Aperture Width		
Description	**Width**	
Open	Greater than 0.2 in.	Greater than 5 mm
Narrow	0.05 in. to 0.2 in.	1 mm to 5 mm
Tight	Less than 0.05 in.	Less than 1 mm
B. Surface Roughness		
Description	**Criteria**	
Very Rough	Near vertical steps and ridges occur on the discontinuity surface	
Slightly Rough	Asperities on the discontinuity surface are distinguishable and can be felt	
Slicken sided	Surface has a smooth, glassy finish with visual evidence of striations.	

Table 2.39 Rock testing methods (ODOT, 2022)

Test Method	ASTM Designation
Slake Durability	D 4644
Point Load Strength Index	D 5731
Unconfined Compressive Strength of Intact Rock	D 7012, Method C
Compressive Strength and Elastic Moduli	D 7012, Method D

(17) Oklahoma

The specifications and guidelines for the state of Oklahoma follow the Geotechnical Engineering Circular No. 5 – Evaluation of Soil and Rock Properties, AASHTO, and ASTM test procedures. The DOT recommends ASTM D 2113 for rock core drilling and sampling of rock for site investigation and ASTM D4220 for preserving and transporting of samples.

(18) Oregon

The Oregon Department of Transportation Geotechnical Design Manual is consistent with the guidelines provided in Sabatini et al. (FHWA, April 2002) for detailed measurement and interpretation of soil and rock properties. The rock cores extracted are tested in the laboratory for the estimation of various properties.

(19) Pennsylvania

The Pennsylvania Department of Transportation (PennDOT) Geotechnical Investigation Manual (2022) has an approximate rock hardness scale that helps to differentiate and describe the rocks. Hardness is a function of mineralogy of the rock and state of weathering, which is described in Table 2.40. Table 2.41 and 2.42 show the classification based on bedding thickness and dip, respectively.

Table 2.40 Rock hardness descriptors (PennDOT, 2018)

Descriptor (Abbrev.)	Test Criteria for Hand Specimen	Typical PA Rock Type	Approx. Mohs Hardness Scale	Materials in Hardness Range
Very Soft (Versus)	Scratched by a wood dowel or fingernail	Gypsum, evaporites, some shale	1 – 2	PVC, fingernail
Soft (Sf)	Scratched by rubbing against the surface of a copper pipe or fitting, but not scratched by a wood dowel or fingernail	Schist, shale, most limestone	3 – 3.5	copper pipe
Medium Hard (Mh)	Scratched by rubbing against the surface of a common steel nail, but not scratched by rubbing against the surface of a copper pipe or fitting	Siltstone, sandstone, some limestone	5 – 5.5	common nail, glass
Hard (Hd)	Scratched by rubbing against a hardened steel file, but not scratched by rubbing against the surface of a common steel nail	Some sandstone, chert, granite, gneiss	7.5 – 8	hardened steel, porcelain
Very Hard (Vh)	Not scratched by rubbing against a hardened steel file	Some hornfels	>8	corundum

Table 2.41 Rock bedding descriptions (PennDOT, 2018)

Bedding Thickness (Abbrev.)	Description
Indistinct Bedding (Inb)	Bedding structure not clearly defined
Laminated Bedding (Lmb)	Bedding thickness < 0.24 inch
Thin Bedding (Tnb)	Bedding thickness 0.24 to 0.98 inch
Narrow Bedding (Nrb)	Bedding thickness 0.98 to 2.95 inch
Moderate bedding (Mob)	Bedding thickness 2.95 to 8.86 inch
Medium Bedding (Meb)	Bedding thickness 8.86 to 23.62 inch
Thick bedding (Tkb)	Bedding thickness 1.97 ft to 5.91 ft
Massive Bedding (Mab)	Bedding thickness > 5.91 ft

Table 2.42 Rock bedding/discontinuity dip descriptions (PennDOT, 2018)

Bedding/Discontinuity Dip (Abbrev.)	Description
Flat Dip (Fld)	Beds/Discontinuities dipping < 5 degrees
Shallow Dip (Sld)	Beds/Discontinuities dipping from 5 to 15 degrees
Moderate Dip (Mdd)	Beds/Discontinuities dipping from 15 to 30 degrees
Steep Dip (Std)	Beds/Discontinuities dipping from 30 to 45 degrees
Very Steep Dip (Versusd)	Beds/Discontinuities dipping from 45 to 60 degrees
Sheer Dip (Srd)	Beds/Discontinuities dipping > 60 degrees

The discontinuity spacing is defined as the measure of the distance between each discontinuity, and PennDOT description of rocks based on discontinuity spacing are shown in Table 2.43.

Table 2.43 Rock discontinuity spacing descriptions (PennDOT, 2018)

Spacing	Abbreviation	Description
Laminated	Lmd	Discontinuity spacing < 0.24 inch
Narrow	Nrd	Discontinuity spacing from > 0.24 up to 0.98 inch
Close	Cld	Discontinuity spacing > 0.98 up to 2.95 inch
Moderate	Mod	Discontinuity spacing > 2.95 inch up to 0.66 ft
Medium	Med	Discontinuity spacing > 0.66 up to 1.97 ft
Wide	Wdd	Discontinuity spacing > 1.97 up to 5.91 ft
Massive	Mad	Discontinuity spacing > 5.91 ft

(20) South Carolina

The South Carolina Department of Transportation (SCDOT) Geotechnical Manual (2019) recommends the use of ASTM D2113 – Standard Practice for Rock Core Drilling and Sampling of Rock for Site Investigation, and AASHTO T225 – Standard Method of Test for Diamond Core Drilling for Site Investigation for rock core sampling. SCDOT describes the rock classification in terms of grain size, as described in Table 2.44. Table 2.45, 2.46, 2.47, and 2.48 describe the classification of rocks in terms of texture or stratification, rock strength, rock hardness, and aperture size discontinuity terms, respectively.

Table 2.44 Rock classification in terms of grain size (SCDOT, 2019)

Description	Diameter (Inch)	Characteristics
Very Coarse-grained	> 0.19	Grain-sizes greater than popcorn kernels
Coarse-grained	0.079-0.19	Individual grains easy to distinguish by eye
Medium-grained	0.017-0.079	Individual grains distinguished by eye
Fine-grained	0.003-0.017	Individual grains distinguished with difficulty
Very Fine-grained	< 0.003	Individual grains cannot be distinguished by unaided eye

Table 2.45 Rock classification in terms of texture (SCDOT, 2019)

Descriptive Term	Layer Thickness
Very Thickly bedded	> 3.28 ft
Thickly bedded	1.64 to 3.28 ft
Thinly bedded	1.97 to 19.696 inch
Very Thinly bedded	0.39 to 1.97 inch
Laminated	0.098 to 0.39 inch
Thinly laminated	< 0.098 inch

Table 2.46 Rock classification in terms of rock strength (SCDOT, 2019)

Description	Recognition	Approx. UCS (Psi)
Extremely Weak Rock	Can be indented by thumbnail	34.81-149.39
Very Weak Rock	Can be peeled by pocketknife	149.39-725.19
Weak Rock	Can be peeled with difficulty by pocketknife	725.19-3501.21
Medium Strong Rock	Can be indented 3/16 inch with sharp end of pick	3501.21-7251.89
Strong Rock	Requires one hammer blow to fracture	7251.89-14503.80
Very Strong Rock	Requires many hammer blows to fracture	14503.80-36259.40
Extremely Strong Rock	Can only be chipped with hammer blows	> 36259.40

Table 2.47 Rock classification in terms of rock hardness (SCDOT, 2019)

Description	Characteristics
Soft (S)	Plastic materials only
Friable (F)	Easily crumbled by hand, pulverized, or reduced to powder
Low Hardness (LH)	Can be gouged deeply or carved with a pocketknife
Moderately Hard (MH)	Can be readily scratched by a knife blade
Hard (H)	Can be scratched with difficulty
Very Hard (VH)	Cannot be scratched by pocketknife

Table 2.48 Rock classification in terms of aperture size discontinuity (SCDOT, 2019)

Aperture opening	Description	
< 0.0039 inch	Very Tight	Closed Features
0.0039-0.0098 inch	Tight	
0.0098-0.020 inch	Partly Open	
0.020-0.098 inch	Open	Gapped Features
0.098-0.39 inch	Moderately Open	
> 0.39 inch	Wide	
0.39-3.94 inch	Very Wide	Open Features
3.94-39.37 inch	Extremely Wide	
>3.28 ft	Cavernous	

(21) Virginia

The Virginia Department of Transportation (VDOT) recommends unconfined compressive strength (ASTM D7012) and point load index (ASTM D5731) as appropriate tests for intact rock properties, and ASTM D2113 – Standard Practice for Rock Core Drilling and Sampling of Rock for Site Investigation and AASHTO T225 – Standard Method of Test for Diamond Core Drilling for Site Investigation for rock core sampling.

2.5.5 Summary of current site investigation and methods for estimating rock properties

In the study of current practices for site investigation and methods for estimating rock properties, it was found that only 21 states have a geotechnical manual with information about rock drilling, transporting, classifying, and testing. The 21 states are shown in Figure 2.13. All these states refer to AASHTO R13 for site investigation and AASHTO T225 for diamond core drilling of rocks. For testing purposes, ASTM D 4543 is used for sample preparation and ASTM 7012, ASTM D 5731, ASTM D 3148, and ASTM D 4644 are used for unconfined compressive strength, point load strength, strength deformation test, and durability test, respectively.
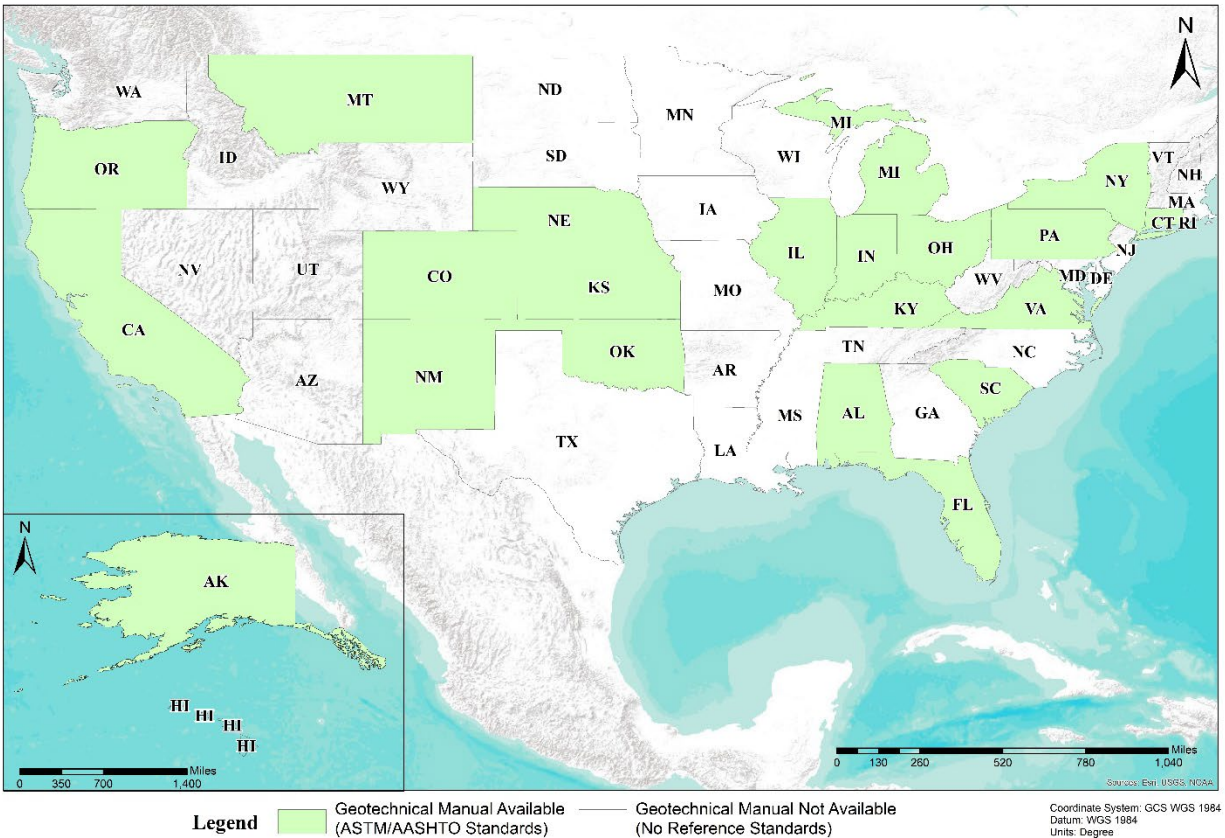
Figure 2.13 States with a geotechnical manual at the time of this study

3. LABORATORY ROCK TESTING AND MEASUREMENTS

3.1 Introduction

Mechanical properties of natural rocks vary significantly due to rock texture, discontinuities, bedding, and mineral composition. This variation is due to their mineralogy, geological age, formations, and other natural processes. Anisotropic rocks have highly variable mechanical properties, which cannot be easily reproduced (Jaeger et al., 2007). This chapter describes the rock core drilling procedure, triaxial experimental procedure, and porosity measurement for rock samples collected across the state of Wyoming. The laboratory measurement of the mechanical properties of the different rock types is necessary to evaluate their failure behavior, mechanical properties, and strength parameters.

In this chapter, preparation of the rock specimen for testing, including drilling, cutting, and polishing of the specimen, is discussed. The triaxial compression setup for hard rocks using GCTS RTR-1500 and for soft rocks using GeoJac testing equipment is described. In addition, the procedure for measuring the porosity of the rocks is described.

This study includes various rock types (sandstone, siltstone, shales, etc.), tested at varying confining pressure using the triaxial equipment. The rock samples collected from Wyoming include both drilled cores and surface boulders. Most samples were tested for at least one unconfined compression (UCS) test and several compression triaxial tests at different confinements. For the compression triaxial tests, the stress condition of $\sigma_1 > \sigma_2 = \sigma_3$ is applied.

3.2 Preparation of Rock Specimens

According to the ASTM standard, a specific specimen size must be attained before proceeding with the mechanical testing of the rock specimen. The height to diameter ratio of the tested specimen should be equal to or greater than two but not less than two. The procedure for the rock specimen preparation is discussed.

3.2.1 Drilling of Rock Specimens from Surface Rock Boulders

The drilling equipment used for coring the rocks is a 1200-hp top drive table drill from Anchor drilling company. Figure 3.1 shows a schematic representation of drilling process using the Anchor drill. For the top drive drill, thrust (force) is applied from the top and the torque generated due to the spinning of drill bit cuts through the rock boulder, as shown in Figure 3.1a and 3.1b. Once the drill bit passes through the rock, the thrust (force) and torque is not applied, and the drill bit is lifted up with the drilled rock core inside it, as shown in Figure 3.1c. Figure 3.2 shows the drill used to core rock specimens from surface rock boulders. It has four adjustable drilling speeds of 250 rpm, 500 rpm, 800 rpm, and 1400 rpm. Drill bits with outer diameters of 1.3 and 2.2 inch were used for drilling 1-inch and 2-inch diameter rock specimens, respectively. The drill bits are specially designed for wet drilling using a sufficient supply of water during the drilling to prevent damage to the drill bits by overheating. The dry drilling can be done on soft rocks, such as fine sandstone, which break with water. The drilling setup and process are described below.
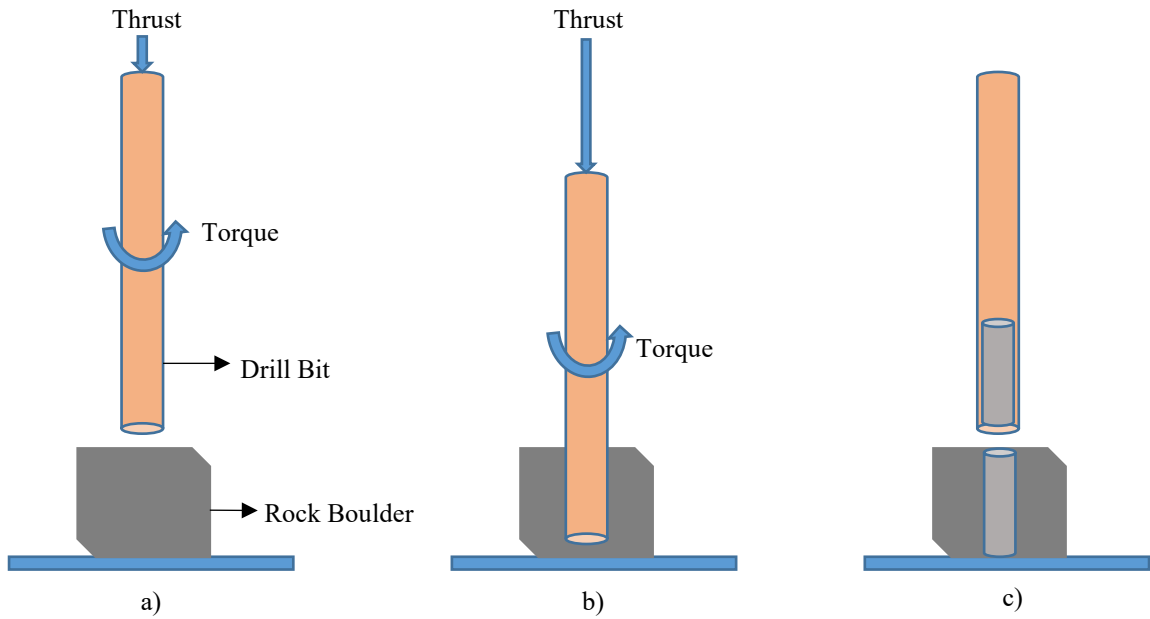
Figure 3.1 Schematic representation of rotary drilling of cores from rock boulders
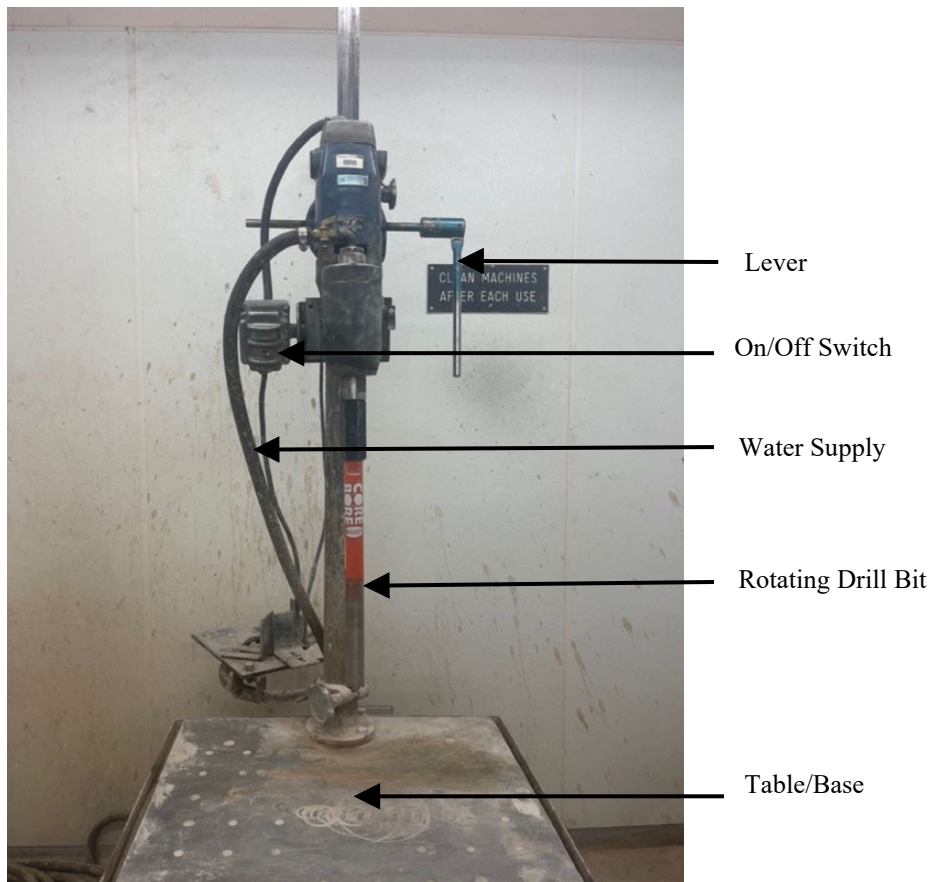
Figure 3.2 Drilling equipment and setup for rocks

(a) Fastening the rock boulder

The rock boulder to be drilled must be fastened tightly on the table before drilling. The regular-shaped boulder can be held easily but not the irregular-shaped boulder. Although many setups can be used to fasten the rock onto the table, 2×4 Irwin quick grip clamps and C-clamps, as shown in Figure 3.3a, were found to be adequate. The drilling process could encounter several problems if the rock boulder is not held properly. First, if the boulder is not fastened properly, it might get thrown off the table during drilling. Second, if the rock is allowed to move during a high-speed rotation, the drill bit could hit the rock and cause rock vibration, preventing the drilling through the rock. This could break the rock specimen, as shown in Figure 3.3b. Finally, if the boulder moves or shifts during the drilling process, a perfectly vertical and straight cylindrical rock specimen cannot be obtained. Similar setup is made when drilling a smaller diameter core from large diameter rock cores.
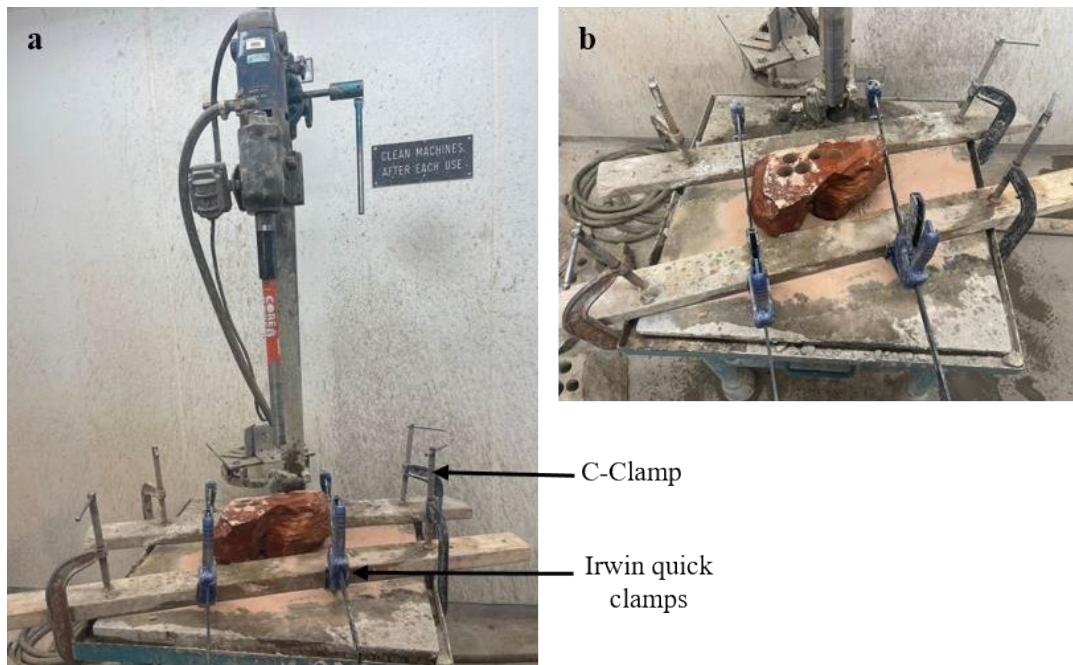
Figure 3.3 Fastening the rock boulder on the table using clamps (a) and broken rock sample (b)

(b) Determining the rotation speed of the drill

After fastening the rock boulder on the table underneath the drill bit, a rotation speed of the drill bit was chosen depending on the rock hardness. For hard rocks like the gneiss and volcanic breccia, a slower drilling speed of 250-500 rpm with a full supply of water to cool the drill bit is recommended. Using a higher rotation speed risks damaging the drill bit and takes a lot more effort to push the drill bit through the rock. On the other hand, a higher drilling speed of 850-1400 rpm with a controlled water supply is recommended for the soft rocks like sandstones and shales. The longer the soft rocks are subjected to the vibration effect from the rotatory drill, the more likely breakage will occur.

(c) Controlling the drilling process

After fastening the rock boulder and determining the drilling speed, the drill bit is lowered using the lever control shown in Figure 3.2. For soft rocks, the lever should be held to maintain a constant force and achieve a smooth drilling through the rock. For hard rocks, force should be applied to the lever to facilitate rock drilling and prevent the idle rotation at one place. Before and after the drilling process, the lever should be held tightly and fixed in place to avoid sudden falling of the drill setup and risk breakage of the drill bit, bottom table, or rock sample, or human injury. The operation process produces deafening sound and splashes of water, so it is important to wear ear and eye protection gears during drilling. The drill bit rotates at a very high speed to produce the torque required for drilling the rock, thus it is very important to not wear loose clothing during the drilling process as it might contact the rotating drill and cause injuries. Figure 3.4a shows the drilled sandstone sample and Figure 3.4b shows four long cylindrical rock cores obtained from the rock boulder.

Figure 3.4 Drilled rock boulder (a) and drilled rock cores (b)

3.2.2 Cutting of rock cores

After the rock cores are extracted from the rock boulder, the rock core length was cut to obtain a length to diameter ratio (L/D) equal to 2. The rock cutting is accomplished using the 7-inch portable wet cutting saw equipment shown in Figure 3.5. The cutting equipment has a 7-inch continuous rim diamond blade, and water is used during the cutting process to keep the blade cool. The excess water from the tabletop is collected in a tray. The cutting equipment has a scale printed on the top and an adjustable linear guide that can be fixed at the desired distance from the saw to get a precise cut. The equipment can reach a saw cutting speed up to 3400 rpm.

The housing is made from an fire-resistance plastic material, and the tabletop is stainless steel. The equipment must be cleaned before and after each cutting operation to ensure the best cutting performance. The sample should be held tightly during cutting to get a smooth and even cut. Care should be taken while cutting as the blades of the cutting saw are exposed and injuries may occur if your hands touch the running blade. During the cutting process, a lot of water is splashed onto the body and eyes, thus wearing proper safety gear is highly recommended.
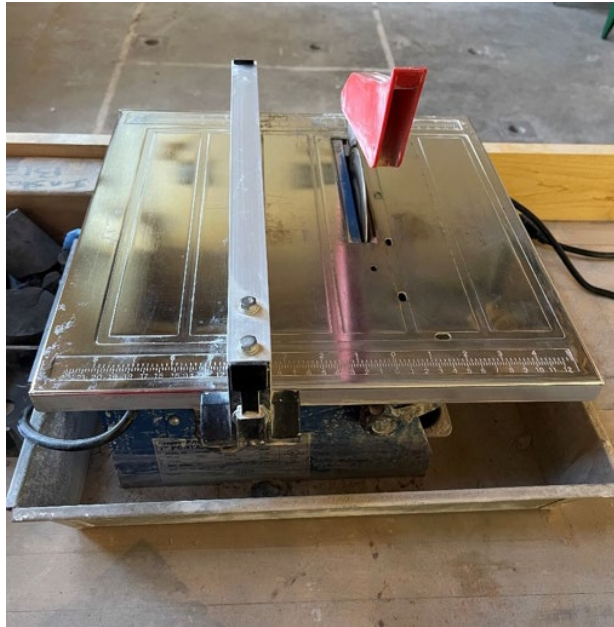
Figure 3.5 Equipment for cutting and trimming rock specimens

3.2.3 Rock trimming and polishing

After the rock specimens are cut to their desired lengths, both ends of the rock specimens are trimmed and polished to obtain a uniformly planar surface for testing, as the top and bottom of the test specimen should be parallel to each other and perpendicular to the longitudinal axis. The finished top and bottom surfaces should not exceed a tolerance of 0.001-inch (ASTM D4543 (withdrawn), 2008). Care should be taken while polishing softer rocks like sandstone to avoid breaking at the edges or making it too short. The polishing is accomplished by rotating the rock specimen and the miter gauge worktable assembly with an attached sanding belt, as shown in Figure 3.6. The aluminum worktable can be tilted from 0 to 45 degrees, and the sanding belt sander is 4×36 inch. There are two cast aluminum worktables for vertical and horizontal polishing. The maximum disc speed is 3450 rpm. A miter gauge is provided to fix the rock specimen's proper angle, and a vacuum is connected to the machine to collect the produced dust particles.

Figure 3.6 Polishing equipment with sanding belt

3.3 Rock Testing System

There were two types of rocks tested in the laboratory. The hard rocks were tested using the GCTS rapid triaxial rock testing equipment RTR-1500, and the soft soil-based rocks were tested using the GeoJac triaxial equipment. The two testing systems are described in Sections 3.3.1 and 3.3.2, respectively.

3.3.1 GCTS rapid triaxial rock (RTR-1500) testing equipment

The GCTS rapid triaxial rock (RTR-1500) testing equipment shown in Figure 3.7 was used for the unconfined compression test and the triaxial test of the hard rock specimens. An automatic hydraulic lift and sliding base, a triaxial cell made of stainless steel, and two pressure intensifiers for controlling the cell and pore pressures are provided in the setup. The triaxial cell can accommodate cylindrical specimens of up to 3 inches. The equipment has a load frame with a stiffness of 1.75 MN/mm. This equipment is a digitally regulated closed-loop servo control of the axial actuator and operated using a computer, as shown in Figure 3.8.

The setup includes a fully integrated SCON-2000 digital signal controller and CATS-TRX-ROCKS software. GCTS RTR-1500 has rapid, easy, and safe operation with automated cell assembly and meets the specifications of the ISRM and ASTM standards for triaxial testing of the rock samples. The axial load actuator has a capacity ranging up to 337.2 kips, and the triaxial cell can apply a maximum confining pressure of 20.3 ksi. The confinement is applied using oil filled inside the stainless-steel chamber inside the frame. For the confinement, a pressure intensifier for cell pressure is used. The pressure intensifier is housed inside a metal cabinet and includes a 20-liter fluid reservoir, precise analog gauges, high pressure valves, and flow indicators. Both the cell and pore pressure intensifiers have a pressure transducer and linear variable differential transformer (LVDT) connected allowing for the servo control as a function of pressure, fluid volume control, or any other measured or calculated test parameter.

A heat-shrink membrane is used to protect and separate the rock specimen from the oil. The connected computer controls the testing system and can be programmed for testing at different ASTM testing standards. The equipment was setup for testing 25-mm and 50-mm diameter rock specimens. Two axial and one radial strain linear variable differential transformers (LVDTs) were used for strain measurements. At the bottom, feed-through lines from the radial LVDT, axial LVDTs, and top and bottom platen are

49

connected to measure the deformation and post-failure behavior studies. The equipment is also equipped with an ultrasonic measurement capacity to yield P-wave and S-wave velocities. The high-performance equipment has a servo-controlled axial actuator used to control the maximum deformation of the axial strain for automatically completing the triaxial test.

Figure 3.7 GCTS RTR-1500 triaxial testing equipment

Figure 3.8 Computer operated SCON controller for RTR 1500 triaxial testing equipment

3.3.2 GeoJac Triaxial Equipment

The GeoJac triaxial equipment shown in Figure 3.9 is a compact and lightweight automated testing system for mechanical testing of soil-based rock specimens. The machine has an axial load capacity of 2.02 kips and a 1.2-ft stroke that can be configured to perform various triaxial tests. The setup is operated using a computer system that can be programmed to perform unconsolidated undrained (UU), consolidated undrained (CU), and consolidated drained (CD) tests.

The test setup consists of a load actuator mounted on two vertical stands that can be used to automate the three triaxial test types. The GeoJac equipment can perform testing under a closed-loop control of the axial deformation, load, or pressure. The triaxial tests are mainly conducted under a controlled axial deformation, with 15% as the peak stress. As the rock specimens are soil-like, it undergoes bulging when load is applied, hence for the safety of equipment and to avoid complete destruction of sample, the test is stopped at 15% strain limit.

The specimen can be sheared in various modes like constant deformation rate, constant rate of loading, or a series of step loads to reach the final axial deformation value. The GeoJac device has a cylindrical glass side wall placed on the base part with a bottom pedestal to place the rock specimen. The top of the cylindrical sidewall is mounted with the piston setup. Water is used to apply the uniform confining pressure to the specimen during the test, and the device can withstand a confining pressure up to 79.8 Psi. A plastic membrane is used to protect the rock specimen from the water. A cell pressure sensor is placed on the top part of the cell chamber to take the stress-strain measurements during the shearing stage.
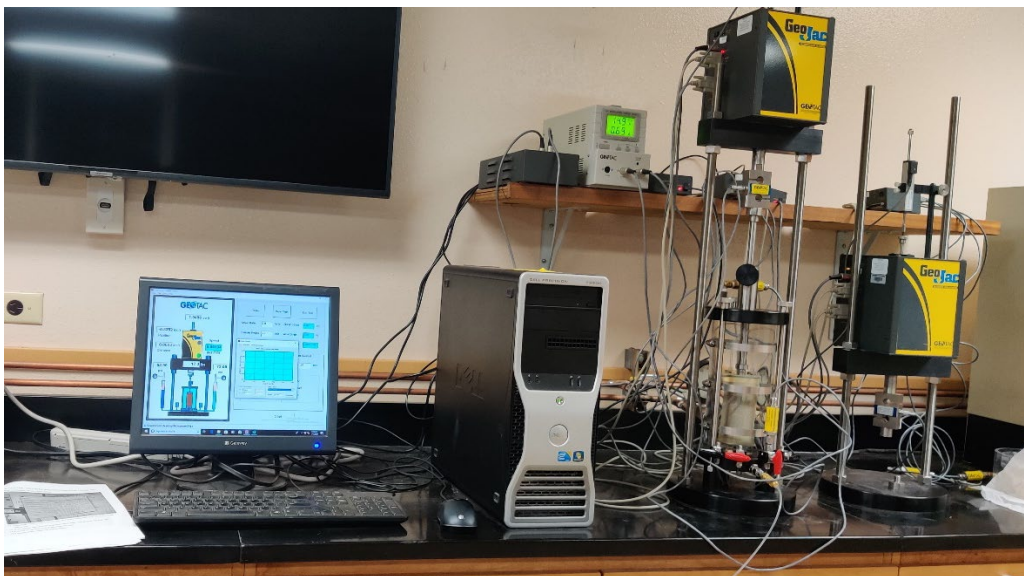
Figure 3.9 GeoJac equipment setup in our UW laboratory

3.4 Rock Testing Procedure

3.4.1 GCTS Rapid Triaxial Rock Testing Procedure

The height, diameter, and weight of each rock specimen are measured as shown in Figure 3.10. The specimen is then placed between the bottom and top platens. A heat-shrink tubing was then wrapped on the rock specimen and extended to its length using a heat gun. Two rings for guiding the LVDTs' installation are mounted on the 2-inch diameter specimens or fastened on the platen groove lines for the 1-inch diameter specimen.

A steel chain for the radial LVDT sensor is wrapped around the mid depth of the rock specimen. For the measurement of the axial deformation of the rock sample, two axial LVDTs are then inserted vertically through the two rings, and for the measurement of the radial deformation, the radial LVDT is inserted horizontally through the chain. The wires of these LVDTs and the platens are inserted into the respective feed-through at the base of the setup, as shown in Figure 3.11. The installed specimen setup is then slid into the loading frame and beneath the cylindrical cell wall, and the cell wall is lowered and closed. The cell wall is then filled with oil, and the desired confining pressure is applied to the rock specimen.

The initial seating pressure of 50 Psi is applied before the shearing stage. The rock is then subjected to an axial shearing stage using a controlled axial strain setup at a constant strain rate of 0.1% per minute for hard rocks and 0.05% per minute for softer rocks. The rock fails, and the test is stopped. After that, the specimen's failure plane and failure angle are determined, as shown in Figure 3.12 for sample 13c. The results of the confining stage and the shearing stage are stored in two separate files for analysis.
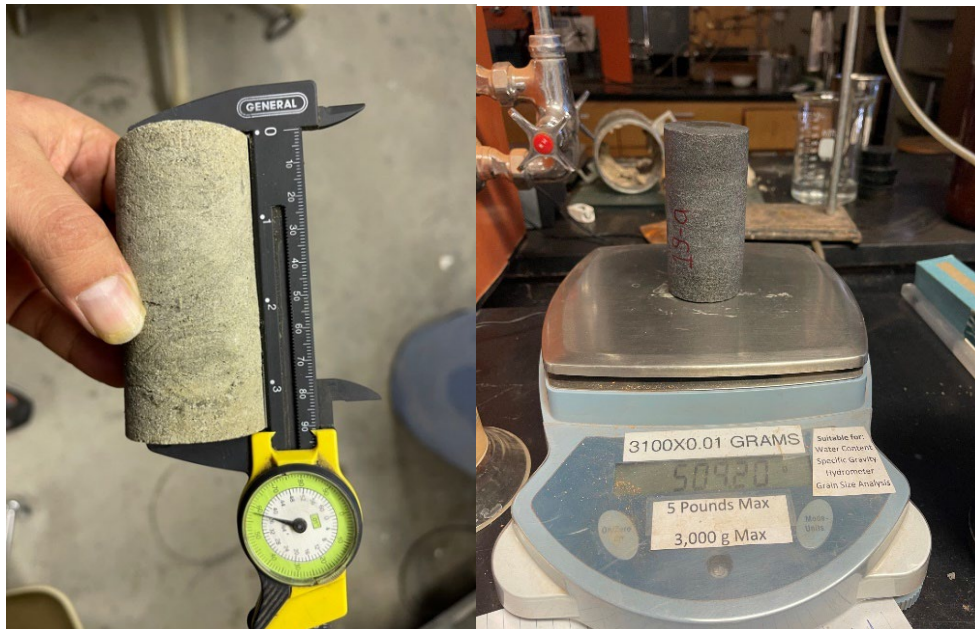
Figure 3.10 Measurement of height, diameter, and weight of each rock specimen
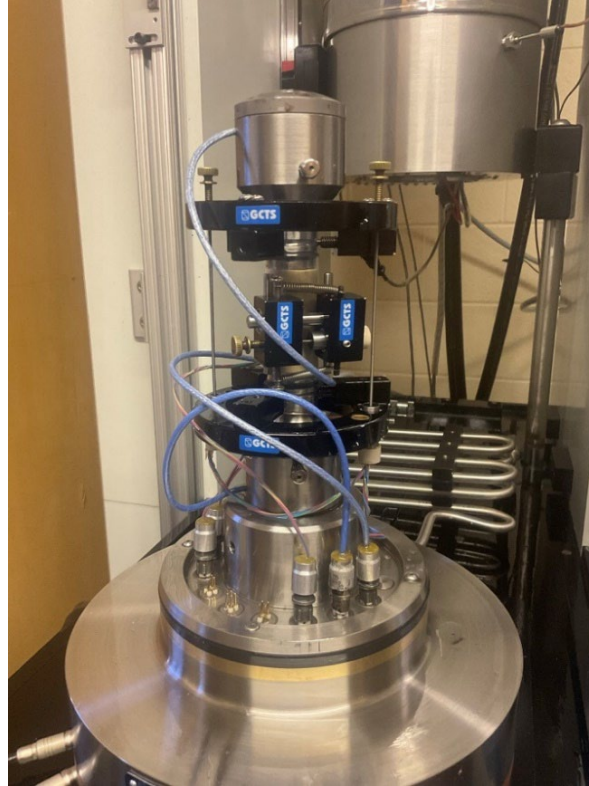
Figure 3.11 Triaxial setup with three LVDT sensors

Figure 3.12 Rock specimen after testing

3.4.2 GeoJac Triaxial Procedure

The height, diameter, and weight of the specimen are measured. A porous stone is placed on the base pedestal, followed by a filter paper. The rock specimen is placed on top of the filter paper followed by a top filter paper and the top pedestal. The specimen is wrapped in a rubber membrane, reaching the top and bottom pedestals. The rubber membrane is held tightly against the top and bottom platens using O-rings. The specimen was enclosed in the cylindrical glass cell wall, and a piston is placed on the top of the cell wall, which is fixed in place using three rods, as shown in Figure 3.13a.

The cell is then filled with water, and the cell pressure is changed to confining pressure using the valve in a red circle (Figure 3.13b). The top piston is unlocked to allow the application of axial load, and the specimen is then shear until the axial strain reaches the maximum limit of 15%. The applied strain rate should fall between 0.3% to 1% per minute so that failure occurs in more than 15 minutes. The specimen during loading and at failure is shown in Figure 3.14a and 3.14b. The experimental data are then recorded and saved for further analysis.
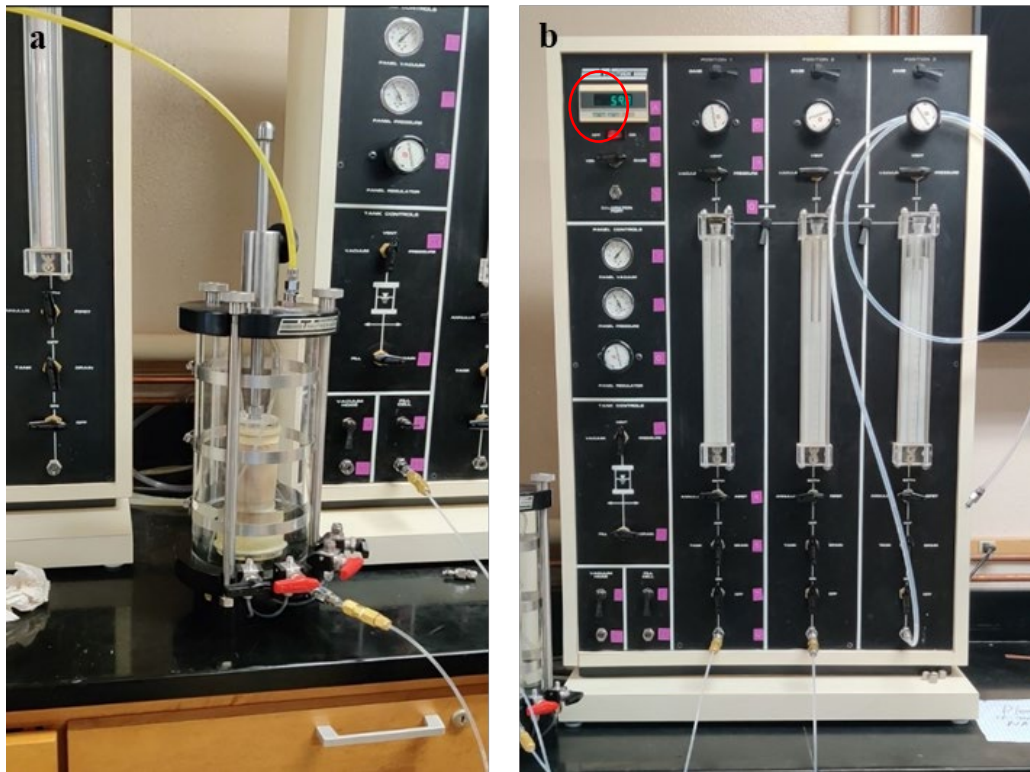
Figure 3.13 GeoJac triaxial setup (a) and switch board for applying confining pressure (b)

Figure 3.14 Application of axial load during the shearing stage (a) and final deformed shape of the specimen (b)

3.5   Determination of Porosity

The porosity (ϕ) is the total volume available inside a rock for passage and storage of fluid and gas. It can be represented as $1 - (V_s/V)$, where *Versus* is the volume of rock solid and V is the total volume of the rock. The porosity of a rock is intrinsic to the rock's bulk matrix, which controls the flow and transport processes inside the rock. The porosity of the rock typically decreases with age and depth of burial and differs with rock type, pore distribution, and composition. Depending upon the rock type, porosity can be determined using the saturation method or calculated using measured specific gravity of rock solid. Saturation method is suitable for harder rocks that would not break or integrate in water while specific gravity method is recommended for softer rocks that break or disintegrate on the action of the water. These two methods for the determination of porosity are described in Sections 3.5.1 and 3.5.2.

3.5.1 Porosity Determination Using the Specific Gravity Method

To determine rock's porosity using this method, we first determine a rock specimen's specific gravity (G_s) and moisture content. The specific gravity is determined using the AASHTO-100 standard test method. The rock specimen is grinded into solid particles and tested using the calibrated 250 ml Pycnometer, described in Section 3.4.1 of AASHTO-T100. The dry weight (weight of Pycnometer filled with de-aired water) and temperature are noted. The weight of the Pycnometer with water at 2° above and below the measured one is calculated using Table 3.5 and equation 3.8 in section 3.4.1 of AASHTO-T100. The solid particles between 30-40 gm are added to ¾ full Pycnometer and vacuumed for 10 minutes (Figure 3.14 left). The Pycnometer is then filled up to the mark and its weight is measured. The

whole mix is then transferred onto an evaporating dish, leaving no solid particles in the Pycnometer. The flow of the mixture coming out from the Pycnometer is controlled by lowering the lip above the water (Figure 3.15 right). The evaporating dish with the mixture is placed inside the oven for at least 24 hours to dry out the water completely. The weight of the evaporating dish with the remaining solids is measured and deducted from the empty weight of the dish to get the weight of the solids. The calculation for the specific gravity is then given by the equations 3.9 in the AASHTO-T100 and Eq. (3.1) below.

$$G_{s,T} = \frac{W_o}{[W_o + (W_a - W_b)]} \tag{3.1}$$

The specific gravity can be calculated using the equation below for K selected based on temperature T_o using Eq. (3.2).

$$G_{s,20C} = K \times G_{s,T_x} = \frac{K \times W_o}{[W_o + (W_a - W_b)]} \tag{3.2}$$

Where, K is the prediction equation factor, W_o is the dry weight of solids, W_a is the weight of Pycnometer and de-aired water, W_b is the weight of Pycnometer, solid and de-aired water.

After specific gravity, we determine the moisture content of the rock specimen. The moist weight of the rock is measured and oven-dried for at least 24 hours before measuring the dry weight. Then we calculate moisture content from these two weights using Eq. (3.3),

$$Moisture\ Content\ (\%) = \frac{W2 - W3}{W2 - W1} \times 100\% \tag{3.3}$$

Where, W1 = empty weight of a can, W2 = weight of the can and moist rock specimen before drying, and W3 = weight of can and rock specimen after oven-drying.

When the porosity and moisture content of the rock has been measured, we then measure the height (L) and diameter (D) of an intact rock specimen before testing in inches using a caliper and the moist weight of the rock specimen (W_m) in grams using the weighing scale. We calculate the intact rock's volume, dry weight, and dry bulk density from these. We then determine the porosity of the intact rock using Eq. (3.4),

$$Porosity\ (\%) = \frac{1 - Dry\ Bulk\ Density}{Specific\ Gravity} \times 100 \tag{3.4}$$
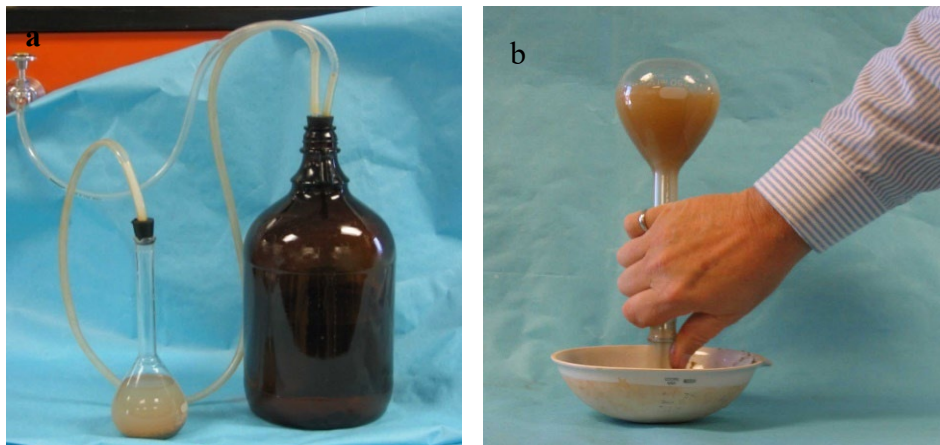
Figure 3.15 Vacuuming the sample and deaired water mix (a) and pouring the mix into evaporating dish for drying (b)

3.5.2 Porosity Determination Using the Saturation Method

Prepare the rock specimen to be tested with length (L) and diameter (D) such that $\frac{L}{D} \geq 2$. The rock specimen is then placed inside an oven to dry for at least 24 hours, and the dry weight of the rock (W_d) is measured. The oven-dried sample is then placed inside the saturation vessel (Figure 3.16 left), and the vacuum is turned on for 24 hours (Figure 3.16 right). After 24 hours, the first saturated weight is taken, and the vacuum is turned on again for the next 24 hours. This process is repeated until the difference in the last two consecutive weights is less than 1%. The previous weight measurement is noted as W_s. From the length and diameter, the volume of the intact rock specimen is calculated, and the porosity of the rock is calculated using Eq. (3.5),

$$Porosity\ (\%) = \frac{W_s - W_d}{Dw(gm/cc) \times V\ (in\ cc)} \times 100\% \tag{3.5}$$

Where, W_s is the saturated weight, W_d is the dry weight, D_w is the density of water, and V is the volume of the rock.

3.6   Result Analysis Plan

The uniaxial and triaxial test results for each tested sample are exported in a Microsoft Excel file format. UCS test data for the axial strain-controlled shearing stage are exported in a single output file. The triaxial test data are exported in two output files with one for the confining stage and the other for the shearing stage. An example of output file on information regarding test setup and tested specimen is shown in Figure 3.17. The output file also contains the maximum peak, deviator, axial, radial, and volumetric strains of the tested specimen, as shown in Figure 3.18 as an example. A plot of the deviator stress against the axial, radial, and volumetric stresses is shown in Figure 3.19. The test results are recorded at an interval of 0.5 seconds.
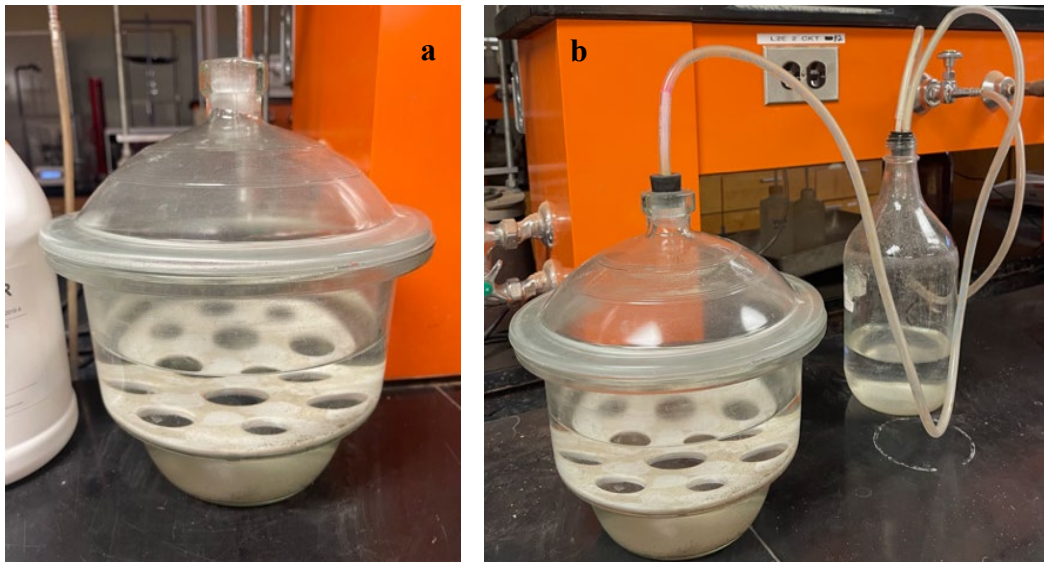
Figure 3.16 Saturation vessel (a) and saturation vessel connected to vacuum (b)

Test Results:	Stopped by User					
Stages:	1					
	Type:	Static Loading				
	Specimen:					
		Height:	4	(inch)		
		Axial Gauge Length:	3.21	(inch)		
		Diameter:	1.99	(inch)		
		Area:	3.11	in^2		
		Volume:	12.13	in^3		
Max (Peak) Sd - Deviator Stress:		7217.6		(psi)		
		Time:	396.362	(Seconds)	=>	6:36
		CP - Cell Pressure:	580.4	(psi)		
		U - Pore Pressure:	-14.6	(psi)		
		Ea - Axial Strain:	0.441	(%)		
		Er - Radial Strain:	-0.961	(%)		
		Ev - Volumetric Strain:	-1.482	(%)		
		Sa - Axial Stress:	7798	(psi)		
		Sa' - Axial Effective Stress:	7812.7	(psi)		
		Sc' - Cell Effective Pressure:	595	(psi)		
End (Residual) Sd - Deviator Stress:		5832.5		(psi)		
		Time:	937.932	(Seconds)	=>	15:37
		CP - Cell Pressure:	579.7	(psi)		
		U - Pore Pressure:	-16.3	(psi)		
		Ea - Axial Strain:	1.03	(%)		
		Er - Radial Strain:	-2.39	(%)		
		Ev - Volumetric Strain:	-3.758	(%)		
		Sa - Axial Stress:	6412.2	(psi)		
		Sa' - Axial Effective Stress:	6428.5	(psi)		
		Sc' - Cell Effective Pressure:	596	(psi)		
Data Points (Rows):	1878					

Figure 3.17 Information regarding test setup and tested specimen

Time	Sd - Deviator Stress	Cell Pressure	Pore Pressure	Ea - Axial Strain	Er - Radial Strain	Ev - Volumetric Strain
sec	(psi)	(psi)	(psi)	(%)	(%)	(%)
0.000	63.65	580	-14.3	0.0495	0.0224	0.0943
0.500	87.07	579.7	-14.6	0.0508	0.0223	0.0954
1.000	90.42	579.7	-14.3	0.0515	0.0223	0.096
1.500	90.45	580	-14.3	0.0517	0.0223	0.0962
1.999	97.12	579.7	-14.6	0.0522	0.0222	0.0965
2.499	100.5	580	-14.6	0.0527	0.0221	0.0969
2.999	110.56	580	-14.6	0.053	0.022	0.097
3.499	113.87	579.7	-14.3	0.0534	0.022	0.0975
3.999	117.22	579.7	-14.3	0.0539	0.022	0.098
4.499	123.99	580.4	-14.3	0.0542	0.022	0.0982
4.998	133.97	579.7	-14.3	0.0548	0.0219	0.0986
5.498	137.32	579.7	-14	0.0552	0.0219	0.099
5.998	144.02	579.7	-14.3	0.0555	0.0218	0.0991
6.498	154.14	580.4	-14.6	0.0559	0.0218	0.0994
6.998	160.77	579.7	-14.3	0.0563	0.0217	0.0996
7.498	167.47	579.7	-14	0.0567	0.0217	0.1001
7.997	177.56	580	-14.3	0.0573	0.0216	0.1005
8.497	184.19	579.4	-14.3	0.0577	0.0216	0.1008
8.997	190.96	580	-13.6	0.0581	0.0216	0.1013
9.497	197.69	580.4	-14.3	0.0583	0.0215	0.1013
9.997	204.36	580	-14	0.0589	0.0215	0.1017
10.497	214.41	580	-14.3	0.0593	0.0214	0.1021
10.997	217.72	579.7	-14	0.0596	0.0214	0.1023
11.496	227.84	580.4	-14	0.06	0.0213	0.1026
11.996	237.86	580	-14.3	0.0607	0.0213	0.1033
12.496	241.21	580	-14	0.0609	0.0212	0.1034
12.996	251.26	580	-13.6	0.0614	0.0212	0.1037
13.496	257.96	580	-14.3	0.0617	0.0211	0.1039
13.996	264.62	579.7	-13.6	0.0623	0.0211	0.1044
14.495	268.01	580	-14	0.0627	0.0211	0.1048
14.995	278.02	579.7	-14	0.0629	0.021	0.1049
15.495	288.07	579.7	-14	0.0634	0.0209	0.1053
15.995	291.46	580	-14	0.0639	0.0209	0.1058
16.495	301.51	580	-13.6	0.0643	0.0209	0.106
16.995	308.21	580	-13.6	0.0646	0.0208	0.1061
17.494	314.91	580	-13.6	0.065	0.0209	0.1067
17.994	321.61	580	-14	0.0656	0.0207	0.107
18.494	328.31	580	-13.6	0.066	0.0207	0.1073
18.994	338.36	580	-13.6	0.0664	0.0207	0.1076
19.494	345.06	580	-14	0.0668	0.0206	0.1079

Figure 3.18 Measured deviator stress, axial strain, radial strain, and volumetric strain data of tested specimen

Young's modulus and Poisson's ratio are determined from the stress-strain values using a moving average regression analysis method. The moving average method is a statistical approach which takes multiple averages of a dataset and its subsets from continuous terms in a series. The moving average method helps capture the average change in a data series. First, axial stress versus axial strain is plotted for each specimen. From the complete stress-strain plot we obtain the linear part of the stress-strain plot using visual inspection. After the linear section is identified, linear regression is performed on the data to obtain a best fit equation of those stress-strain data. The data in the linear portion are added or removed to make the statistical parameter R^2 as close to 1 as possible. Young's Modulus is calculated from the gradient of the equation obtained from the linear portion.

We see the gradient of the linear portion as 125.62, to obtain the E of this rock, we multiply the gradient by 100 to obtain the value in the same unit as the axial stress as the strain is in percentage. The linear portion of the stress-strain plot used for calculating the Young's modulus is used to calculate the Poisson's ratio. Poisson's ratio is that of radial strain to axial strain. The RTR-1500 testing machine provides a series of data shown in Figure 3.18 at 0.5-second intervals. Poisson's ratio for each data point is calculated by dividing the measured radial strain by the measured axial strain. Poisson's ratio of the rock is obtained by taking the average of the calculated Poisson's ratio of the data points that are used in the linear section while calculating the Young's modulus.

4.   EXPERIMENTAL RESULTS

4.1   Introduction

Fifty-six (56) rock samples were collected from different locations around the state of Wyoming. These samples are a mix of different rock types, formations, geologic ages, and depths. Figure 4.1 shows the location of the individual samples on the Wyoming geographical map. Each sample is identified with an identification number from 1 to 56. The prominent rock types are sandstones, shales, and siltstones while other less common rock types tested in this study are indicated as other rocks. Among the 56 samples, six samples (3, 7, 8, 26, 38, and 52) were not usable for various reasons indicated in Table 4.1, and hence, 50 rock samples are considered usable.

4.2   Master Summary of Tested Samples

The 56 rock samples with their ages, formations, rock types, depths, and locations are summarized in Table 4.1, and 50 samples with a sufficient rock core length for rock specimen preparation are considered usable. The information about the individual samples obtained are shown in Table 4.1. Representative rocks from all three geological eras, Precambrian, Mesozoic, and Cenozoic, are collected and tested in this project. The samples also represent all three geological rock types: igneous, sedimentary, and metamorphic.

The samples collected are a mixture of surface boulders and rock cores obtained from a depth up to 65 m, so that the strength properties of rocks can be compared for all major civil engineering applications. The number of samples based on rock types, ages, and depths are shown in Tables 4.2, 4.3, and 4.4, respectively. Table 4.2 shows 13 rock types collected and tested in this project, their geological type, and the count of each rock type. Table 4.3 shows the list of geological era, their respective geological era, and the count of rock samples from each geological era. Table 4.4 shows the number of rock samples that are obtained either as a surface boulder or from a subsurface depth by various coring methods.
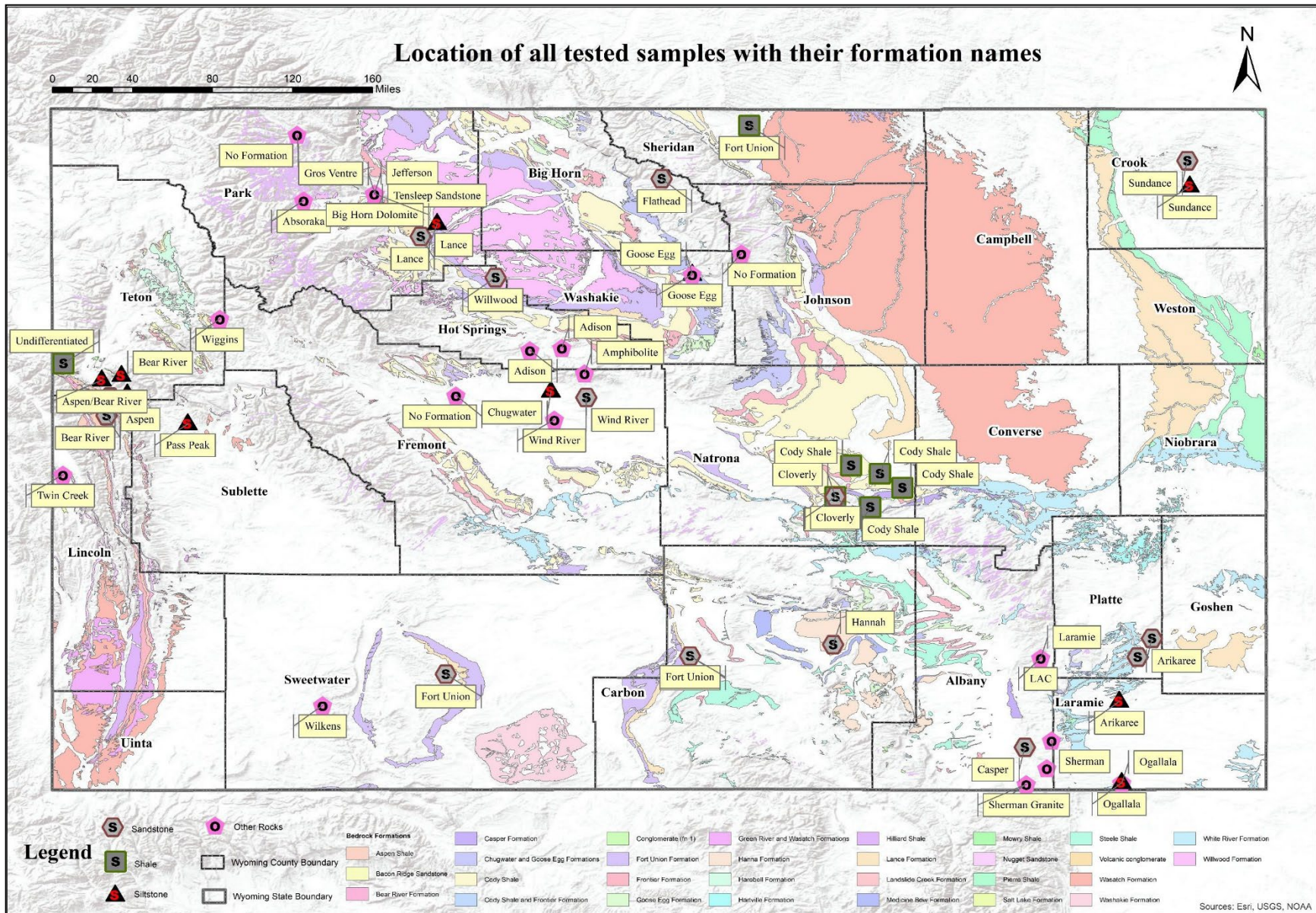
Figure 4.1 Location of tested samples with their formation names

Table 4.1 Summary of 56 rock samples with different identifications, ages, formations, types, depths, and locations

Sample ID	Age	Formation	Rock Type	Depth (ft)	Location	Comments
1	Miocene	Ogallala	Claystone	65.03 - 6.28	Terry Ranch Road	
2	Cretaceous	Cody Shale	Shale	51.02 - 3.02	Walsh Drive, Casper	
3	Jurassic	Morrison	Shale	6.30 - 9.19	Narrow Backslope	Dried out and short length of cores
4	Cretaceous	Undifferentiated	Shale	43.01 - 5.02	Mail Cabin Landslide	
5	Permian	Goose Egg	Siltstone	11.71- 12.99	Toms Pit	
6	Jurassic	Sundance	Siltstone	26.51 - 33.01	Lower Red Canyon Slide	
7	Cretaceous	Aspen/Bear River	Siltstone	39.50 - 44.23	Bear River Slide 3	Dried out and short length of cores
8	Eocene	Pass Peak	Clayey Siltstones	45.02 - 57.81	Spud Slide	Dried out and short length of cores
9	Oligocene	Wiggins	Volcanic Breccia	212.67- 214.68	The Rock, Togwotee Pass	
10	Cretaceous	Cloverly	Conglomerate	91.93 - 95.44	Narrows Backslope	
11	Eocene	Wasatch	Siltstone	58.40 - 71.53		
12	Paleogene	White River	Siltstone	71.13 - 75.63		
13	Cretaceous	Aspen/Bear River	Siltstone	34.22 - 36.22	Swinging Bridge	
14	Cretaceous	Cody Shale	Shale	58.83 - 78.02	North Platte River Bridge	
15	Cretaceous	Cody Shale	Shale	43.01 - 53.02	Walsh Drive	
16	Cambrian	Flathead	Sandstone	10.01 - 65.52	Ski Area Slide	
17	Cretaceous	Cloverly	Sandstone	98.04 - 100.23	Narrows Backslope	
18	Jurassic	Sundance	Sandstone	2.99 - 58.01	Lower Red Canyon Slide	
19	Cretaceous	Aspen/Bear River	Sandstone	20.01 - 41.01	Hoback Jct. Bridge	
20	Cretaceous	Aspen/Bear River	Sandstone	26.51 - 35.21	Hoback Jct. Bridge	
21	Paleocene	Fort Union	Shale	48.00 - 53.02	Tongue River Bridge	

Table 4.1 Continued

Sample ID	Age	Formation	Rock Type	Depth (ft)	Location	Comments
22	Cretaceous	Cody Shale	Shale	51.02 - 59.52	F-St. Bridge over North Platte	
23	Cretaceous	Lance	Graywacke Sandstone	Surface	MP 65.8, US 120, South of Cody	
24	Cretaceous	Lance	Siltstone	Surface	MP 65.8, US 120, South of Cody	
25	Mississippian	Madison Limestone	Limestone	Surface	MP 122.5, US20/WY789, Wind River Canyon	
26	Eocene	Willwood	Sandstone	Surface	Paddy Pit, Hot Springs County	Rock boulder broke during drilling and no cores were extracted
27	Permian	Goose Egg	Limestone	Surface	Toms Pit, Washakie County	
28	Precambrian	No Designation	Granite	Surface	MP 7.6, WY 296	
29	Archean	No Designation	Hornblende Gneiss	Surface	MP 56, US16, Powder River Basin	
30	Cretaceous	Bear River	Siltstone	38.03 - 44.00	Bear River Slide	
31	Pennsylvanian	Tensleep Sandstone	Sandstone	Surface	MP 44.3, US16/14/20 West of Cody	
32	Lower Miocene	Arikaree	Coarse Sandstone	Surface	TY Bluff Road	
33	Lower Miocene	Arikaree	Medium Sandstone	Surface	I25 cut at Chugwater	
34	Lower Miocene	Arikaree	Siltstone	Surface	East I25 Frontage Road, MP 38	
35	Paleogene	Hanna	Siltstone	187.05-190.07	Hanna Power Pole	
36	Triassic	Chugwater	Siltstone	Surface	US20/WY789, MP 112.9, Red Bed Slide	
37	Miocene	Ogallala	Siltstone	81.04 - 96.03	Terry Ranch Road, Cheyenne	
38	Paleogene	Hanna	Claystone	31.01-44.00, 66.01 - 74.02	Hanna Power Pole	Only two testable samples
39	Paleogene	Hanna	Fine Sandstone	143.05 - 157.06	Hanna Power Pole	
40	Paleogene	Hanna	Shale	106.04 - 116.05	Hanna Power Pole	
41	Paleogene	Hanna	Coarse Sandstone	76.02 - 86.03	Hanna Power Pole	
42	Jurassic	Twin Creek	Limestone	Surface	MP 94.7, US89, North of Afton	

Table 4.1 Continued

43	Eocene	Wind River	Medium Sandstone	Surface	MP 95.5, US20/26, East of Shoshoni	
44	Eocene	Wind River	Silty Claystone	Surface	MP 95.5, US20/26, East of Shoshoni	
45	Ordovician	Big Horn Dolomite	Dolostone	Surface	MP 45.05, US14/16/20	
46	Cambrian	Gros Ventre	Limestone Pebble Conglomerate	Surface	MP 45.1, US14/16/21	
47	Devonian	Jefferson Formation	Limestone	Surface	MP 44.84, US14/16/22	
48	Eocene	Absoraka Supergroup	Welded Tuff	Surface	MP 23.6, US 14/16/23	
49	Eocene	Bridger	Medium Sandstone	Surface	MP 3.0, WY530	
50	Paleocene	Fort Union	Medium Sandstone	Surface	MP 131, I-80	
51	Paleocene	Fort Union	Fine Sandstone	Surface	MP 206, I-80	
52	Proterozoic	Sherman Granite	Granite Pegmatite	Surface	MP 422.6, US 287	Rock boulder broke during drilling and no cores were extracted
53	Proterozoic	Lac Wheatland	Anthracite	Surface	MP 25, WY34	
54	Archean	No Designation	Amphibolite	Surface	MP 116.6, US20	
55	Proterozoic	Sherman Granite	Granite	Surface	MP 28.8, WY210	
56	Permian	Casper	Sandstone	Surface	MP 323.6, I-80	

*Sample ID refers to the order in which samples were obtained and tested; M–Medium; MP–Mile post.

Table 4.2 shows that sandstone (30.36%), siltstone (23.24%) and shale (14.29%) make up the majority of rock samples used in this study; hence most of the rock samples are sedimentary rocks. Other notable rock types encountered are limestone (7.14%), granite (5.36%), and claystone (5.36%). Other less notable rock types are amphibolite (1.79%), anorthosite (1.79%), conglomerate (3.57%), dolostone (1.79%), gneiss (1.79%), volcanic breccia (1.79%), and welded tuff (1.79%).

Table 4.2 Summary of rock sample counts based on rock types

Rock Type	Geological Rock Type	Count	Weightage (%)
Amphibolite	Metamorphic	1	1.79
Anorthosite	Igneous	1	1.79
Claystone	Sedimentary	3	5.36
Conglomerate	Sedimentary	2	3.57
Dolostone	Sedimentary	1	1.79
Gneiss	Metamorphic	1	1.79
Granite	Igneous	3	5.36
Limestone	Sedimentary	4	7.14
Sandstone	Sedimentary	17	30.36
Shale	Sedimentary	8	14.29
Siltstone	Sedimentary	13	23.21
Volcanic Breccia	Igneous	1	1.79
Welded Tuff	Igneous/Sedimentary (Pyroclastic)	1	1.79

Based on the geological age of rocks summarized in Table 4.3, most rock samples are from the Cretaceous Period (26.79%), followed by Eocene (12.5%), Paleogene (10.71%), Miocene (8.93%), Jurassic (7.14%), Permian (5.36%), and Paleocene (5.36%). This suggests that most rock samples are from the Mesozoic Era (250-66 million years ago) and the Cenozoic Era (66 million years ago to present). The Cretaceous Period (135-66 million years ago) is the youngest, whereas the Cambrian Period (570-500 million years ago) is the oldest in the Mesozoic Era, and Pliocene Epoch (5-2 million years ago) is the youngest, whereas Paleocene Epoch (66-58 million years ago) is the oldest in the Cenozoic Era. The details of the geological time scale are shown in Table 2.1.

Table 4.3 Summary of rock sample counts based on geological ages and eras

Rock Age	Geological Era	Count	Weightage (%)
Miocene	Cenozoic	5	8.93
Cretaceous	Mesozoic	15	26.79
Jurassic	Mesozoic	4	7.14
Permian	Paleozoic	3	5.36
Eocene	Cenozoic	7	12.50
Oligocene	Cenozoic	1	1.79
Paleogene	Cenozoic	6	10.71
Paleocene	Cenozoic	3	5.36
Mississippian	Mesozoic	1	1.79
Precambrian	Precambrian	1	1.79
Archean	Precambrian	2	3.57
Pennsylvanian	Mesozoic	1	1.79
Triassic	Mesozoic	1	1.79
Ordovician	Mesozoic	1	1.79
Cambrian	Mesozoic	1	1.79
Devonian	Mesozoic	1	1.79
Proterozoic	Precambrian	3	5.36

The rock samples were collected either as surface boulders or rock cores from drilling. One- or two-inch diameter rock specimens were drilled out from the surface boulders using the drilling machine for testing described in Chapter 3. Table 4.4 indicates that that the number of rock samples collected as surface boulders and the rock cores are almost equal at 48.21% and 51.79%, respectively.

Table 4.4 Summary of rock sample counts based on rock depths

Sample No.	Rock Depth	Count	Weightage (%)
1	Surface	27	48.21
2	Rock cores from subsurface drilling	29	51.79

5. MECHANICAL PROPERTIES AND PREDICTION EQUATIONS

5.1 Research Methods and Analysis

The prediction equation development is done using OriginPro 2022b, CurveExpert Professional 2.7.5, and Microsoft Excel. OriginPro is a data analysis and graphing software with advanced customization capacities such as fitting multiple datasets, weighted fitting, residual analysis, and fitting comparison of the nonlinear fitting analysis. CurveExpert Professional is a cross-platform solution similar to that of OriginPro, which helps in data analysis and curve fitting.

Linear regression models and nonlinear regression models can be modeled using built-in fitting function or user-defined fitting function. The best fit from CurveExpert is found by comparing the data to each built-in and user-defined models to choose the best curve. The ranking of the models is based on scores of correlation coefficient, standard error, or coefficient of determination. Akaike information criterion (AIC) (Akaike 1974) and Bayesian information criterion (BIC) (Schwarz 1978) are selected as the comparison criteria since they are widely used for nonlinear prediction equations that are proposed for describing the strength relationships. The equations used to calculate these statistical criteria are described in Masud et al. (2022) and given by Eq. a, b, and c. Residual standard error (RSE) and root mean square error (RMSE) is also implemented to facilitate the comparison. The nonlinear prediction equations are developed using the statistical software RStudio version 2022.02.2 (R Core Team 2022).

$$L\left(\hat{\beta}, \hat{\sigma}^2 | \underline{y}\right) = \prod_{i=1}^{n} \frac{1}{\sqrt{2\pi\hat{\sigma}^2}} exp\left(-\frac{1}{2\hat{\sigma}^2}\left(y_i - f\left(x_i, \hat{\underline{\beta}}\right)\right)^2\right) \tag{a}$$

$$AIC = -2\ln\left(L\left(\hat{\beta}, \hat{\sigma}^2 | \underline{y}\right)\right) + 2(p+1) \tag{b}$$

$$BIC = -2\ln\left(L\left(\hat{\beta}, \hat{\sigma}^2 | \underline{y}\right)\right) + \ln(n)(p+1) \tag{c}$$

5.2 Analysis Dataset

5.2.1 Shales

Among the eight shale samples tested, all samples were obtained as rock cores drilled out from various projects around the state. Table 5.1 shows the description of the tested shale samples. The uniaxial compressive strength (UCS) is a standard strength parameter for an intact rock and is widely used in engineering projects to evaluate structure stability (Gholami & Fakhari, 2017). The UCS test results described in this chapter are primarily based on unpublished test data of rock cores obtained from the state of Wyoming. Wyoming shales are from a shallow depth of below 98.4 feet. The UCS and triaxial test results are summarized in Table 5.2.

Table 5.1 Summary of tested shale samples

Sample ID	Age	Formation	Specimen ID	Depth (ft)	Moisture Content (%)	Specific Gravity	Porosity (%)
2	Cretaceous	Cody shale	2a	51.02	12.47	2.730	31.000
			2b	51.41	12.47		30.000
			2c	51.81	12.47		29.000
			2d	50.20	12.47		30.000
3	Jurassic	Morrison	N/A	N/A	N/A	N/A	N/A
4	Cretaceous	Undifferentiated	4a	44.00	10.16	2.650	29.200
			4b	43.01	10.16		27.800
			4c	43.41	10.16		35.500
14	Cretaceous	Cody Shale	14a	73.76	20.37	2.477	23.800
			14b	74.28	20.37		23.800
			14c	76.02	20.37		23.200
			14d	77.27	20.37		24.700
			14e	78.02	20.37		24.100
			14f	78.45	20.37		24.500
			14g	70.51	20.37		23.800
15	Cretaceous	Cody Shale	15a	43.60	13.26	2.529	26.900
			15b	46.52	13.26		21.900
			15c	47.02	13.26		21.000
			15d	47.80	13.26		20.100
			15e	49.90	13.26		24.400
			15f	50.92	13.26		23.100
			15g	51.61	13.26		24.100
			15h	52.20	13.26		23.800
21	Paleocene	Fort Union	21a	48.03	22.24	2.536	36.240
			21b	48.82	22.24		36.500
			21c	49.22	22.24		38.280
22	Cretaceous	Cody Shale	22a	Surface	11.59	2.624	24.397
			22b	Surface	11.59		21.417
			22c	Surface	11.59		22.954
			22d	Surface	11.59		22.242
			22e	Surface	11.59		22.654
40	Paleogene	Hanna	40a	106.44	5.01	N/A	12.940
			40b	107.22	5.01		13.200
			40c	108.34	5.01		12.760

*Specimen ID refers to the individual test specimen ; N/A refers to unavailability of test specimen

Table 5.2 Summary of test results of tested shales

Sample ID	Formation	S ID	σ_c (Psi)	σ_p (Psi)	β (deg)	E (ksi)	Failure Behavior	Failure Angle (deg)
2	Cody shale	2a	42.05	198.65	0	7.25	Ductile	90
		2b	82.65	249.40	0	5.80	Ductile	30
		2c	59.45	218.95	0	5.80	Ductile	90
		2d	0	158.05	0	2.90	Ductile	90
3	Morrison	N/A	N/A	N/A	N/A	N/A	N/A	N/A
4	Undifferentiated	4a	43.5	184.15	N/A	10.15	Ductile	60
		4b	78.3	182.70	N/A	4.35	Ductile	90
		4c	59.45	152.25	N/A	2.90	Ductile	90
14	Cody Shale	14a	145	388.60	N/A	29068.15	Brittle	50
		14b	580	859.85	N/A	24926.95	Brittle	50
		14c	0	484.30	N/A	30857.45	Brittle	10
		14d	290	633.65	N/A	28994.20	Brittle	75
		14e	1160	1660.25	N/A	40644.95	Brittle	90
		14f	1450	1824.10	N/A	21993.6	Brittle	80
		14g	0	269.70	N/A	12136.5	Brittle	80
15	Cody Shale	15a	145	250.85	N/A	1474.65	Ductile	80
		15b	580	838.10	N/A	11234.6	Transitional	60
		15c	290	694.55	N/A	27687.75	Transitional	50
		15d	290	696	N/A	29842.45	Transitional	45
		15e	580	729.35	N/A	9607.7	Ductile	65
		15f	435	556.80	N/A	4178.9	Brittle	20
		15g	1200	1328.20	N/A	5043.1	Transitional	45
		15h	1450	1596.45	N/A	4148.45	Transitional	75
21	Fort Union	21a	20.3	82.65	N/A	NA	Ductile	60
		21b	24.65	100.05	N/A	NA	Ductile	60
		21c	59.45	113.10	N/A	NA	Ductile	60
22	Cody Shale	22a	580	871.45	90	14.5	Transitional	60
		22b	1450	1864.70	90	30.45	Brittle	45
		22c	145	833.75	90	31.9	Brittle	60
		22d	870	1452.90	90	36.25	Brittle	65
		22e	145	426.30	90	10.15	Transitional	80
40	Hanna	40a	0	4670.45	N/A	1116.5	Brittle	70
		40b	580	11842.1	N/A	780.1	Brittle	80
		40c	1450	12893.4	N/A	1425.35	Brittle	45

*S ID= Specimen ID; σ_c = Confining stress; σ_p = Peak stress; β= Bedding angle; S=Shear; TS=Tensile Splitting; MTS=Multiple Tensile Splitting.

Table 5.3 presents the Mohr-Coulomb parameters of the tested shales. The lowest UCS is observed in shale from undifferentiated formation of Cretaceous Period, and friction angle is lowest in Cody Shale formation of Cretaceous Period. The greatest difference between the UCS and cohesion is observed in the Hanna formation of the Paleogene Period, whereas the least difference is seen in undifferentiated formations of the Cretaceous Period. The difference is due to the contribution of friction angle.

The intact rock material constant (mi) values for all the shale samples are provided in Table 5.4 along with the cohesion (c), friction angle (φ), and tensile strength (σ_t) based on Hoek and Brown (HB) criteria. Hoek & Brown (1997) and Marinos & Hoek (2001) provided the range of mi value of shale as 6 ± 2. However, we observed that the calculated values of mi range from 0.28 to 21.05, significantly lower and higher than the proposed range. Hoek & Brown (1997) reported that the value of mi can change significantly with variations in the rock bedding angle as the failure will occur along a weakness plane. The reason for variation observed could be because the values reported are for intact rock specimens, which are tested normal to bedding whereas the intact rock specimens tested in this project do not show any apparent beddings.

Table 5.3 Mohr-Coulomb results of tested shales

Sample ID	Formation	UCS, measured (Psi)	Cohesion, c (Psi)	Friction Angle, φ (deg)
2	Cody Shale	153.7	50.75	23
3	Morrison	N/A	N/A	N/A
4	Undifferentiated	46.4	23.2	13
14	Cody Shale	269.7	127.6	5
15	Cody Shale	145	44.95	2
21	Fort union	N/A	7.25	
22	Cody Shale	195.75	98.6	10
40	Hanna	4670.45	1149.85	44

*N/A indicate no specimen for testing.

Table 5.4 Hoek and Brown results of tested shales

Sample ID	Formation	m_i (measured)	C (Psi)	φ (deg)	σ_t (Psi)
2	Cody Shale	2.86	53.65	21.00	53.65
3	Morrison	N/A	N/A	N/A	N/A
4	Undifferentiated	2.32	18.85	13.00	20.3
14	Cody Shale	0.28	131.95	1.00	961.35
15	Cody Shale	1.64	30.45	48.00	88.45
21	Fort union	N/A	N/A	N/A	N/A
22	Cody Shale	1.74	81.2	12.00	113.1
40	Hanna	21.05	1087.5	44.00	220.4

*C=Cohesion; σ_t=Tensile strength; ϕ=Friction angle; m_i=HB parameter; N/A=No specimen Available for testing /not enough tests for calculations.

5.2.2 Siltstone

A total of 42 siltstone samples from 11 locations in Wyoming are tested for UCS and used in the triaxial tests. Most siltstone samples are collected from depths of 20 to 92 feet, and three surface samples are collected for testing. The siltstones have moisture contents (w) ranging from 0.57% to 21% and porosity (ϕ) from 1.5% to 43.5%. In addition, historical UCS test data from WYDOT for 11 siltstone formations are also included in the analyses. Table 5.5 summarizes the properties of tested siltstones. A series of uniaxial compressive strength, triaxial, porosity, and specific gravity tests were conducted on these samples, and the results in terms of Mohr-Coulomb failure parameters, HB failure parameters, and elastic properties are discussed in the following subsections. Table 5.6 summarizes the test results of the siltstone samples.

Table 5.5 Summary of tested siltstone samples

Sample ID	Age	Formation	Specimen ID	Depth (ft)	Moisture Content (%)	Specific Gravity	Porosity (%)
5	Permian	Goose Egg	5a	38.32	0.57	2.67	21.660
			5b	39.73	0.57		20.600
6	Jurassic	Sundance	6a	85.27	5.32	2.62	24.086
			6b	86.55	5.32		25.491
			6c	101.74	5.32		28.486
			6d	103.02	5.32		26.202
7	Cretaceous	Aspen/Bear River	N/A	N/A	N/A	N/A	N/A
8	Eocene	Pass Peak	N/A	N/A	N/A	N/A	N/A
11	Eocene	Wasatch	11a	190.33	22.25	2.69	36.158
			11b	191.61	22.25		35.572
			11c	193.22	22.25		35.944
			11d	194.86	22.25		31.340
			11e	198.17	22.25		31.811
			11f	203.13	22.25		31.786
			11g	201.42	22.25		32.487
			11h	205.06	22.25		31.619
			11i	207.00	22.25		31.813
12	Paleogene	White River	12a	233.28	N/A	N/A	N/A
			12b	241.78	N/A		N/A
			12c	248.01	N/A		N/A
13	Cretaceous	Aspen/Bear River	13a	112.18	1.48	N/A	2.943
			13b	113.79	1.48		5.729
			13c	115.82	1.48		2.227
			13d	117.46	1.48		2.096
24	Cretaceous	Lance	24a	Surface	1.30	N/A	3.430
			24b	Surface	1.69		4.400
			24c	Surface	1.34		3.690
30	Cretaceous	Bear River	30a	38.09	1.32	N/A	1.490
			30b	38.58	1.10		1.820
			30c	39.40	1.23		1.740
34	Lower Miocene	Arikaree	34a	Surface	1.95	N/A	12.960
			34b	Surface	3.01		13.180
			34c	Surface	3.00		12.800
35	Paleogene	Hanna	35a	187.25	1.53	N/A	4.250
			35b	187.84	1.55		4.540
			35c	188.26	1.73		4.380
			35d	188.76	1.75		4.050
			35e	189.35	1.68		4.020
36	Triassic	Chugwater	36a	Surface	0.67	N/A	7.810
			36b	Surface	0.58		6.700
			36c	Surface	0.62		6.970
37	Miocene	Ogallala	37a	82.22	21.29	N/A	43.480
			37b	82.81	21.29		42.660
			37c	84.22	21.29		42.630

*Specimen ID refers to the individual test specimen of the sample; N/A refers to unavailability of test specimen

Table 5.6 Summary of test results of siltstone

ID	Formation	S ID	σ_c (Psi)	σ_p (Psi)	β, deg	E (ksi)	Failure	Failure
5	Goose Egg	5a	145	4512.4	90	29	Brittle	75
		5b	1450	6052.3	90	29	Brittle	70
6	Sundance	6a	145	1336.9	90	29	Brittle	80
		6b	1450	2827.5	90	14.5	Brittle	60
		6c	580	2489.6	90	14.5	Brittle	60
		6d	1450	3368.3	90	14.5	Brittle	70
7	Aspen/Bear River	N/A	N/A	N/A	N/A	N/A	N/A	N/A
8	Pass Peak	N/A	N/A	N/A	N/A	N/A	N/A	N/A
11	Wasatch	11a	0	62.35	N/A	14.5	Ductile	30
		11b	42	118.9	N/A	14.5	Ductile	30
		11c	0	37.7	N/A	14.5	Ductile	30
		11d	78.3	178.35	N/A	14.5	Ductile	45
		11e	0	104.4	N/A	1268.46	Ductile	30
		11f	320	442.25	N/A	1709.41	Ductile	60
		11g	160	232	N/A	1855.42	Ductile	45
		11h	1450	1612.4	N/A	706.01	Ductile	45
		11i	160	276.95	N/A	1109.98	Ductile	60
12	White River	12a	104.4	388.6	N/A	867.53	Ductile	N/A
		12b	20.3	197.2	N/A	N/A	Ductile	N/A
		12c	40.6	243.6	N/A	N/A	Ductile	N/A
13	Aspen/Bear River	13a	1450	19860.6	45	2032.47	Brittle	90
		13b	580	23675.6	15	1856.29	TN	45
		13c	2900	32158.1	90	1927.49	TN	90
		13d	145	17814.7	90	1105.48	Brittle	90
24	Lance	24a	0	3220.45	N/A	1519.17	Brittle	90
		24b	580	11056.2	N/A	2055.81	TN	45
		24c	1450	15329.4	N/A	4810.38	Ductile	45
30	Bear River	30a	145	11714.5	N/A	9876.97	Brittle	90
		30b	580	13817.0	N/A	2136.58	Brittle	90
		30c	0	11811.7	N/A	13.78	Brittle	90
34	Arikaree	34a	580	6504.7	N/A	14.935	Ductile	45
		34b	1450	11961.0	N/A	23.2	Ductile	45
		34c	0	2485.3	N/A	7283.21	Brittle	90
35	Hanna	35a	0	1120.85	N/A	6524.13	Brittle	45
		35b	592	8301.25	N/A	4320.28	Brittle	60
		35c	0	4861.85	N/A	5672.11	Brittle	90
		35d	1450	13512.5	N/A	902.48	Ductile	90
		35e	580	4112.2	N/A	1642.42	Ductile	45
36	Chugwater	36a	0	2395.4	N/A	2329.43	Brittle	90
		36b	1450	8972.6	N/A	2511.4	TN	90
		36c	580	5127.2	N/A	2154.99	TN	90
37	Ogallala	37a	59.45	72.5	N/A	2906.24	Ductile	N/A
		37b	40.6	53.65	N/A	1046.76	Ductile	N/A
		37c	65.25	85.55	N/A	6140.17	Ductile	N/A

*S ID= Specimen ID; σ_c = Confining stress; σ_p = Peak stress; β= Bedding angle; S=Shear; TS=Tensile Splitting; MTS=Multiple Tensile Splitting; TN= Transitional; N/A= Test data not available.

Table 5.7 represents Mohr-Coulomb failure parameters. The UCS ranges from 62.4 to 17,731 Psi, the cohesion (C) ranges from 29 to 4000 Psi, and the friction angle ranges from 5 to 49 degrees. All formations with larger friction angles have higher cohesion values. Table 5.8 represents the HB failure parameters. The HB criterion is applied by taking the HB parameters a=0.5 and s=1 to estimate the cohesion and friction angle. The calculated mi values in Table 5.8 are comparable to the values proposed by Hoek and Brown (1997) for siltstones as 7± 2, and hence are used in the calculation of the cohesions and friction angles.

Table 5.7 Mohr-Coulomb results of tested siltstones

Sample ID	Formation	Measured UCS (Psi)	Calculated UCS (Psi)	Cohesion, c (Psi)	Friction Angle, φ (deg)
5	Goose Egg	2520.1	2520.1	1985.05	5
6	Sundance	800.4	800.4	400.2	17
7	Aspen/Bear River	N/A	N/A	N/A	N/A
8	Pass Peak	N/A	N/A	N/A	N/A
11	Wasatch	62.35	62.35	29	8
12	White River	153.7	153.7	50.75	23
13	Aspen/Bear River	17730.6	17730.6	4000.55	43
24	Lance	3220.45	3220.45	1000.5	49
30	Bear River	11811.7	11811.7	3049.35	36
34	Arikaree	2485.3	2485.3	580	47
35	Hanna	4861.85	4861.85	1149.85	45
36	Chugwater	2396.85	2396.85	549.55	40
37	Ogallala	N/A	N/A	N/A	N/A

*UCS= Uniaxial compressive strength (MPa); N/A = no specimen for testing.

Table 5.8 Hoek and Brown results of tested siltstones

Sample ID	Formation	m_i	c (Psi)	φ (deg)	σ_t (Psi)
5	Goose Egg	4.73	1068.65	11.00	533.6
6	Sundance	3.55	298.7	18.00	224.75
7	Aspen/Bear River	N/A	N/A	N/A	N/A
8	Pass Peak	N/A	N/A	N/A	N/A
11	Wasatch	0.73	29	2.00	84.1
12	White River	2.86	53.65	21.00	53.65
13	Aspen/Bear River	8.39	4677.7	38.00	2111.2
24	Lance	42.67	682.95	48.00	75.4
30	Bear River	4.61	3552.5	31.00	2562.15
34	Arikaree	26.42	539.4	47.00	94.25
35	Hanna	16.04	1106.35	45.00	303.05
36	Chugwater	12.47	607.55	39.00	191.4
37	Ogallala	N/A	N/A	N/A	N/A

*C=Cohesion; σ_t=Tensile strength; ϕ=Friction angle; m_i=HB parameter; N/A=No specimen available for testing/not enough tests for calculation.

5.2.3 Other Rock Types

Among the 17 rock samples tested, 14 were obtained as surface boulders, and three samples were obtained as rock cores drilled out from various projects around the state. Table 5.9 shows the description of the tested rock samples. The test specimens are prepared at either a 1-inch diameter or 2-inch diameter. The length to diameter ratio (L/D) ratio of the test specimen is maintained from 2 to 2.5. The top and bottom of the test specimen should be parallel to each other and perpendicular to the longitudinal axis. A series of uniaxial compressive strength, triaxial, porosity, and specific gravity tests were conducted on these samples, and the results in terms of Mohr-Coulomb failure parameters, HB failure parameters, and elastic properties are analyzed. Table 5.10 shows the results of the tested rock samples.

Table 5.9 Summary of tested rock samples

Sample ID	Age	Formation	Rock Type	S ID	Depth (ft)	Moisture Content (%)	Specific Gravity	Porosity (%)
1	Miocene	Ogallala	Claystone	1a	65.03	15.90	2.580	28.00
				1b	65.42	15.90		28.00
				1c	65.82	15.90		28.00
9	Oligocene	Wiggins	Volcanic Breccia	9a	212.87	3.83	2.680	23.95
				9b	213.27	3.83		19.23
				9c	213.66	3.83		20.52
				9d	214.25	3.83		24.29
10	Cretaceous	Cloverly	Conglomerate	10a	91.93	1.69	2.560	13.24
				10b	92.33	1.69		15.34
				10c	92.72	1.69		13.25
				10d	95.02	1.69		14.39
25	Mississippian	Madison Limestone	Limestone	25a	Surface	2.18	N/A	7.93
				25b	Surface	2.18		2.60
				25c	Surface	2.18		3.23
27	Permian	Goose Egg	Limestone	27a	Surface	1.84	N/A	12.41
				27b	Surface	1.84		11.96
				27c	Surface	1.84		12.18
				27d	Surface	1.84		12.23
28	Precambrian	No Designation	Granite	28a	Surface	0.23	N/A	0.81
				28b	Surface	0.23		0.72
				28c	Surface	0.23		0.98
29	Archean	No Designation	Hornblende Gneiss	29a	Surface	0.38	N/A	1.08
				29b	Surface	0.38		0.74
				29c	Surface	0.38		0.89
38	Paleogene	Hanna	Claystone	38a	Surface	6.58	N/A	7.86
				38b	Surface	6.58		7.45
44	Eocene	Wind River	Silty Claystone	44a	Surface	7.85	N/A	5.41
				44b	Surface	7.85		5.03
				44c	Surface	7.85		4.96
45	Ordovician	Big Horn Dolomite	Dolostone	45a	Surface	1.41	N/A	8.50
				45b	Surface	1.41		8.27
				45c	Surface	1.41		8.09
46	Cambrian	Gros Ventre	Limestone Pebble Conglomerate	46a	Surface	2.23	N/A	0.82
				46b	Surface	2.23		1.01
				46c	Surface	2.23		1.47
				46d	Surface	2.23		1.10

Table 5.9 continued

				47a	Surface	1.87		2.12
47	Devonian	Jefferson Formation	Limestone	47b	Surface	1.87	N/A	1.55
				47c	Surface	1.87		1.90
				48a	Surface	0.15		13.62
48	Eocene	Absoraka Supergroup	Welded Tuff	48b	Surface	0.15	N/A	13.08
				48c	Surface	0.15		13.01
52	Proterozoic	Sherman Granite	Granite Pegmatite	N/A	Surface	N/A	N/A	N/A
				53a	Surface	3.15		5.07
53	Proterozoic	LAC	Anthracite	53b	Surface	3.15	N/A	4.56
				53c	Surface	3.15		4.68
				54a	Surface	2.46		5.26
54	Archean	No Designation	Amphibolite	54b	Surface	2.46	N/A	7.42
				54c	Surface	2.46		5.78
				55a	Surface	1.24		3.49
55	Proterozoic	Sherman Granite	Granite	55b	Surface	1.24	N/A	4.85
				55c	Surface	1.24		4.38

*S ID refers to the individual test specimen of the sample; N/A refers to unavailability of test specimen/no tests conducted.

Table 5.10 Summary of test results of tested rocks

Sample ID	Formation	Rock Type	σ_c (Psi)	σ_p (Psi)	E (Ksi)	Failure Mode	Failure Behavior	Failure Angle (deg)
			0	59.45	1.45	S	Ductile	45
1	Ogallala	Claystone	46.4	143.55	1.45	S	Ductile	45
			82.65	185.6	2.9	S	TN	65
			0	1110.7	2650.6	S	Brittle	55
9	Wiggins	Volcanic Breccia	115	1322.4	1947.35	MTS	Brittle	90
			580	4258.6	2256.2	S	Brittle	25
			1450	8259.2	1609.5	TS	Brittle	90
			0	1632.7	1711	TS	Brittle	60
10	Cloverly	Conglomerate	147	3094.3	1277.45	TS	Brittle	90
			580	4928.5	2689.75	TS	Brittle	90
			1450	4116.5	2099.6	TS	Brittle	90
			145	5598.4	2218.5	TS	TN	90
25	Madison Limestone	Limestone	580	13057.25	2027.1	TS	TN	90
			1450	4593.6	11304.2	TS	Brittle	90
			0	8884.15	4293.5	MTS	Brittle	90
27	Goose Egg	Limestone	145	9719.35	2270.7	TS	TN	90
			290	9135	4719.8	TS	TN	90
			1160	17333.3	4676.3	MTS	Brittle	90
			0	12755.65	4989.5	MTS	Brittle	90
28	No Designation	Granite	870	22418.45	3105.9	TS	TN	90
			1450	29040.6	5070.7	S	TN	80
			0	5318.6	6504.7	TS	Brittle	90
29	No Designation	Hornblende Gneiss	145	9452.55	14646.5	S	Brittle	70
			1450	22298.1	2438.9	S	Brittle	90
38	Hanna	Claystone	0	2988.45	662.7	TS	TN	90
			580	7325.4	519.1	TS	TN	90

Table 5.10 continued

S ID	Formation	Rock Type	σ$_c$	σ$_p$				
44	Wind River	Silty Claystone	0	1232.5	566.9	S	TN	45
			580	7322.5	635.1	S	Brittle	60
			1450	10096.35	651.1	S	TN	75
45	Big Horn Dolomite	Dolostone	0	3353.85	1425.4	TS	TN	90
			580	11536.2	1100.6	S	Brittle	60
			1450	5589.75	1116.5	MTS	Brittle	90
46	Gros Ventre	Limestone Pebble Conglomerate	0	5901.5	2102.5	TS	Brittle	90
			582.9	5950.8	2427.3	S	Brittle	60
			870	13777.9	1248.5	S	Brittle	60
			1450	3926.6	2920.3	TS	TN	90
47	Jefferson Formation	Limestone	0	1642.85	2228.7	TS	Brittle	90
			580	7651.65	974.4	MTS	Brittle	90
			1450	21277.3	2920.3	MTS	TN	90
48	Absoraka Supergroup	Welded Tuff	0	3063.85	2762.3	MTS	TN	90
			580	7792.3	3027.6	TS	Brittle	90
			1450	10814.1	3819.3	MTS	Brittle	90
52	Sherman Granite	Granite Pegmatite	N/A	N/A	N/A	N/A	N/A	N/A
53	Lac Wheatland	Anthracite	0	6417.7	3071.1	S	Brittle	45
			580	9139.35	2826.1	TS	Ductile	90
			1450	20975.7	2117	S	TN	60
54	No Designation	Amphibolite	0	8775.4	6356.8	TS	Brittle	90
			580	16608.3	2698.5	TS	TN	90
			1450	26768.45	4819.8	MTS	TN	90
55	Sherman Granite	Granite	0	3881.65	2466.5	TS	Brittle	90
			580	9607.7	823.6	MTS	Ductile	90
			1450	18165.6	1160	S	TN	60

*S ID= Specimen ID; σ$_c$ = Confining stress; σ$_p$ = Peak stress ; S=Shear; TS=Tensile Splitting; MTS=Multiple Tensile Splitting; TN= Transitional; N/A= Test data not available.

UCS, c, and φ for other rock types are summarized in Table 5.11. The lowest UCS and cohesion in limestone are observed from the Jefferson formation of the Devonian Period, and the lowest friction angle was observed from the Madison formation of Mississippian Period. Similarly, for claystone, the lowest UCS, cohesion, and friction angle are observed from the Ogallala formation of the Miocene Epoch. The greatest difference between the UCS and cohesion for limestone is observed in the Madison formation of the Permian Period, with cohesion being 85% lower than UCS. In the Jefferson formation of the Devonian Period, cohesion is 75% lower than UCS.

Similarly, for claystone, the greatest difference between the UCS and cohesion is observed in the Ogallala formation of the Miocene Epoch (78%) and the least difference in the Wind River formation of the Eocene Epoch (71%). The difference is due to the contribution of friction angle.

Table 5.11 Mohr-Coulomb results of tested rocks

Sample ID	Age	Rock Type	UCS, measured (psi)	Cohesion, c (Psi)	Friction Angle, φ (deg)
1	Miocene	Claystone	59.45	13.05	25
9	Oligocene	Breccia	1110.7	179.8	43
10	Cretaceous	Conglomerate	1632.7	539.4	40
25	Mississippian	Limestone	4000.55	600.3	6
27	Permian	Limestone	8884.15	1719.7	50
28	Precambrian	Granite	12755.65	2499.8	56
29	Archaeon	Gneiss	5318.6	1000.5	57
38	Paleogene	Claystone	2988.45	800.4	46
44	Eocene	Claystone	1232.5	349.45	46
45	Ordovician	Dolostone	3353.85	849.7	50
46	Cambrian	Conglomerate	5900.05	1100.55	53
47	Devonian	Limestone	1642.85	449.5	58
48	Eocene	Welded Tuff	3063.85	700.35	44
52	Proterozoic	Granite	N/A	N/A	N/A
53	Proterozoic	Anthracite	6417.7	1300.65	53
54	Archean	Amphibolite	8775.4	1550.05	58
55	Proterozoic	Granite	3881.65	900.45	54

*N/A indicate no specimen for testing.

The non-linear failure criterion proposed by Hoek and Brown (1997) is used to calculate the non-linear shear strength of the tested samples. The HB material constant for intact rock (mi) is calculated using the statistical method proposed by Hoek (2019) based on test results on a principal axis plane. The HB criterion is applied on the intact rock taking the HB parameters, a=0.5 and s=1, to estimate the cohesion and friction angle. The calculation of the material constant mi is conducted from a series of triaxial tests and uniaxial tests performed on the intact rock specimens for each sample. In this process, the major and minor principal stresses of the tested specimens are plotted, and a curve HB line is fitted through the points by substituting a=0.5, s=1, and mb=mi in the generalized HB criterion. Table 5.12 represents Hoek and Brown failure parameters.

The intact rock material constant (mi) values for all the tested rock samples are summarized in Table 5.12 along with the cohesion (c), friction angle (φ), and tensile strength (σ_t). Hoek & Brown (1997) and Marinos & Hoek (2001) recommended the range of mi values of limestone as 12 ± 3, claystone 4 ± 2, granite 32 ± 3, and gneiss 28 ± 5. However, we observed that the calculated values of mi range from 17.42 to 125 for limestone and 1.63 to 46.27 for claystone, which significantly varies from the proposed range. Hoek & Brown (1997) reported that the value of mi can vary significantly with variations in the rock bedding angle as the failure will occur along a weakness plane. The reason for the variations observed could be because the values reported are for intact rock specimens that tested normal to bedding, whereas the intact rock specimens tested in the project do not show any apparent beddings.

Table 5.12 Hoek and Brown results of tested rocks

Sample ID	Age	Rock Type	m_i	c (Psi)	φ (deg)	σ_t (Psi)
1	Miocene	Claystone	1.63	24.65	14.00	37.7
9	Oligocene	Breccia	24.18	365.4	26.00	46.4
10	Cretaceous	Conglomerate	18.33	397.3	42.00	88.45
25	Mississippian	Limestone	53.80	787.35	51.00	73.95
27	Permian	Limestone	17.42	2112.65	43.00	510.4
28	Precambrian	Granite	30.55	2576.65	50.00	417.6
29	Archaean	Gneiss	54.02	858.4	58.00	98.6
38	Paleogene	Claystone	N/A	N/A	N/A	N/A
44	Eocene	Claystone	46.27	319	39.00	27.55
45	Ordovician	Dolostone	39.40	745.3	46.00	85.55
46	Cambrian	Conglomerate	13.30	1742.9	32.00	442.25
47	Devonian	Limestone	125.00	449.5	58.00	208.8
48	Eocene	Welded Tuff	19.19	807.65	38.00	159.5
52	Proterozoic	Granite	N/A	N/A	N/A	N/A
53	Proterozoic	Anthracite	28.39	1068.65	57.00	226.2
54	Archean	Amphibolite	41.99	1816.85	49.00	208.8
55	Proterozoic	Granite	41.93	704.7	54.00	92.8

*C=Cohesion; σ_t=Tensile strength; ϕ=Friction angle; m_i=HB parameter; N/A=No specimen available for testing/not enough tests for calculation.

6. SUMMARY, CONCLUSIONS AND RECOMMENDATIONS

6.1 Summary

This study focuses on understanding the mechanical and deformation behaviors of Wyoming bedrocks to improve the design and construction of transportation infrastructures in the state. To accomplish the objective, 56 samples were tested under different confining stresses. Test rock samples are mostly sandstone (30%), siltstone (23%), shale (14%), and others (33%).

Bedrocks in Wyoming are from different geological eras, and a conscious effort is made to include samples from different eras. The tested samples are mostly from Cretaceous (27%), Eocene (13%), Paleogene (11%), and others. The rock samples are from all three geological rock types: sedimentary (86%), igneous (11%), and metamorphic (3%). The rock samples are obtained as surface boulders (48%) and rock cores from subsurface drilling (52%). The rock specimens prepared for testing are either 1-inch or 2-inch diameter with the height to diameter of two.

Triaxial and uniaxial compression tests are conducted using GCTS RTR-1500 rapid triaxial rock testing equipment on hard rocks and GeoJac triaxial equipment on soft and soil-like rocks. The physical properties like moisture content, porosity, and specific gravity of tested specimens are measured before compression testing. Laboratory compressive tests are performed to measure the stress and strains of each rock specimen, and elastic properties (Young's modulus and Poisson's ratio) are determined from the linear stress-strain relationship. Shear strength parameters, such as cohesion and friction angle, are determined from the Mohr-Coulomb criterion constructed from a series of Mohr's circles. The nonlinear Hoek and Brown criterion is also applied to determine the tensile strength and material constant (m_i) for each rock sample.

This report focuses on presenting the results of laboratory tests and prediction equation analyses to relate mechanical properties to physical properties for claystone, shale, and siltstone. An extensive study is conducted to compile available test data on shale, claystone, and siltstone from the literature for the prediction equation analyses. Two sets of prediction equations are proposed with one based on test data from the literature and Wyoming and another based solely on Wyoming data. Statistical analyses are conducted to evaluate the performance of proposed prediction equations, which are compared against prediction equations from literature based on RMSE.

6.2 Conclusions

The prediction equations developed from this study for UCS, E, and strength parameters of claystone, shale, and siltstone are summarized in Table 6.1.

Table 6.1 Developed prediction equations for UCS, E, and strength parameters of claystone, shale, and siltstone from this study

Rock	Developed Equation	Test Condition	RMSE	Data Source
Shale	$\widehat{UCS} = 6.25\, e^{-\frac{x}{7.66}}$	UC	10.60	Wyoming
	$\widehat{UCS} = 4.81\, (1 - \frac{\phi}{47.5})^{1.7}$	UC	34.43	Wyoming
	$\widehat{UCS} = 0.000015 \times e^{5.354\rho}$	UC	-	Wyoming
	$\hat{E} = 4.9896\, w^{-2.273}$	UC	1.25	Wyoming
	$\hat{E} = 2065.8\, \phi^{-3.604}$	UC		Wyoming
	$\hat{E} = 0.121\, UCS - 0.032$	UC	15.53	Wyoming
	$\hat{E} = 0.00004 \times \rho^{8.801}$	UC	-	Wyoming
	$\hat{E} = 0.266\, x^{-2.106}$	UC	-	Wyoming
	$\hat{E} = 21.83 \times (0.93)^{\phi}$	Triaxial	4.71	Wyoming
Claystone	$\widehat{UCS} = 28.71 e^{-0.251w}$	UC	9.79	Wyoming
	$\widehat{UCS} = 62.29\, e^{-0.17\phi}$	UC	8.23	Wyoming
	$\hat{E} = 1.7407 e^{-0.273w}$	UC	0.74	Wyoming
	$\hat{E} = 3.3678 e^{-0.174\phi}$	UC	0.67	Wyoming
	$\hat{E} = 0.0654 \times UCS + 0.0287$	UC	-	Wyoming
Siltstone	$\widehat{UCS} = 39.18 \times 0.83^{w}$	UC	9.47	Wyoming (All)
	$\widehat{UCS} = 42.99 \times 0.81^{w}$	UC	-	Wyoming (Cretaceous)
	$\widehat{UCS} = 69.40 \times 0.7^{w}$	UC	-	Wyoming (Triassic)
	$\widehat{UCS} = 29.77(1 - \frac{\phi}{47.5})^{2.15}$	UC	15.62	Wyoming (All)
	$\widehat{UCS} = 27.64 - 0.93\phi$	UC	-	Wyoming (Cretaceous)
	$\widehat{UCS} = 48(1 - \frac{\phi}{47.5})^{3.8}$	UC	-	Wyoming (Triassic)
	$\widehat{UCS} = 0.16 \times \rho^{5.387}$	UC	9.81	Wyoming
	$\hat{E} = 4.4725 w^{-1.45}$	UC	0.45	Wyoming
	$\hat{E} = 0.564 e^{-0.658\phi}$	UC	0.78	Wyoming
	$\hat{E} = 0.0255 + 0.0647 \times UCS$	UC	-	Wyoming
	$\hat{E} = 0.0003 e^{3.1359\rho}$	UC	0.45	Wyoming
	$\hat{c} = 32.17 \times \phi^{-0.674}$	Triaxial	2.13	Wyoming
	$\frac{\hat{c}}{\phi} = 542.82 e^{-0.614w}$	Triaxial	-	Wyoming

*UCS= Uniaxial compressive strength (MPa); w= moisture content (%); ϕ= Porosity (%); ρ= Bulk density (g/cm³); x= Axial strain at peak stress (%); PS= Peak Stress; E= Young's modulus (GPa); c= Cohesion (MPa); φ= Friction angle (deg); UC= Uniaxial compression test; Triaxial= Triaxial compression test.

Based on the experimental results and prediction equation studies, the following conclusions are drawn:

(a) <u>**Shale**</u>

- The unconfined compressive strength (UCS) of shale decreases with the increase in moisture content (w). The relationship between UCS and w for all shale data from the literature and Wyoming can be described by the power prediction equation. A decreasing trend of UCS with w is also observed on Wyoming shale. The power prediction equation developed using all shale data will yield a better prediction of UCS in terms w.

- The UCS of shale decreases with the increase in porosity (ϕ). The UCS versus ϕ relationship for all shale data and Wyoming only shale data can be described by power prediction equations. Power prediction equation describing all shale data is better among the two.

- The bedding angle influences the UCS of shales. It was found that the UCS is lowest when the bedding angle is between 30^0 and 60^0 and highest when bedding angle is either 0^0 or 90^0.

- The UCS increases with the increase in bulk density ($\square$) of shales as described by the exponential prediction equations, based on all shale data and Wyoming shale data, respectively.

- Axial strain at peak stress for shale shows no relationship with UCS.

- Young's modulus (E) of shale decreases with the increase in w. The relationship between E and w for both all shale data and Wyoming shale data are described by power prediction equations.

- A negative relationship between E and ϕ of shale can be described by the exponential prediction equation developed based on all shale data and the power prediction equation, for Wyoming shale only.

- The E increases with the increase in UCS of shale, which can be described by the power prediction equation, based on all shales and the linear prediction equation, based on Wyoming shales only.

- In terms of Young's modulus for Wyoming shales, some data show that E increases with the increase in bedding angle while most data show the lowest E occurred in shales with bedding angles between 30^0 and 60^0 and the highest E of shales with the bedding angle at either 0^0 or 90^0.

- E has a decreasing trend with the axial strain at peak stress defined by the power prediction equation.

- The effect bedding angle on rock strength is similarly observed in the triaxial test condition. The lowest peak stress occurred at the bedding angle between 30^0 and 60^0 and the highest peak stress at the bedding angle of either 0^0 or 90^0.

- A linear relationship between the peak stress and confining stress for all bedding angles 0^0, 15^0, 30^0, 45^0, 60^0, 75^0, and 90^0.
- No relationship is observed between a ratio of peak stress to confining stress versus porosity for bedding angles 0^0, 15^0, 30^0, 45^0, 60^0, 75^0, and 90^0.
- No relationship is observed between Young's modulus and a ratio of confining stress to porosity for bedding angles 0^0, 15^0, 30^0, 45^0, 60^0, 75^0, and 90^0.

- Cohesion of shales decreases with the increase in porosity.

- No relationship is observed between friction angle and porosity for shale data from the literature. However, an increasing trend between friction angle and porosity is observed in Cody shale.

- The Young's modulus decreases with the increase in the porosity of the triaxial condition.

(b) Claystone

- UCS decreases with the increase in w defined by the exponential prediction equation for Wyoming claystone.

- UCS decreases exponentially with ϕ.

- No apparent relationship is observed between UCS and bulk density as well as the axial strain at peak stress.

- A linear relationship is observed between E and UCS.

- E decreases exponentially with the increase in moisture content.

- E decreases exponentially with ϕ.

- No relationship is observed between E and bulk density as well as the axial strain at peak stress.

(c) Siltstone

- UCS decreases with the increase in moisture content (w). The relationships between UCS and w for all siltstone data and Wyoming data only are defined by the power prediction equation.

- The relationship between UCS and w improves when siltstones are analyzed from individual geological ages as indicated by the improved statistical indices.

- The negative relationships between UCS and ϕ for all siltstone data and Wyoming siltstone data only are described by power prediction equations.

- The relationship between UCS and ϕ is found to be improved when siltstones are analyzed from individual geological ages as indicated by the improved statistical indices.

- A positive relationship between UCS and bulk density (ρ) can be described by power prediction equation.

- No relationship is observed between UCS and axial strain at peak stress.
- E decreases with the increase in w.

- The negative relationship between E and ϕ can be described by the exponential prediction equation.

- The linear relationship between E and UCS can be described by the linear prediction equation.

- The positive relationship between E and ρ can be described by the exponential prediction equation.

- No relationship is observed between E and axial strain at peak stress.

- The peak stress under the triaxial compression condition has a positive relationship with the normalized confining stress with porosity described by the power prediction equation.

- Cohesion (c) decreases with the increase in porosity, which can be described by the power prediction equation.

- A ratio of cohesion to porosity also decreases with the moisture content, which can be described by the power prediction equation.

- Friction angle shows no relationship with porosity.

- No relationship is observed between the Young's modulus and porosity as well as confining stress.

The recommended prediction equations can be used for estimating mechanical properties of various shale formations with reasonable accuracy. The prediction equations for UCS are developed using Wyoming claystone data only, and they should be applied with caution to other claystone formations of other regions.

6.3   Recommendations

The study on the bedrock characterization of Wyoming in this study focused on the strength properties of the rocks at their in-situ moisture conditions. The rock cores obtained are either surface samples or samples from shallow depths (around 98 feet). The effect of temperature has not been studied in this study. Sedimentary rocks like shale and claystone are known to undergo rock hardening at an elevated temperature, and hence, studying the behaviors of these bedrocks at elevated temperatures can be a point of interest.

The mineral composition of rocks affects shear and compressive strengths of the rocks. Percentage clay content and clay fraction in the overall composition of shale and claystone significantly alter the strength and deformation behaviors of these rocks. The mineral composition can be quantified in a future study to understand the anisotropic effect on the rock strength. No apparent bedding is noticed on Wyoming rocks, but it has been found that the rock strength is highly influenced by the degree of bedding. A future study on Wyoming shales and claystone with different bedding planes should be considered.

There is a lack of research regarding the mechanical properties of claystone and siltstone in terms of their physical properties. The shear and compressive strengths of claystone and siltstone from Wyoming are very low as compared with the strengths of rocks reported in the literature. Additional research on different claystone and siltstone formations will help to populate more test data and help better understand their mechanical behaviors.

7. REFERENCES

AASHTO. (2017). AASHTO LRFD Bridge Design Specifications 8th Ed U.S. Customary Units. American Association of State Highway and Transportation Officials (AASHTO), Washington, D.C.

Adhikari, P., Ng, K. W., Gebreslasie, Z. Y., Wulff, S. S., and Sullivan, T. A. (2019). "Geomaterial Classification Criteria for Design and Construction of Driven Steel H-Piles." *Canadian Geotechnical Journal*, 57(4), 616-621.

Akaike, H. (1974). "A new look at the statistical model identification." *IEEE Transactions on Automatic Control, AC-19*, 716–723.

Amadei, B. (1996). "Importance of anisotropy when estimating and measuring in situ stresses in rock." *International Journal of Rock Mechanics and Mining Sciences & Geomechanics Abstracts*, 33, 293-325.

Amadei, B., and Savage, W. Z. (1989). "Anisotropic Nature of Jointed Rock Mass Strength." *J. of Mech. of ASCE*, 115, 525–542.

ASTM. (2014). *Standard Test Methods for Compressive Strength and Elastic Moduli of Intact Rock Core Specimens under Varying States of Stress and Temperature. ASTM Standard D7012-14.* ASTM International, West Conshohocken, PA.

Atkinson, B. K. (1979). "A fracture mechanics study of subcritical tensile cracking of quartz in wet environments." *Pure Appl Geophys*, 117, 1011–1024.

Barton, N. R. (1974). "A review of the shear strength of filled discontinuities in rock." *Norwegian Geotech. Inst.*, 105, 1–19.

Baud, P., Zhu, W., and Wong, T. F. (2000). "Failure mode and weakening effect of water on sandstone." *J Geophys Res*, 105(B7), 16371– 16389.

Bian, K., Liu J., Liu, Z.P., and Liu, J. (2019). "Mechanism of large deformation in soft rock tunnel: a case study of Huangjiazhai Tunnel." *Bull Eng Geol Environ*, 78, 431–444.

Bian, K., Liu, J., Zhang, W., Zheng, X., Ni, S., and Liu, Z. (2019). "Mechanical behavior and damage constitutive model of rock subjected to water-weakening effect and uniaxial loading." *Rock Mech Rock Eng*, 52, 97–106.

Bieniawski, Z. T. (1973). "Engineering classification of jointed rock masses." *Trans S. Afr. Inst. Civ. Engrs*, 15, 335-344.

Bieniawski, Z. T. (1978). "Determining Rock Mass Deformability: Experience from Case Histories." *International Journal of Rock Mechanics Mineral Science & Geomechanics Abstracts*, 15(5), 237-247.

Bieniawski, Z. T. (1989). *Engineering Rock Mass Classifications: A Complete Manual for Engineers and Geologists in Mining, Civil, and Petroleum Engineering.* Wiley, New York.

Bonewitz, R. L. (2012). *Rocks and Minerals*. DK Publishing, UK.

Carmichael, R. S. (1982). *Handbook of Physical Properties of Rocks.* 1st Edition, Volume III, CRC Press, Boca Raton.

Carter, J. P., and Kulhawy, F. H. (1988). *Analysis and Design of Foundations Socketed into Rock*. Report No. EL-5918, Empire State Electric Engineering Research Corporation and Electric Power Research Institute, Palo Alto, California.

Chang, C., and Haimson, B. (2007). "Effect of fluid pressure on rock compressive failure in a nearly impermeable crystalline rock: implication on the mechanism of borehole breakouts." *Eng Geol*, 89, 230–242.

Deere, D. U., and Miller, R. P. (1966). *Engineering classification and index properties for intact rock. Air Force Weapons Lab Tech Report*. Report No. AFWL-TR-65-116: Air Force Weapon Laboratory, New Mexico.

Duveau, G., Shao, J.F., and Henry, J. P. (1998). "Assessment of some failure criteria for strongly anisotropic geomaterials." *Mech. Cohesive-Frictional Mater.*, 3, 1-26.

Erguler, Z. A., and Ulusay, R. (2009). "Water-induced variations in mechanical properties of clay-bearing rocks." *Int J Rock Mech Min Sci*, 46(2), 355–370.

Fahy, M. P., and Guccione, M. J. (1979). "Estimating strength of sandstone using petrographic thin-section data." *Bulletin of the Association of Engineering Geologists*, 16(4), 467-485.

Fjaer, E., and Nes, O. M. (2013). "Strength anisotropy of Mancos shale." *Proceedings of the 47th US Rock Mechanics Symposium,* San Francisco, CA.

Franklin, J. A., and Dusseault, M. B. (1989). *Rock Engineering*. McGrill Hill, New York.

Gholami, R., and Fakhari, N. (2017). *Chapter 27 - Support Vector Machine: Principles, Parameters, and Applications.* Handbook of Neural Computation, 515-535.

Gholami, R., and Rasouli, V. (2013). "Mechanical and elastic properties of transversely isotropic slate." *Rock Mech Rock Eng*, 1–11.

Goodman, R. E. (1989). *Introduction to Rock Mechanics*. 2nd Edition, John Wiley & Sons, New York.

Griffith, A. (1924). *The theory of rupture. In Proceedings of the 1st International Congress for Applied Mechanics*, April 22-26, Delft.

Hadizadeh, J., and Law, R. D. (1991). "Water-weakening of sandstone and quartzite deformed at various stress and strain rates." *Int J Rock Mech Min Sci*, 28(5), 431–439.

Handin, J., Rex, V., Hager, J., Melvin, F., and Feather, J. N. (1963). "Experimental Deformation of Sedimentary Rocks Under Confining Pressure: Pore Pressure Tests." *Am. Assoc. Pet. Geol. Bull*, 47, 717–755.

Hawkins, A. B., and McConnell, B. J. (1992). "Sensitivity of sandstone strength and deformability to changes in moisture content." *Q. J. Eng. Geol. Hydrogeol*, 25, 115–130.

Hoek, E., and Brown, E. T. (1980). *Underground Excavations in Rock*. CRC Press, Florida.

Hoek, E., and Brown, E. T. (1997). "Practical Estimates of Rock Mass Strength." *International Journal of Rock Mechanics and Mining Sciences*, 34(8), 1165-1186.

Hoek, E., Carranza-Torres, C., and Corkum, B. (2002). "Hoek–Brown Failure Criterion—2002 Edition." *Proceedings of North American Rock Mechanics Society Meeting,* Toronto, Canada, 1, 267-273.

Hoek, E., Carter, T. G., and Diederichs, M. S. (2013). "Quantification of the Geological Strength Index Chart." *Proceedings of 47th US Rock Mechanics and Geomechanics Symposium,* San Francisco, CA, Paper No. ARMA 13-672, 23-26.

Hoek, E., and Marinos, P. (2000). "Predicting tunnel squeezing problems in weak heterogeneous rock masses." *Tunnels and Tunnelling International*, 32(11), 45-51.

Hossain, M. S., and Lane, D. S. (2015). *Development of a Catalog of Resilient Modulus Values for Aggregate Base for Use with the Mechanistic-Empirical Pavement Design Guide.* Final Report VCTIR 15-R13, Virginia Center for Transportation Innovation and Research, Charlottesville, VA.

Hu, D. W., Zhang F., Shao, J. F., and Gatmiri, B. (2014). "Influences of mineralogy and water content on the mechanical properties of argillite." *Rock Mech Rock Eng*, 47, 157–166.

Hudson, J. A., and Harrison, J. P. (2000). *Engineering Rock Mechanics—An Introduction to the Principles.* Elsevier, New York.

Jaeger, J. C., and Cook, N. G. W. (1976). *Fundamentals of Rock Mechanics*. Chapman and Hall, UK.

Jaeger, J., Cook, N. G. W., and Zimmerman, R. W. (2007). *Deformation and Failure of Rocks. Fundamentals of Rock Mechanics*. 4th Edition, Blackwell Publishing, 80.

Jizba, D. (1991). "Mechanical and acoustical properties of sandstones and shales." PhD thesis, Stanford University, CA.

Kim, K. Y., Zou, W., Holland, S., and Sachse, W. (2003). "Measurements of the longitudinal wave speed in thin materials using a wideband PVDF transducer." *The Journal of the Acoustical Society of America*, 114(3), 1450-1453.

Kirby, S. H. (1984). "Introduction and digest to the Special Issue on Chemical Effects of Water on the Deformation and Strengths of Rocks." *J. Geophys. Res.*, 89(B6), 3991– 3995.

Kumar, R., Sharma, K. G., and Varadarajan, A. (2010). "Post-peak Response of Some Metamorphic Rocks of India under High Confining Pressures," *International Journal of Rock Mechanics & Mining Sciences*, 47(8), 1357–1362.

Lashkaripour, G. R., Ajalloeian, R. (2000). "The effect of water content on the mechanical behaviour of fine-grained sedimentary rocks." *Proceedings of the ISRM International Symposium,* Paper Number ISRM-IS-2000-216, November, Melbourne, Australia.

Li, B., Liu, J., Bian, K., Ai, F., Hu, X., Chen, M., and Liu, Z. (2019). "Experimental study on the mechanical properties weakening mechanism of siltstone with different water content." *Arabian Journal of Geosciences,* 12(21).

Lu, Y. L., Wang, L. G., Sun, X. K., and Wang, J. (2017). "Experimental study of the influence of water and temperature on the mechanical behavior of mudstone and sandstone." *Bull Eng Geol Environ*, 76, 645–660.

Liu, T. Y., and Cao, P. (2016). "Testing study of subcritical crack growth mechanism during water-rock interaction." *Geotech Geol Eng*, 34, 923–929.

Lorig, L. J., and Varona, P. (2013). "Guidelines for numerical prediction equations of rock support for mines," *Proceedings of the Seventh International Symposium on Ground Support in Mining and Underground Construction*, Australian Centre for Geomechanics, Perth, 81-105.

Topinka, L. http://vulcan.wr.usgs.gov/Volcanoes/WestIndies/Pelee/description_l902_eruption.html, United States Geological Survey, Reston, VA, February 24 (1997).

Martin, C. D., and Chandler, N. A. (1994). "The progressive fracture of Lac du Bonnet granite." *Int. J. Rock Mech. Min. Sci*, 31, 643–659.

Masud, N., Ng, K. W., Johnson, T., and Wulff, S. S. (2022). "New static analysis methods for the prediction of driven piles resistances in siltstone." GeoCongress 2022, *Geotechnical Special Publication No. 332,* ASCE, March 20 to 23, Charlotte, NC, 93-103.

Mokwa, R., and Brooks, H. (2008). Axial Capacity of Piles Supported on Intermediate Geomaterials. Report No. FHWA-MT-08-008/8117-32, Montana State University/Western Transportation Institute, Bozeman, MT.

Noël, C., Baud, P., and Violay, M. (2021). "Effect of water on sandstone's fracture toughness and frictional parameters: Brittle strength constraints." *International Journal of Rock Mechanics and Mining Sciences*. 147.

Palmström, A. (1982). "The volumetric joint count—a useful and simple measure of the degree of rock jointing." *Proc. 4th Congr. Int. Assn Engng Geol.,* 221-228.

Paterson M. S., and Wong, T. F. (2004). *Experimental rock deformation—The Brittle Field*. Springer, Heidelberg, Berlin.

Romana M., and Vásárhelyi, B. (2007). "A discussion on the decrease of unconfined compressive strength between saturated and dry rock samples." *Proceedings of 11th ISRM Congress,* Lisbon, Portugal, 1, 139-142.

Roy, D. G., Singh, T. N., Kodikara, J., and Das, R. (2017). "Effect of water saturation on the fracture and mechanical properties of sedimentary rocks." *Rock Mech Rock Eng*, 50(10), 2585–2600.

Rybacki, E., Reinicke, A., Meier, T., Makasi, M., and Dresen, G. (2015). "What controls the mechanical properties of shale rocks? – Part I: Strength and Young's modulus." *Journal of Petroleum Science and Engineering*, 135, 702–722.

Schwarz G. (1978). "Estimating the dimension of a model." *Ann Stat*, 6, 461–464.

Shakoor, A., and Bonelli, R. E. (1991). "Relationship between petrographic characteristics, engineering index properties, and mechanical properties of selected sandstones." *Bulletin of the Association of Engineering Geologists*, 28(1), 55-71.

Singh, S. K. (1988). "Relationship among fatigue strength, mean grain size and compressive strength of a rock." *Rock Mechanics and Rock Engineering*, 21(4), 271-276.

Song, R., Zheng, L., Wang, Y., and Liu, J. (2020). "Effects of pore structure on sandstone mechanical properties based on micro-CT reconstruction model." *Advanced in Civil Engineering*, Volume 2020, 1-21.

Sonmez, H., and Ulusay, R. (1999). "Modification to the Geological Strength Index (GSI) and Their Applicability to Stability of Slopes." *International Journal of Rock Mechanics and Mining Sciences*, 36, 743-760.

Tien, Y. M., Kuo, M. C., and Juang, C. H. (2006). "An experimental investigation of the failure mechanism of simulated transversely isotropic rocks." *International Journal of Rock Mechanics and Mining Sciences*, 43, 1163–1181.

Torres-Suareza, M. C., Alarcon-Guzman, A., and Moya, R. D. (2014). "Effects of loading-unloading and wetting-drying cycles on geomechanical behaviors of mudrocks in the Colombian Andes." *J Rock Mech Geotech Eng*, 6, 257–268.

Travis, R. B. (1955). *Classification of Rocks*. Volume 50-51, Quarterly of the Colorado School of Mines, Golden, CO.

Ulusay R., and Hudson, J. (2007). "The complete ISRM suggested methods for rock characterization, testing and monitoring: 1974–2006." Commission on Testing Methods, International Society for Rock Mechanics, Ankara, Turkey.

Van Eeckhout, E. M. (1976). "The mechanisms of strength reduction due to moisture in coal mine shales." *Int. J. Rock Mech. Min. Sci. Geomech*, 13, 61–67.

Vásárhelyi, B. (2002). "Influence of water saturation on the strength of volcanic tuffs in Eurock." *Proceedings of ISRM International Symposium on Volcanic Rocks*, Maderia, Portugal, November, 89–96.

Vásárhelyi, B., and Ván, P. (2006). "Influence of water content on the strength of rock." *Eng Geol*, 84 (1–2), 70–74.

Vasarhelyi, B. (2002). "Influence of water saturation on the strength of volcanic tuffs in Eurock." *International Symposium on Volcanic Rocks. Maderia*, 89–96.

Verstrynge E., Adriaens, R., Elsen, J., and Van Balen, K. (2014). "Multi-scale analysis on the influence of moisture on the mechanical behavior of ferruginous sandstone." *Constr Build Mater*, 54, 78–90.

Vutukuri, V. S. (1974). "The effect of liquids on the tensile strength of limestone." *Int. J. Rock Mech. Min. Sci*, 11, 27–29.

Wickham, G. E., Tiedemann, H. R., and Skinner, E. H. (1972). "Support determination based on geologic predictions." *North American Rapid Excavation & Tunneling Conference*, Chicago.

Wong, T. F., and Baud, P. (2012). "The brittle-ductile transition in porous rock: A review." *Journal of Structural Geology*, 44, 25–53.

Wong, L. N. Y., Maruvanchery, V., and Liu, G. (2016). "Water effects on rock strength and stiffness degradation." *Acta Geotech,* 11, 713–737.

Wyllie, D. C., and Norrish, N. I. (1996). "Rock strength properties and their measurement." *Transportation Research Board*, 372–379.

Xie, H. P., Liu, J. F., Ju, Y., Li, J., and Xie, L. Z. (2011). "Fractal property of spatial distribution of acoustic emissions during the failure process of bedded rock salt." *International Journal of Rock Mechanics and Mining Sciences*, 48, 1344–1351.

Zhang Z. H., Jiang, Q. H., Zhou, C. B., and Liu, X. (2014). "Strength and failure characteristics of Jurassic red-bed sandstone under cyclic wetting-drying conditions." *Geophys J Int*, 198, 1034–1044.

Zhang, Q. B., and Zhao, J. (2014). "A review of dynamic experimental techniques and mechanical behavior of rock materials." *Rock Mech. Rock Eng*, 47, 1411–1478.

Zhou, Z., Cai, X., Cao, W., Li, X., and Xiong, C. (2016). "Influence of water content on mechanical properties of rock in both saturation and drying processes." *Rock Mech. Rock Eng*, 49, 3009–3025.